The Impact of Path Dependent Degradation on the Lifetime of Lithium-Ion Batteries

Trishna Raj

Department of Engineering Science

University of Oxford

This dissertation is submitted for the degree of

Doctor of Philosophy

St.Hilda's College

October 2021

Declaration

I hereby declare that except where specific reference is made to the work of others, the contents of this dissertation are original and have not been submitted in whole or in part for consideration for any other degree or qualification in this, or any other university. This dissertation is my own work and contains nothing which is the outcome of work done in collaboration with others, except as specified in the text and Acknowledgements.

Trishna Raj

October 2021

Acknowledgements

Firstly, I would like to thank my supervisor, Prof. David Howey, for his encouragement, patience and guidance. His advice has been invaluable and has motivated me through my DPhil journey.

I would like to express my appreciation to the Engineering and Physical Sciences Research Council and Jaguar Land Rover for the financial support that has enabled me to conduct my research. I am indebted to Prof. Charles Monroe and the Monroe group for allowing me to use their equipment to conduct experiments.

It has been a great pleasure to be part of the BIL group. I could not have asked for a more friendly and supportive environment in which to work. Special thanks to Jorn Reniers for the continuous encouragement, debates, and friendship; to Andrew Wang for technical insight and expertise which led to a fruitful collaboration; to Samuel Greenbank and Howie Chu: our invaluable discussions and laughs have kept me going; to Jorge Valera Barreras for imparting knowledge on conducting empirical research and to Asna Dodhy, Firoza Patel and Solveig van der Vegt for standing by me through it all.

Finally, my sincere thanks to my parents. Appa and Amma, thank you for inspiring me and supporting me in every way imaginable.

Abstract

To ensure lithium-ion batteries are reliable in terms of lifetime and performance, a detailed understanding of their ageing behaviour is essential. Models that predict battery lifetime require knowledge of the causes of degradation and operating conditions that accelerate it. Batteries experience two ageing modes: calendar ageing at rest and cyclic ageing during the passage of current. Existing empirical ageing models treat these as independent, but degradation may be sensitive to their order and periodicity – a phenomenon known as "path dependence". This empirical study investigates whether interactions between ageing modes can impact the rate of degradation. Eight groups of graphite/NCA 18650 lithium-ion cells were exposed to load profiles consisting of the same ratio of calendar and cyclic ageing applied in various orders. The profiles incorporate different C-rates, cycling methods and calendar ageing conditions, to gain insight into the conditions that encourage path dependent ageing. The data collected indicates that under certain conditions cells exposed to the same amount of calendar/cyclic ageing, but in different orders, can lead to a difference in degradation trends. The divergence in degradation rates is more pronounced when constant current cycling at higher C-rates and is limited when constant voltage steps are incorporated during cycling. Comparing the rate of degradation experienced by cells exposed to combined load profiles versus the degradation predicted using the cumulative empirical model indicates that the cumulative model underestimates the cell lifetime. These findings suggest that including the possible coupling between calendar and cyclic ageing modes can improve the accuracy of lifetime predictions.

Publications

Parts of the research presented in this thesis has been published. The experimental set up and initial results from the first experimental campaign presented in chapters 2 and 3 has been published in [1]. That paper did not include the complete data set because data collection from the experiments was ongoing and did not include any post-mortem results. The data presented in [1] has been shared under an open access licence [2]. The second half of the data from the first experimental campaign, and the data from the second experimental campaign, have also been published with open access licences [3],[4].

Dr. Jorge Varela Barreras and I have co-authored two conference papers [5],[6]. A screening study on 208 pouch cells were conducted to gain some insight into the cell-to-cell variation at the beginning of life [5]. To understand the impact that derating strategies can have on the rate of degradation of cells, a study was conducted that highlights the benefits of derating through simulations [6]. Although the research from these papers is not presented in this thesis, knowledge from the design of experiments and data collection techniques influenced the experiments conducted in this study.

[1] Trishna Raj, Andrew A. Wang, Charles W. Monroe, and David A. Howey. Investigation of Path-Dependent Degradation in Lithium-Ion Batteries. Batteries & Supercaps, pages 1377–1385, 2020.

[2] Path Dependent Battery Degradation Dataset Part 1, Trishna Raj and David A. Howey,2020. Oxford Research Archive, https://ora.ox.ac.uk/objects/uuid:de62b5d2-6154-426d-bcbb-30253ddb7d1e , DOI: 10.5287/bodleian: v0ervBv6p

[3] Path Dependent Battery Degradation Dataset Part 2, Trishna Raj and David A. Howey,2021. Oxford Research Archive, https://ora.ox.ac.uk/objects/uuid:be3d304e-51fd-4b37-a818-b6fa1ac2ba9d , DOI: 10.5287/bodleian:2zvyknyRg

[4] Path Dependent Battery Degradation Dataset Part 3, Trishna Raj and David A. Howey,2021. Oxford Research Archive, https://ora.ox.ac.uk/objects/uuid:78f66fa8-deb9-468a-86f3-63983a7391a9, DOI: 10.5287/bodleian:2zvyknyRg

[5] Jorge Varela Barreras, Trishna Raj, David A. Howey, and Erik Schaltz. Results of screening over 200 pristine lithium-ion cells. 2017 IEEE Vehicle Power and Propulsion Conference, VPPC 2017 - Proceedings, 2018-January(Cccv):1–6, 2018.

[6] Jorge Varela Barreras, Trishna Raj, and David A. Howey. Derating Strategies for Lithium-Ion Batteries in Electric Vehicles. IECON 2018 - 44th Annual Conference of the IEEE Industrial Electronics Society, 1:4956–4961, 2019.

Table of contents

List of figures

List of tables

Nomenclature

Abbreviations

BoL Beginning of Life

CC Constant Current

CCCV Constant Current Constant Voltage

DoD Depth of Discharge

DVA Differential Voltage Analysis

EIS Electrochemical Impedance Spectroscopy

EoL End of Life

EV Electric Vehicles

FEC Full Equivalent Cycles

GITT Galvanostatic Intermittent Titration Technique

ICA Incremental Capacity Analysis

LAM Loss of Active Material

LAM_{ne} Loss of Active Material at the Negative Electrode

LAM_{pe} Loss of Active Matterial at the Positive Electrode

LLI Loss of Lithium Inventory

MoL Middle of Life

NCA Lithium Nickel Cobalt Aluminium Oxide

OCV Open Circuit Voltage

PPC Pulse Power Characterisation

$Q_{balance}$ Electrode Balance Capacity

R_{CT} Charge Transfer Resistance

R_{DC} DC Resistance

R_{Ohmic} Ohmic Resistance

R_{SEI} SEI Resistance

RPT Reference Performance Test

SEI Solid Electrolyte Interphase

SoC State of Charge

Chapter 1

Introduction

The research presented in this thesis aims to explore whether the order and periodicity of calendar/cyclic ageing can impact the rate of degradation i.e., is degradation path dependent? Empirically, batteries can experience two forms of ageing "calendar ageing" (at open circuit) and "cyclic ageing" (at non-zero applied current). In the case of an EV, calendar ageing occurs when the vehicle is parked, while cyclic ageing occurs during driving and charging. Predicting the remaining useful life and tracking the state of health of batteries continues to be a challenge, especially for cells operating under realistic use conditions, where lifetime is affected by factors such as external temperature, pack cooling, intensity of usage, etc.[2]. In order to minimise model complexity, empirical ageing models either account for only a single mode of ageing (calendar or cyclic) or treat these modes separately and add their contributions together to form a combined model under the assumption that calendar/cyclic ageing is cumulative [3–6]. The data used for these empirical models tend to be state dependent, which means that the degradation is dependent on cells that have been exposed to either calendar or cyclic ageing under a controlled stress conditions like C-rate, state of charge, temperature etc. Realistically, a battery will experience a combination of both calendar ageing (i.e. relaxation periods with no load) and cycling (i.e. charging and discharging), making it essential to understand their combined impact on cell lifetime, however most data-driven

empirical models that are used to predict cell lifetime disregard the impact on degradation caused by the interaction of degradation mechanisms as a result of calendar/cyclic ageing, a phenomenon which is referred to as the "path dependence" of battery degradation [7]. Where state dependent degradation is the degradation experienced by a cell being held under specific ageing conditions (i.e., calendar ageing at a single SoC, continuous cycling through a constant SoC window, etc) path dependent degradation is influenced by the degradation the cell has experienced in the past. In this study we limit the investigation of path dependence to investigate whether cells exposed to the same duration of calendar/cyclic ageing but in different orders can impact the rate of degradation to answer the hypothesis of whether a previously experienced mode of ageing (calendar or cyclic) can interact with future ageing types to affect the rate of degradation. The experiments designed to answer this research question take into consideration the following conditions: the method of cycling (constant current or constant current constant voltage), different C-rates, the voltage window for cycling, the duration of cycling, the SoC during calendar ageing, the duration of calendar ageing, and the ambient temperature during testing.

Understanding how different operating conditions impact cell ageing can improve the accuracy of lifetime and performance prediction. It is crucial for manufacturers and original equipment manufacturers (OEMs) to have an in-depth understanding of how batteries degrade in order to ensure the reliability and performance of their product. Accounting for path dependence in lifetime models and understanding its impact on cell lifetime allows for a better understanding of when the cell will reach the end of life condition and what impact combined profiles will have on the rate of degradation. This is valuable for OEMS and manufacturers as they will be equipped with the models required to provide accurate warranties on batteries. This also ensures that batteries are being used to their maximum potential and reaching their true end of life condition before being transitioned into second-life applications or being recycled.

The following sections provide some background on the fundamentals of batteries, an overview of the degradation mechanisms that affect the lifetime of a cell and a review of research that has been conducted to understand battery ageing. The rest of the chapter identifies the gap in current literature and explains how the research in this thesis aims to improve the understanding of path dependence.

1.1 Lithium-ion Batteries

A lithium-ion cell consists of two porous electrodes, a separator, electrolyte and current collectors. While charging, the lithium oxidises and deintercalates from the positive electrode. The deintercalation releases an electron which is conducted through the current collectors to the external circuit. The lithium ions act as the charge carriers and are transported through the separator via the electrolyte. The electron is absorbed at the negative electrode and the lithium ions in the electrolyte intercalate into the electrode. [8]. The cell components can be configured into three cell designs, cylindrical cells, prismatic cells and pouch cells. The electrodes in cylindrical cells are wound to form a 'jelly roll'. Prismatic cells also have a would electrode configuration while the electrodes in pouch cells are stacked.

The electrolyte provides the medium for ion exchange which allows for the production of electricity. The commonly used electrolyte is a mixture of organic solvents, conducting salts and additives. A porous polymer foil is used as the separator to allow the transport of lithium ions through the electrolyte while preventing electrical contact between the electrodes [9]. The cell contains two electrodes, the anode is the negative electrode upon discharge and the cathode is the positive electrode. Although strictly speaking these swap upon charging, the positive electrode will be referred to as the 'cathode' and the negative electrode will be referred to as the anode throughout this thesis. The anode is commonly a slurry consisting of graphite, binder solution and carbon black coated onto a copper current collector foil[10]. The positive electrode (cathode) is made up of an aluminium current collector coated in a

lithium metal oxide. The cathode material can have an olivine structure (e.g. lithium iron phosphate), a layered structure (e.g. nickel cobalt aluminium oxide) or a spinel structure (e.g. lithium manganese oxide) [11]. Selecting the cell chemistry according to the application is critical—currently lithium nickel manganese cobalt oxide (NMC) or lithium nickel cobalt aluminium oxide (NCA) are commonly used in electric vehicles (EVs) due to their high energy density and good power capability and cycle life [12, 13].

1.2 Degradation of Lithium-ion batteries

During operation, lithium-ion cells are exposed to two modes of ageing, calendar ageing and cyclic ageing. Calendar ageing occurs when the cell is at rest under open circuit conditions; in an electric vehicle this would be when the car is parked. Cyclic ageing occurs when cells are experiencing dis/charging i.e. when an EV is being driven or recharged [14]. Cells undergo degradation during both ageing modes and this leads to the reduction of cell lifetime and the deterioration of performance characteristics. The rate of degradation is dependent on the stress factors that the cells are exposed to during calendar or cyclic ageing. For calendar ageing, stress factors such as the temperature and state of charge (SoC) can influence the rate of degradation. The SoC is the total charge stored in the cell relative to the maximum charge the cell can store within the operating limits of the cell. Degradation during cyclic ageing is more complex and is dependent on temperature, C-rate (the cell current divided by the nominal capacity) , cycle depth, charge throughput, etc. In this section we will focus on the degradation mechanisms experienced by a cylindrical NCA cell. Fig. 1.1 presents a schematic summary of degradation mechanisms that can impact cell lifetime. Significant degradation mechanisms will be discussed in this section.

Being exposed to different ageing modes and stress factors encourage various degradation mechanisms that affect cell components. The degradation mechanisms result in the loss of lithium inventory (LLI) and the loss of active material (LAM) at electrodes. Degradation

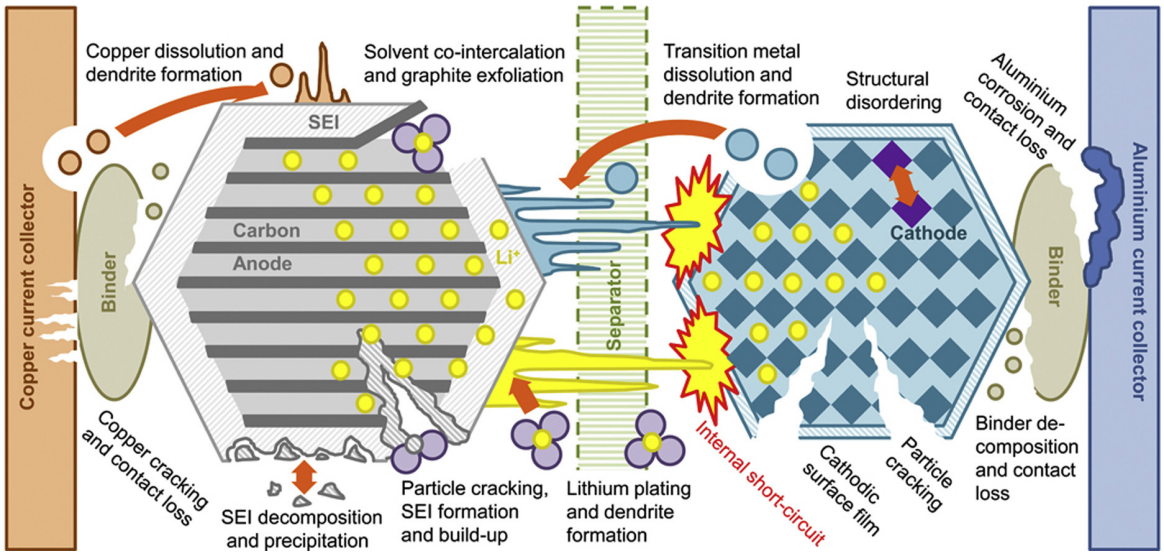

Fig. 1.1 A schematic summary of degradation mechanisms, from Birkl et al. [1] CC BY 4.0

of a cell can be tracked by monitoring its capacity fade and/or power fade [1]. Loss of lithium inventory is a result of lithium ions being consumed by side reactions such as solid electrolyte interphase formation or lithium plating resulting in less lithium ions available to cycle through the electrodes which can result in capacity fade. The loss of active material can occur at the negative or positive electrodes. LAM at the negative electrode means a portion of the negative electrode is no longer active and is not able to accept lithium ions. This can be a product particle cracking and loss of electrical contact or the pore blocking due to surface film formations. Similarly, the positive electrode can also lose active material due to particle cracking, structural disordering or loss of electrical contact. If the loss of active material occurs while the electrode is lithiated, this can also attribute to the LLI.

The degradation mechanisms causing LLI/LAM that impact the lifetime and performance of a cell are discussed below.

1.2.1 Anode Degradation

The most commonly used Li-ion battery anode material is graphite, especially in electric vehicles. The anode can experience a range of degradation mechanisms that lead to the

loss of active anode material (in either a lithiated or delithiated state) and consume lithium inventory.

Solid Electrolyte Interphase

Solid electrolyte interphase (SEI) is considered to significantly contribute to cell degradation. Formation of the SEI layer is a result of lithium ions reacting with electrolyte at the electrode/electrolyte interphase leading to a thin solid deposit on the anode surface[15]. When the anode is at low potentials during charging, it reduces the electrolyte into insoluble salts that result in the formation of the surface layer [16]. The morphology and properties of the SEI layer depends on the local voltage as studied by Lu et al [17]. The growth of the SEI layer is encouraged by high temperatures and, high C-rates and high SoCs. The SEI layer built during the initial cycles also knows as the formation layer is actually crucial for stable battery operation, as it has low electrical conductivity whilst still allowing ions to pass through, and is impermeable to other electrolyte components which limits further side reactions. The passivation layer however does not completely isolate the electrode and hence the SEI layer continues to grow over time [18]. As the SEI layer grows, it can penetrate through the pores of the electrode leading to a reduced area of accessible active material and results in increased current density on the remaining active material[19]. The formation of the SEI layer leads to the irreversible loss of lithium inventory (i.e. loss of otherwise useful lithium that could be cycled). The formation of the SEI layer is usually accompanied by the formation of gaseous electrolyte decomposition products[20]. The formation of the SEI layer leading to the irreversible loss of lithium inventory and access to active anode material impacts both capacity and power fade. [21]

Lithium Plating

Lithium plating occurs when lithium ions that are dissolved in the electrolyte deposit as metallic lithium onto the surface of the electrode instead of intercalating into the electrodes. Plating can take place when the anode is fully lithiated before the end of charge or due to kinetic factors caused by extreme charging conditions [22]. As the cell charges, the reduced available sites for lithium intercalation and the sluggish solid-state diffusion rate limits the intercalation rate into the anode. High SoC can encourage lithium plating due to the limited available sites for lithium intercalation at the electrode and the slower diffusion through the electrode. Low temperature conditions can encourage lithium plating as the reaction rates slow down which influences the rate of intercalation. This leads to a growth of metallic lithium on the electrode that can insulate areas of the electrode. The anode is most vulnerable to plating at the end of a constant current charge when the anode potential is at its lowest with respect to Li/Li+ [23]. Applying a constant voltage step or relaxation period after constant current charging can prevent lithium plating and can allow plated lithium to reintercalate into the electrode [22]. While some of the plated lithium can be recovered, the plating that remains on the electrode surface can encourage more SEI to form [24]. Lithium plating consumes lithium inventory and can cause pore clogging that leads to the loss of active surface area which impacts the lifetime and performance of the cell. Under extreme circumstances, the plating can lead to the formation of dendrites, small metallic structures that grow away from the electrode surface. If the dendrites pierce through the separator, they can cause internal short circuits leading to thermal runaway. Lithium plating is hence not only detrimental to the performance of a cell but also is a potential hazard [25].

Mechanical Stress

When a cell is dis/charged the volume of the anode changes, as the lithium ions intercalate the electrode material expands and the electrode material contracts during deintercalation. The

distance between the layers of graphite can expand up to 10% during intercalation [26]. This can lead to weakened particle to particle contact, loss of contact between the active material and the current collector or loss of contact of the binder to the active material/current collector leading to loss of active material and subsequently resulting in capacity fade. The weakened contact between the particles, current collector and binder can lead to inhomogeneous current and potential distributions. The mechanical stress in the electrodes is encouraged by cycling at high C-rates [27]. The mechanical stress leads to cracks forming in the SEI which brings 'fresh' electrode material into contact with electrolyte and causes more SEI formation which consumes active lithium[28]. Electrode material may be lost in a lithiated state leading to a decrease in cyclable lithium inventory. The resulting reduced active surface area can also lead to an increase in resistance.

1.2.2 Cathode Degradation

This section will describe the degradation mechanisms at the cathode that can lead to loss of active material and lithium inventory. The cells used in this thesis have NCA cathodes and hence the degradation mechanisms discussed in this section will focus mainly on NCA cells.

Passive Film Formation

Similar to the anode, a passive film forms at the interphase between the cathode and electrolyte. The layer is composed of organic components from the electrolyte decomposition and inorganic species from conductive salt decomposition[29]. The formation is encouraged by storing the cell at high SoC. The passivation film has similar properties to the layer of SEI at the anode, and the growth of the layer leads to an increase in cell resistance.

Transition Metal Dissolution

During operation, the transition metals such as manganese, cobalt and nickel in the cathode can become unstable. Transition metals can oxidize into cations at high cathode potentials which is encouraged by high temperatures and high cathode potentials [30]. The resulting dissolved metal can be transported in the electrolyte and may encourage SEI growth at the anode resulting in capacity fade[31].

Mechanical Stress

Mechanical stress caused by de/intercalation of lithium ions into NCA electrode can cause changes similar to that experienced at the anode, including the formation of microcracks and the isolation of NCA active material[32]. Studies have shown that there can be a significant increase of impedance at the cathode due to the loss of contact between segments of the cathode after cycling. High energy lithium-ion cells that have thicker electrodes are more susceptible to the adverse effects of mechanical stress leading to a higher rate of degradation. The impedance increase seen when an NCA cell ages can be partially attributed to the cathode[33, 34].

1.2.3 Degradation of other cell components

Components other than the electrodes may also deteriorate as the cell ages which can influence the rate of degradation. The current collectors may experience direct mechanical stress leading to their deformation. The volume changes in the electrodes during de/intercalation may also result in deformation of the current collector foils. The deformation in the jelly roll is especially evident in cells cycled at high C-rates and can lead to loss of electrical contact resulting in loss of capacity [35].

The pores of the separator can become clogged with electrolyte decomposition products. This can lead to inhomogeneous current distribution caused high local ionic current densities

which can cause uneven ageing through the electrode [36]. Certain binder materials can react with the charged anode which can lead to mechanical deterioration of the electrode. This results in consumption of the useable lithium inventory [26].

The electrolyte is involved in SEI formation at the anode and the formation of the passivation film at the cathode, which leads to the consumption of cyclable lithium [37]. The decomposition of electrolyte can also lead to gaseous products forming that result in increased pressure within the cell. Prolonged electrolyte decomposition can also lead to drying out of parts of the cell which causes inhomogeneous current distribution within the cell leading to uneven degradation of the electrodes [38, 39].

1.2.4 Calendar versus Cyclic Ageing Modes

Studies have been conducted to understand the relationship between each mode of ageing, stress factors and the degradation mechanisms that result in capacity/power fade.

Batteries in EVs for light duty passenger vehicles (with the exception of taxis) spend much of their lifetime at rest, hence it is valuable to study the influence that calendar ageing conditions can have on cell lifetime. There are two types of calendar ageing that a cell can experience, calendar ageing under a float condition or under open circuit conditions. Float calendar ageing, common with lead acid batteries but less relevant for Li-ion which has very low self-discharge, is conducted by supplying a constant voltage to maintain a stable SoC, while open circuit calendar ageing does not involve any charging [40]. The two stress factors that impact the rate of degradation during rest are the state of charge that the cell rests at and the temperature. Bloom et al. conducted a study that exposed lithium nickel cobalt oxide cells to a combination of 3 SoC points at 4 different temperatures [41]. Groups of cells were calendar aged at 40%, 60% and 80% SoC and at 40°C, 50°C, 60°C and 70°C temperatures. The data shows that calendar ageing is accelerated at higher temperatures and higher SoC. The authors suggest that the associated power fade could be due to the growing passivation

layer at the electrode interphase. To gain further insight, Keil et al. performed a study on three different chemistries, NCA, Lithium Nickel Manganese Cobalt Oxide (NMC) and Lithium Iron Phosphate (LFP) with a more intensive test matrix consisting of 16 SoC points at ambient temperature (25°C) as well as temperature extremes (40°C and 50°C) [27]. As expected, the cells held at higher temperatures experienced greater degradation at all storage SoCs with respect to capacity fade and resistance increase. The data to study the relationship between the rate of degradation due to calendar ageing and SoC indicates that there was not a steady increase in cell degradation with the increase in SoC. The data shows that there is a significant increase in the rate of capacity/power fade for cells held at 60% SoC or higher for NCA and NMC cells . The LFP data suggests that being held at 70% SoC or higher can encourage capacity fade however SoC does not impact the rate of resistance increases. Differential voltage analysis was conducted in order to study the role of the electrodes and electrode balancing in calendar ageing. This revealed that the low anode potentials with respect to Li/Li+ caused by storage at high cell SoCs encouraged loss of lithium inventory which could be due to the growth of the SEI layer. Comparing the conclusions from this paper with various other calendar ageing studies shows agreement that the most prominent degradation mechanism for calendar ageing is the growth of the anode SEI passivation layer which leads to loss of lithium inventory [42–44, 14].

In lab tests, there are commonly two types of cyclic ageing that a cell can be exposed to: constant current constant voltage cycling (CCCV) and constant current (CC) cycling. Constant current cycling means dis/charging to the set cell voltage limits at a fixed C-rate while CCCV cycling holds the cell at the voltage limit after CC charging until the current reduces considerably. Käbitz et al. conducted a study that cycled NMC cells to through multiple different SoC windows and temperatures ranging from 25 °C to 60 °C. The cells were cycled under a CC condition at 1C. The results confirm that cycling around a higher average SoC or at higher temperatures will increase the rate of degradation. A post-mortem

study showed that the cyclic degradation could be attributed to mechanical stress and SEI formation at the anode[43]. By expanding the experimental test matrix to include temperature, depth of discharge (DoD) and C-rate, Wang et al. improved the understanding of cyclic ageing for $LiFePO_4$ cells [45]. Five cycling windows were tested under 5 temperatures at 4 different C-rates under CC cycling conditions. Extreme C-rates and temperatures were used to accelerate ageing and to understand the impact that extreme stress factors have on cell lifetime. The cells cycled at extremely low temperatures, high temperatures and at high C-rates experienced the shortest lifetime. As the C-rate increases, the mechanically induced stress increases leading to the irreversible capacity loss and resistance increase. The authors predict the increased degradation due to accelerated ageing conditions could be due to increased lithium consumption at the negative electrode.

These cyclic and calendar ageing studies do not take into consideration the influence of a more realistic cycling profile that an EV or other application might experience. Laboratory ageing studies tend to accelerate ageing by exposing cells to extreme stress factors in order to speed up data collection, but this may lead to erroneous conclusions about the real world behaviour of batteries. In order to collect data that is representative of realistic cell use in a laboratory environment, there are certain characteristics that can be taken into consideration. Using real drive cycle profiles instead of CC or CCCV cycling allows the stop-and-go nature of driving through traffic and charging power pulses caused by regenerative braking to be accounted for. Keil et al. [46] exposed cells to the US06 highway drive cycle under three different temperatures and within 3 SoC cycling windows. The study focused on understanding the impact of regenerative braking by applying 4 regenerative charging conditions that ranged from no regenerative charging to a maximum of 4 A (1.4 C)of regenerative charging. All cells were exposed to two runs of the US06 drive cycle in series followed by a recharge to the maximum SoC limit within each of the 3 SoC cycling windows. Surprisingly the results showed that the cell experiencing more regenerative braking aged

slower. This trend was especially evident in the cells cycled around a higher SoC or at lower temperatures. The authors conclude that the negative degradation impact due to the short, high C-rate recharging is counteracted by the less aggressive recharge required after the two consecutive runs of the drive cycle. The charge recovered by braking, the higher the overall SoC at the end of the drive cycle and the shorter charging required. Charging the cell at high SoC or low temperatures are known to encourage lithium plating however it was suggested that reducing the time spent during a full recharge of the cell by having more aggressive regeneration peaks, may reduce lithium plating and cell degradation[46]. The second important feature relating to real usage is the relaxation periods. For an application such as an EV, the battery may spend much of the time at rest with less frequent periods of cycling. Since incorporating calendar ageing periods into cycling ageing studies would prolong the duration of a lab test, calendar ageing tests are usually conducted separately. However, having a period of calendar ageing after a period of cyclic ageing can positively influence the capacity fade of a cell. Burrell et al. [47] conducted a study to look into reversible capacity loss in cycle ageing tests. Cells were CCCV cycled through 6 different cycling windows and were calendar aged at 50% SoC for 12 weeks followed by relaxation at 0% SoC for additional 12 weeks. After continuous cycling, the cells that were cycled through a larger SoC window had lost more capacity than the cells cycled through a smaller SoC window. It was shown that cells that had an upper voltage limit of 4.1 V degraded more rapidly than those that were cycled up to 4.2V. This cyclic data goes against most other studies that suggest the rate of ageing is increased with larger cycling SoC windows. After investigating the time spent under constant current and constant voltage conditions during cycling, it was noted that cells cycled within a lower cut off voltage spent longer at constant voltage. The longer time spent under constant voltage at high SoCs will lead to lithium diffusing into the anode overhang region. for which there is no cathode counterpart. This leads to the loss of lithium inventory and hence greater capacity fade, but that loss is

recoverable with very long relaxation times. Allowing the cell to relax for an extended period of time (weeks) after cycling will enable the lithium in the overhang anode area to diffuse evenly throughout the electrode. After the cells in the study were calendar aged at 50% SoC, capacity recovery was observed especially for those cells cycled to a lower cut off voltage (4.1V). A significant capacity recovery was observed by further calendar ageing at 0% SoC with the cells cycled at to a lower cut off voltage showing greater capacity recovery than those cycled to higher voltages. This study not only highlights the importance of relaxation periods to obtain accurate cycling data but also identifies the need to conduct studies that combine calendar and cyclic ageing periods [47].

1.3 Gap Analysis - Path Dependent Degradation

Cell degradation has been studied experimentally by considering calendar and cyclic ageing to be independent [48–51]. Separating calendar and cyclic studies allows for shorter testing durations, making research more time and cost effective. It is also common to expose the cells to stress factors in order to accelerate ageing, such as temperature extremes, high cycling C-rates, high storage SoC, etc. Although this results in a faster experiment, it also influences the degradation mechanisms within the cell and encourages possibly unrealistic degradation.

Path dependence is a phenomenon that has been alluded to in many studies as a factor that could influence the rate of degradation [26, 52–54]. Thomas et al. suggests that cell degradation is a dynamic process and is not a 'memoryless' process. It is explained that a 'memoryless' degradation would mean that the future degradation rate is independent of the stress that led to a cells' current state of health and is only dependent on the current and future ageing conditions of the cell [55]. Path dependent ageing on the other hand can alter the rate of ageing as result of the interaction between degradation mechanisms over time. These degradation mechanisms can be encouraged by calendar and cyclic ageing under various stress factors meaning that the order in which a cell is exposed to different types of

ageing could lead to an altered influence of the various degradation mechanisms. However, research has not been presented that accurately isolates the impact of path dependence on the rate of degradation and assesses the accuracy of the cumulative assumption in empirical lifetime models.

There are a few papers in which cells have been exposed to controlled stress factors to gain some insight into path dependent degradation.

Ma et al. [56] identified that the accuracy of battery state-of-health estimation might be impacted by path dependence, and explored this question experimentally. The study aimed to identify the path dependence caused by different thermal conditions and depths of discharge. Six pairs of cells were aged using a drive cycle at various temperatures and cycled to different DoDs. Since the cells were exposed to three different stress factors, it is unclear whether the degradation seen was caused by the environmental temperature, the DoD variations, or by cell heating due to dynamic cycling. This makes the specific influence of path dependence unclear. The study also did not incorporate any calendar ageing periods other than breaks during the drive cycles and a 4 hour relaxation before characterisation data was collected [56].

Dubarry et al. [7], [57] created an experimental campaign incorporating cycling related to EV driving, charging, calendar ageing during parking, and vehicle-to-grid/grid-to-vehicle power exchange. To accelerate ageing, the profiles were simplified, which resulted in calendar ageing times being reduced compared to a real-world scenario. Separate calendar ageing studies were conducted in parallel at various temperatures. Due to the accelerated degradation conditions used, the influence of degradation on path dependence is not clear.

A study of path dependence was also performed by Gering et al. [58], and this included an investigation of how power pulses influence degradation. Five groups of cells were exposed to charge/discharge power pulses that varied in amplitude and duration. The profiles incorporated calendar ageing periods of varying durations and the profile design ensured that

the cumulative discharge energy was consistent throughout the different profiles to ensure comparability. All the tests however were conducted at 30 °C which may have encouraged some degradation mechanisms. A second study was designed to investigate the influence of thermal cycling along with electrochemical cycling similar to the study conducted by Ma et al. [56]. Due to the limited data collected at the time of the publication of this paper, a conclusive analysis of the results was not presented [58]. These studies have not isolated the impact of path dependence on degradation, since they all involve exposing the cells to varying stress factors, confusing the picture. They also do not address the combined ageing and coupling influence of calendar versus cyclic ageing.

Groot et al. discussed the lack of understanding of the impact of rest periods between cyclic ageing periods and designed an experiment to study the impact that brief relaxation periods can have on cell lifetime [59]. Their combined test profile subjected cells to a 15 minute relaxation period before each charge and discharge condition. A symmetric constant current charge and discharge cycling profile was used with a high C-rate of 3.75C, which was assumed to be a realistic hybrid electric vehicle us C-rate. The design of experiments included an initial set of cells cycled at ambient temperature between 0% SoC to 100% SoC at 3.75C and no relaxation periods, and a second test that incorporated 15 minute relaxation periods at ambient temperature. The third test included the relaxation periods too, and was cycled at a 'medium temperatures' which were not defined in the study but suggested to be around 35 °C. The results suggest that the cells that experienced brief relaxation periods aged more rapidly. The capacity fade data shows the cell exposed to the cyclic and calendar profile at ambient temperature reached the end of life condition first, followed by the cell exposed to the combined profile at higher temperature, with the cell exposed to continuous cycling lasting the longest. The discussion suggests that the relaxation period leaving the cell at SoC extremes encouraged SEI formation leading to the rapid ageing of the cells. This study sheds light on the impact that combined profiles can have on ageing. The three combined

profile conditions, uncontrolled thermal conditions and high cycling rate makes it difficult to understand the extent of influence that path dependent degradation can have on cell lifetime from this work.

Most empirical models only account for a single mode of ageing (calendar or cyclic) [3]. The models that incorporate both calendar and cyclic modes often assume that the degradation caused by each of these can be dealt with separately and that the cyclic/calendar degradation is cumulative.

Schimpe et al. produced a semi-empirical model to predict the capacity loss experienced by cells exposed to varying thermal conditions under calendar and cyclic ageing [6]. To parameterise the model, a calendar study was conducted under 9 SoC conditions and 7 temperature conditions. A separate cyclic ageing study exposed cells to a combination of 3 C-rates and 7 temperatures under different cycling conditions. Four models reflecting the cell capacity behaviour under calendar ageing, cyclic ageing at high temperatures, cyclic ageing at low temperatures, and cyclic ageing at high temperature plus high SoC were developed. The authors then introduced the assumption that the capacity degradation experienced under all 4 conditions are separable and the cumulative degradation can be used to estimate the capacity fade of the cell.

Many other semi-empirical models also implement the cumulative assumption. Guenther et al. state that calendar ageing occurs when no current is applied however they justify the cumulative assumption by saying that calendar ageing occurs during operation [60]. Similarly, the model developed by Wang et al. sums the calendar and cyclic capacity fade influences [4].

This shows that while the battery research community is aware that path dependence could impact the rate of degradation, there is still not a clear understanding of the difference in the rate of degradation caused by path dependence and how it can affect cell lifetime modelling. Due to the lack of experimental evidence, there is no data to prove whether

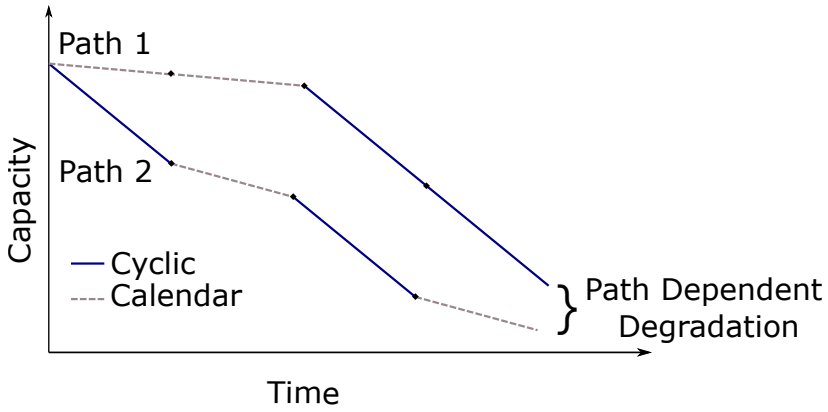

Fig. 1.2 A schematic representation of the impact of path dependent degradation

the cumulative assumption used in empirical lifetime models leads to accurate lifetime predictions under combined ageing modes.

1.4 Motivation and Objectives

Understanding battery ageing is complex and relating laboratory experiments to real world cell use is still an active area of research. Realistically, a cell would not spend a lifetime being only exposed to calendar ageing nor would a cell be continuously cycled till the end of life. Since a cell in the real world would be exposed to a combination of both ageing types, collecting laboratory data to replicate the influence of combined ageing can help bridge the gap between controlled data collection and realistic cell ageing. A schematic representation of the impact of path dependent ageing is presented in Fig. 1.2 , highlighting the importance of understanding how calendar and cyclic ageing interact during realistic combined profiles. Exploring path dependent ageing will improve the understanding of the interaction between the types of ageing and will provide some data to gain insight into the accuracy of the cumulative assumption in empirical models.

This thesis aims to investigate the impact that path dependence has on lithium-ion cell degradation and study the accuracy of empirical models that do not account for path dependent degradation. Due to the lack of data collected to date using controlled combined cycling

profiles, a relationship between path dependence, degradation and cell lifetime/performance has not yet been formed. This study provides the data to address the hypothesis that path dependence as a result of exposure to combined load profiles could influence the rate with which the cell ages. The data improves the understanding of path dependence, and the analysis investigates the degradation modes leading to the differences in degradation resulting from this phenomenon. Comparing the state of health results obtained through the experimental campaigns here and the predicted ageing obtained from empirical models that assume calendar/cyclic degradation is cumulative, provides insight into the accuracy of this assumption.

Improving lifetime and performance models of batteries to reflect a realistic rate of degradation encourages full utilisation of a cell. Underestimating the lifetime of a cell would lead to batteries being over-engineered, involving unnecessary additional cost. Modifying models to incorporate the coupling between both types of ageing mode will reduce the underestimation of cell lifetime that occurs if this coupling is ignored. This is beneficial to cell manufacturers and electric vehicle manufacturers as they will be able to gain a more realistic view of cell lifetime and power capabilities which in turn will improve the accuracy of battery warranties provided. Since degradation can follow non-linear trends, not accounting for path dependence could not only lead to a difference in the time/charge throughput to reach the end-of-life condition but it could also impact the ageing trajectory. For example, two groups of cells exposed to the same duration of calendar/cyclic ageing in different orders may experience a significant divergence in capacity fade from the beginning to middle of life which may reduce as the cells in both groups reach the end of life condition. While the divergence between the end of life condition may not be significant, the significant difference in the degradation trends seen until the middle of life indicates a difference in performance of the cells. Accounting for path dependent degradation and ensuring that the cells are used to their full potential before being transitioned into second-life applications or

being recycled would be financially and environmentally valuable. To summarise, the main objectives of this study are as follows:

1. Design experiments used to collect data in order to test the hypothesis that path dependence exists.

2. Investigate the extent of path dependent degradation under constant current cycling at different C-rates.

3. Examine the difference in the extent of path dependent degradation when cycling under constant current constant voltage conditions

4. Understand the relationship between path dependent degradation and calendar ageing at different states of charge.

5. Gain insight into the degradation modes that encourage path dependent degradation

6. Understand the accuracy of lifetime predictions made under the cumulative degradation assumption in empirical models.

1.5 Scope

To understand the impact of path dependent degradation with a focus on the interaction between degradation mechanisms encouraged by calendar and cyclic ageing, the following considerations were taken into account in this study. Three cells were tested per condition to understand the impact of cell-to-cell variability while also accounting for equipment availability. This study considers the influence of external temperature on the rate of degradation by conducting all the in thermal chambers set to 24 °C to ensure comparability between datasets and to ensure the cell ageing was not accelerated under extreme temperatures. Each group of cells is be exposed to the same duration of calendar or cyclic ageing but in different

orders to isolate the impact of path dependent degradation. Load profiles were designed that combined cyclic and calendar ageing that maintained the ratio of 1:5 across all groups of cells. The calendar ageing is conducted under open circuit conditions at either 90% or 100% SoC. Continuous calendar ageing was conducted for 5 or 10 days in order to ensure the influence of calendar ageing is seen in the degradation data from the combined load profiles. The cyclic ageing is conducted for 1 day or 2 days by continuously cycling the cell between the cell voltage limits (i.e., 2.5 V to 4.2 V). Experiments were conducted to investigate the impact of cycling under constant current conditions and under constant current constant voltage conditions. The constant current cycling was limited to two c-rates, C/2 and C/4, while constant current constant voltage cycling was only conducted at C/2. These calendar and cyclic conditions limits the study of path dependent degradation to the experimental conditions selected and does not account for other ageing conditions that could impact the difference in the rate of degradation such as regenerative braking power pulses, realistic drive cycles, smaller cycling SoC windows and ageing at temperature extremes. For example, by incorporating regenerative braking, the magnitude and frequency of the power pulses could lead to thermal gradients within the cell which may result in accelerated ageing for those cells experiencing more power peaks. Ageing the cells at temperature extremes would have a similar affect where the degradation could be encouraged which would make it difficult to attribute any difference in the rate of degradation to path dependence. The above mentioned cyclic and calendar ageing conditions were hence selected to ensure that data could be collected that can isolate path dependent degradation trends to the best of our ability.

1.6 Outline of Thesis

The literature review, gap analysis and motivation has been covered above in this first chapter. Below is an overview of the following 5 chapters that describes the research conducted and the objectives addressed in each chapter.

Chapter 2 provides information on the cell specifications for the NCA lithium-ion cells used and the equipment used to conduct the experiments. The design of reference performance tests in order to collect the data required for objective 1 and the application of degradation data analysis techniques are discussed. This chapter also covers the construction, testing procedures and data collection of half-cell.

Chapter 3 covers the first experimental campaign, to address objectives 2 and 4, that presents the data and analysis conducted on groups 1,2,3 and 4. The campaign is designed to gain insight into the influence of path dependence by exposing cells to combined load profiles at two C-rates and calendar ageing at 90% SoC. The design of the combined load profiles (objective 1) and cyclic/calendar ageing conditions are discussed. The capacity, resistance, temperature and electrochemical impedance spectroscopy data obtained for the experiments are shown along with the incremental capacity analysis (ICA) and differential voltage analysis (DVA) that were used to gain insight into the degradation trends (objective 5). The capacity and resistance datasets are normalised to allow for a clear comparison of the rate of degradation between the groups. The capacity fade and power fade data are also shown against time and full equivalent cycles to help understand the impact that calendar/cyclic ageing has on the rate of degradation. A discussion of the post-mortem study to inspect the electrodes at the end of the experimental campaign is presented.

Chapter 4 explores the impact that CCCV cycling and calendar ageing at 2 SoC conditions can have on path dependence in response to objectives 3 and 4. A second set of combined load profiles are presented along with the degradation data presented in a similar fashion to the data in chapter 3 collected from groups 7,8,9 and 10. In order to gain insights into the difference in the rate of degradation caused by path dependence as outlined in objective 5, DVA and ICA techniques are used to study the degradation modes. A comparison of the results obtained from the first and second experimental campaigns is presented.

Chapter 5 addresses objective 6 by comparing the difference in cell lifetime between the data collected from cells exposed to combined profiles (chapters 3 and 4) and the lifetime predictions obtained with an empirical model under the cumulative assumption. The cumulative model uses additional cyclic data (group 5) and calendar ageing (group 6) which was collected in order to ensure the cyclic/calendar degradation data used in the model was comparable to the cyclic/calendar conditions used in the combined profiles. The comparisons are split into three plots with the first comparing the data collected in groups 1 and 3 (chapter 3) with the cumulative degradation of groups 5 and 6, the second comparing groups 7 and 8 with the cumulative models and the third compares groups 9 and 10 with the cumulative model created using cyclic/calendar ageing data obtained from other studies.

Chapter 6 presents the conclusions drawn from the study, the contributions made and the future work that could be undertaken to build on the research conducted in this thesis.

Appendix A includes the scripts designed to conduct reference performance tests and the combined load profiles.

Appendix B shares some additional unnormalized capacity and resistance degradation data.

Chapter 2

Experimental Setup, Characterisation Data Collection and Analysis Techniques

This chapter describes the experimental setup including the cell selection and the equipment used to conduct the experiments. The procedures used for cell degradation data collection and the reasoning behind the selection of each technique are discussed. The design of the combined load profiles that are specific to each experimental campaign is presented in section 3.2 and section 4.2. The experimental setup and cells used were kept as similar as possible across both experimental campaigns to ensure comparability between the results.

2.1 Experimental Setup

2.1.1 Cell Selection and Cell Specifications

The cells selected to study are commercially available Panasonic NCR18650BD cells. These cells were selected as they have a nickel cobalt aluminium oxide cathode and a graphite anode, which is the same cell chemistry and format as used in many current electric vehicles on the road, including the Tesla Model S, Model X and Model 3 [13, 61]. Therefore, studying

these cells is practically relevant. The cell specifications obtained from the datasheet provided from the manufacturer are presented in table 2.1. All the cells selected for the study were from the same production batch, and all were stored under the same controlled conditions before testing commenced.

The cells were received in two batches, at two different times (2017 and 2018), and therefore experienced different periods of calendar ageing. Before testing, they were stored at 12 °C and 30% SOC to minimise degradation. The cells for the first campaign were selected from the 20 cells in the 2017 batch and the cells for the second campaign were selected from the second batch of 27 cells received in 2018. In beginning of life tests, the first batch of cells exhibited slightly lower capacities and greater cell-to-cell variability compared to the second batch. The first batch had a mean capacity of 3.02 Ah with standard deviation of 0.04 Ah. The second batch of cells had a mean of 3.11 Ah and a standard deviation of 0.01 Ah. Fig. 2.3 shows a capacity histogram for both batches of cells along with the mean batch capacity indicated by the dashed lines. Baumhöfer et al. [62] studied the influence that variations introduced during manufacturing can have on cell lifetime and found that cells from the same batch can still have significant cell-to-cell variations that influence their rate of degradation. However, there is not necessarily an obvious relationship between the beginning of life performance and the end of life performance [62].

To gain an indication into the cell-to-cell variability and improve statistical confidence whilst also making best use of the available battery tester channels, 3 cells were tested at each test condition. For the first experimental campaign, groups of 3 cells each having similar beginning of life capacities were selected for each testing condition in order to minimise the influence of cell-to-cell variability on the degradation data, as shown in Fig. 2.1. Due to this clustering of similar capacities within each test group, some groups had a lower average initial capacity compared to others. The average initial capacity for group 1 was 3.07 Ah, group 2 had 2.97 Ah, group 3 had 3.04 Ah, group 4 had 3.06 Ah and group 5

had 3.00 Ah. This grouping means that the cells in group 1 has the highest overall BoL capacity as compared to all other groups in the first batch of cells and group 2 had the lowest average initial capacity. In the first experimental campaign presented in chapter 3, the data from groups 1 and 3 are compared which had a difference of 0.03 Ah in the average BoL capacity. The datasets collected for groups 2 and 4 are compared in the study which has a more significant average difference of 0.06 Ah at the BoL. The average initial capacity for all groups of cells tested is presented in table. 2.2.

As an alternative for comparison, when selecting cells for the second experimental campaign, the groups were instead made up of three cells each with overlapping capacities across test groups, i.e. with one cell in each group with a capacity that ranged between 3.124 Ah to 3.128 Ah, one in the range 3.11 Ah to 3.127 Ah, and one in the range 3.1159 Ah to 3.11 Ah respectively as shown in Fig. 2.2 . This provided some qualitative insight into the influence of the initial cell selection criteria on degradation trends and ensures the groups have a similar average capacity at the BoL.

Table 2.1 Battery specifications for Li-ion cells used in the experimental campaign.

Manufacturer	Panasonic
Model Name	NCR18650BD
Cathode	$LiNiCoAlO_2$
Anode	Carbon
Rated Capacity	3 Ah
Maximum Voltage	4.2 V
Minimum Voltage	2.5 V
Maximum Charge Current	1.5 A
Maximum Continuous Discharging Current	10 A

2.1.2 Half Cell Fabrication and Data Collection

Half cells fabricated from harvested electrode material can provide valuable insight into the changes in cathode and anode characteristics as a battery ages. In order to understand

Table 2.2 Average initial capacity for cells in groups 1 - 10

Group	Average Initial Capacity [Ah]
1	3.07
2	2.97
3	3.04
4	3.06
5	3.00
6	3.03
7	3.12
8	3.12
9	3.12
10	3.12

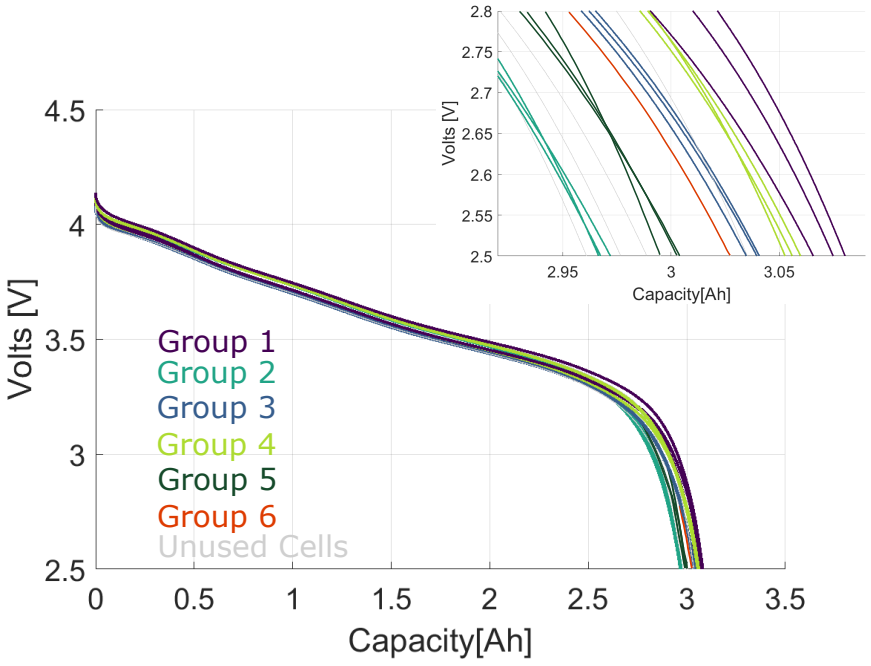

Fig. 2.1 Cell selection for experimental campaign 1

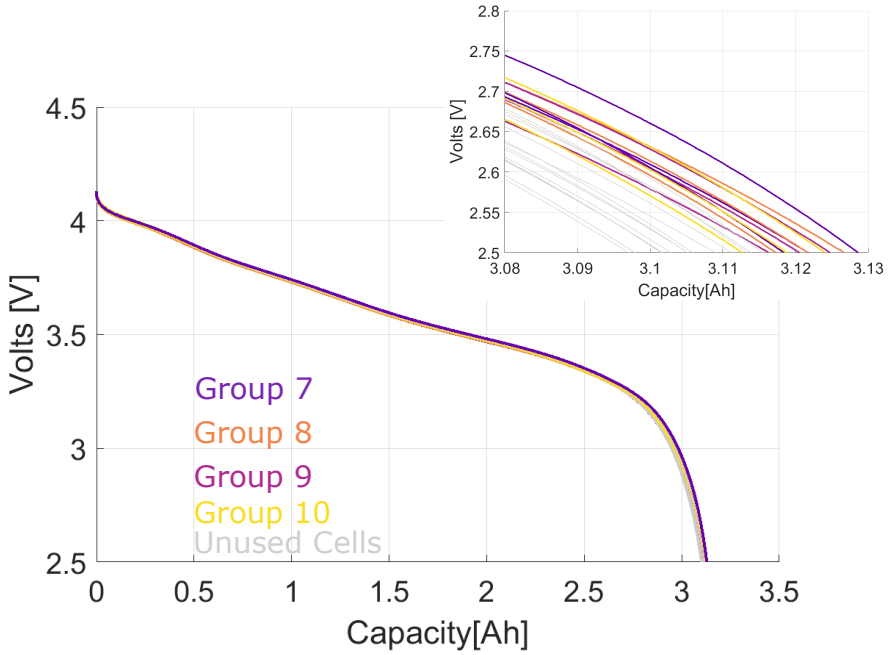

Fig. 2.2 Cell selection for experimental campaign 2

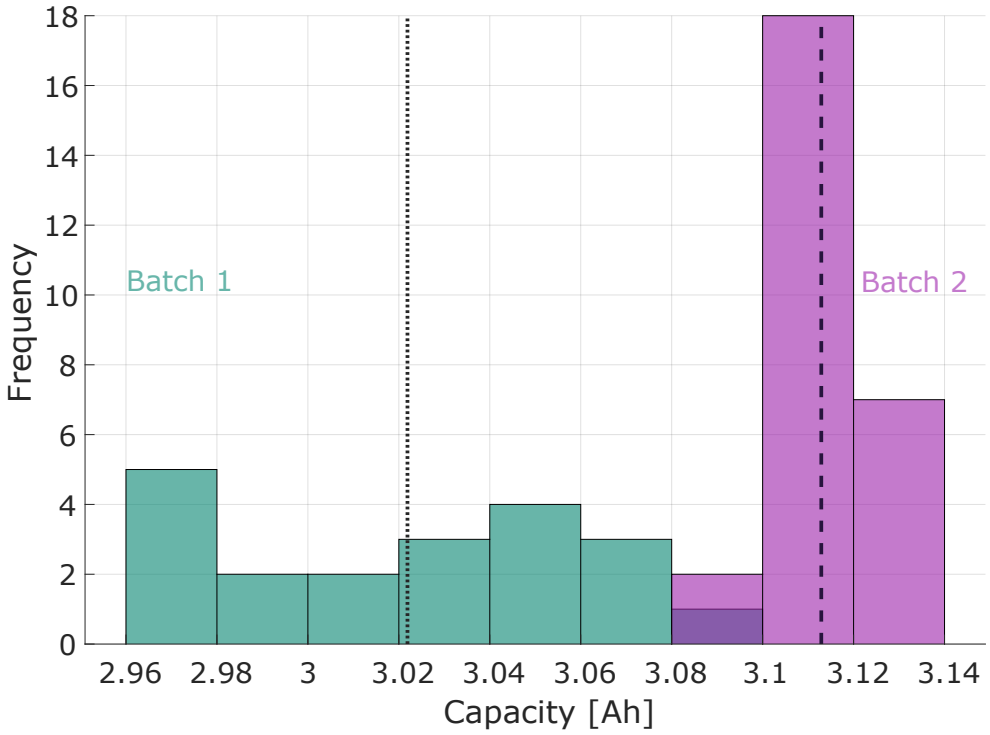

Fig. 2.3 Histogram of cell capacities for batch 1 and batch 2 with the mean capacity of each batch indicated by the black dashed lines

the influence of path dependent degradation on each electrode individually, CR2032 sized half cells were fabricated from pristine electrodes from the 18650 cells. The half cells were constructed in an argon filled glove box using the electrode material harvested from a fresh 18650 NCA cell. The construction of the half cells was performed as described in method 2 outlined by Schmid et al. [63]. In order to prepare the electrode material for half cell construction, the cell can was first cut with a pipe cutter, then the jelly roll was removed and unravelled carefully. The electrodes in commercial 18650 cells are generally coated on both sides of each current collector, however for half cell construction, an electrode with a single coating layer is required. To clean the active material from the current collectors, sections of the electrode were cut and secured to a glass block. A Kimwipe soaked in N-methyl-2-pyrrolidone (NMP) was used to remove the active material from one side of the cathode sample, and correspondingly a dimethyl carbonate (DMC) soaked kimwipe was used to remove anode material from one side of an anode sample.

Electrodes with a diameter of 12mm (1.13 cm^2) were punched from the 726 cm^2 of extracted electrode material using an MSK-T-10 Precision Disc Cutter. Half cells size CR2032 were constructed consisting of a lithium foil of 14 mm diameter as the counter electrode, Celgard 2400 separator material, the punched electrode material, and LP30 electrolyte (1.0 M LiPF6 solution in ethylene carbonate (EC) and dimethyl carbonate (DMC); EC/DMC=50/50). The electrode extraction and half cell construction is shown in Fig. 2.4.

Pseudo OCV (OCV) tests were conducted on the half cells at a C-rate of C/24 to ensure the comparability of the half cell data with the full cell POCV data collected during RPTs. In order to scale down the current to achieve C/24 with the coin cell, the current density of the original 18650 cell had to be determined. The pristine 18650 cell that was used to create the half cells had a capacity of 3.163 Ah and an electrode area of 726 cm^2, resulting in capacity density of 4.36 mAh /cm^2. This results in the half cell at C/24 having a capacity of 4.93 mAh. From this it was determined that a CR2032 cell with an electrode area of 1.13 cm^2 would

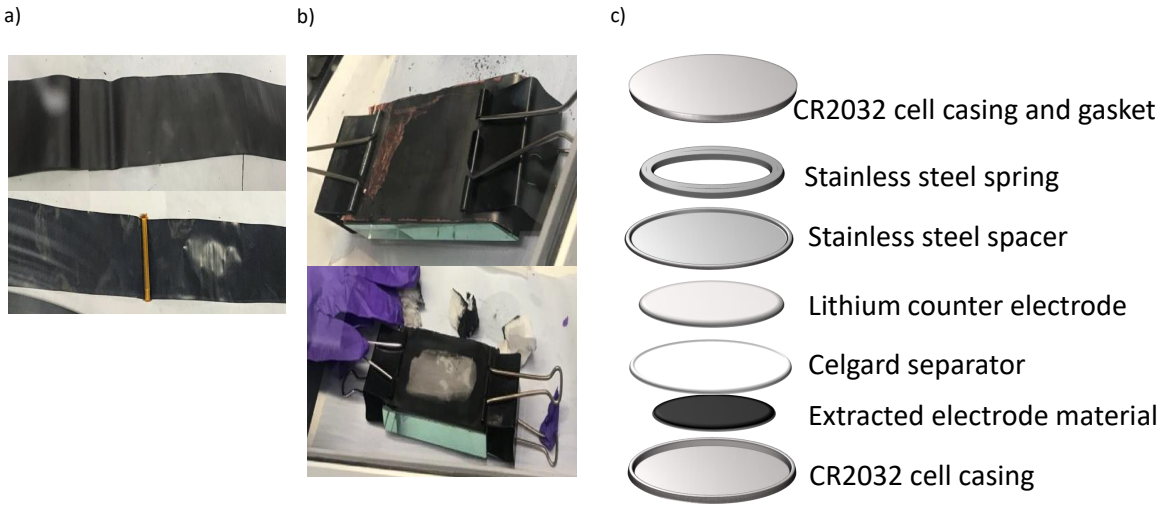

Fig. 2.4 Progression of half cell construction (a) extracted anode and cathode material, (b) electrode cleaning (c) half cell construction with extracted electrode material

need to be dis/charged at 0.19 mA to achieve a C-rate of C/24. The cathode half-cell was tested between 2.49 V vs. Li/Li+ and 4.29 V vs. Li/Li+, while the OCV test on the anode was conducted between 0.04 V vs. Li/Li+ and 1.25 V vs. Li/Li+. A total of 14 half cells were constructed and tested in this study. Data from two sets of anode and cathode half cells were used to confirm the alignment of the half cell OCV curves with the full cell OCV curve.

2.1.3 Experimental Equipment

The cycling tests and reference performance tests were conducted using a Maccor 4200 battery tester and a Maccor 4000 battery tester. The Maccor 4200 provides 16 channels each with range 0-10 V and -10 to +10 A and was used to run the experiments for experimental campaign 1 outlined in chapter 3. Experimental campaign 2 was conducted using the Maccor 4000 system, which can provide 0-5 V and -5 to +5 A. Due to the lower current specifications of the 4000 system, the pulse test during the reference performance tests was altered for

campaign 2 as discussed in chapter 4 . Electrochemical impedance spectroscopy (EIS) data was collected using an 8 channel BioLogic MPG205 tester, which can provide 0-9 V and -5 to +5 A .

All experiments were conducted using 4-terminal cell holders, which consist of a counter electrode connection, a working electrode connection and two voltage sense connections. The counter electrode and working electrode provide the main path for current to flow through the cell. The two sense connections are used for accurate measurement of the cell voltage. Four terminal testing is required for accurate low impedance measurements for batteries—a 2-terminal connection could lead to difficulties in differentiating the impedance of the cables versus the cell, leading to inaccurate impedance data. The additional sense connections for voltage ensure that the voltage measurement is the cell voltage only, and the voltage drop in the working or counter electrode wires is excluded [64]. The cell holder used is pictured in Fig. 2.5 and has 4 spring loaded pogo pins to ensure that consistent torque was applied on all cells. The pins are brass to ensure minimal contact resistance. The cell holder was connected to the battery tester using 4 mm and 2 mm banana plugs to ensure a consistent and robust connection across all cells.

Throughout characterisation and testing, the cells were kept at a constant temperature of 24°C using a Binder MK53 and a Maccor MTC-010 thermal chamber. The temperature of the thermal chambers was set to 24°C to limit degradation mechanisms that are encouraged by extreme temperatures and to isolate the degradation effects caused by path dependency. The surface temperature of each cell was monitored using a T-type thermocouple secured with kapton tape and positioned 4 cm from the positive terminal for all cells to ensure there was no influence of temperature variations due to sensor positioning. The study conducted by Taylor et al. [65] suggests that conducting the same experiment in different thermal chambers set to the same nominal temperature setpoint can still lead to variations of around 1.1% in the

Fig. 2.5 Four terminal spring loaded cell holder

test results. In order to mitigate this error and ensure comparability of the data collected, the groups of cells that were being directly compared were tested in the same thermal chamber.

2.2 Characterisation Data Collection and Analysis Techniques

Reference performance tests (RPTs) , sometimes called 'check-up tests', are a collection of cell characterisation diagnostic tests conducted periodically over the lifetime of a cell in order to track their change in performance and quantify degradation. The RPTs must be designed to obtain useful data that are comparable across datasets, while exposing the cells to minimal additional degradation. Insight into the cause and progression of cell degradation can be gained by analysing the RPT data. Characterisation data collection and analysis techniques are discussed in this chapter along with a description of the reference performance test used in this study.

2.2.1 Capacity Test

Tracking the changes in capacity as the cell ages can be used to quantify degradation and can help determine state of health. Capacity is the total electrical charge stored in a cell between the cell minimum and maximum voltage limits, and it is determined by the number of active material sites available in each electrode for intercalation. As the cell ages, it experiences a loss in lithium inventory (i.e., available lithium to cycle) which could be due to degradation mechanisms such as SEI formation or lithium plating, or loss of lithiated active material which could be a result of loss of electrical contact, resulting in reduced cell capacity. Understanding capacity fade is crucial for practical applications such as cells in an EV, where capacity fade leads to reduced driving range. There are three commonly used tests for capacity, and these are constant current constant voltage (CCCV) tests, galvanostatic

intermittent titration technique (GITT), and pseudo open circuit voltage (OCV) tests. The data collected from these tests can analysed to gain insight into the degradation modes causing the capacity fade [66]. The characterisation tests and analysis techniques are discussed in the following section.

Constant Current Constant Voltage Test

Constant current constant voltage testing is a frequently used characterisation procedure to obtain a quick approximation of a cell's capacity. The capacity is determined by charging or discharging the cell fully, and then conducting a full CCCV discharge or charge respectively until the minimum or maximum voltage limit is reached. Coulomb counting is used to calculate the capacity in Ampere-hours by integrating the current. Using a constant current stage alone to obtain a capacity estimate is not reliable unless the C-rate is very low. After conducting a constant current charge or discharge to a voltage limit and relaxing the cell, the cell voltage can recover because the concentration gradients in the cell equilibrate. This effect is more evident with higher C-rates due to the more extreme concentration gradients. To ensure the cell is fully dis/charged in order to estimate the capacity, either a low C-rate constant current can be used, or in the case of a higher C-rate constant current dis/charge, a constant voltage step can be incorporated after the constant current step. Incorporating the constant voltage step means that once the cell has reached the maximum cut off voltage limit, the cell is held at a constant voltage until the current drops below a predetermined cut off current, which is usually less than 0.05C [67]. This ensures that the lithium distribution within the electrode is homogeneous and that the concentration gradients have relaxed.

CCCV tests have the benefit of being able to provide a quick initial estimation of the capacity. However, the measured capacity is highly dependent on the operational conditions the cell is tested at, such as the C-rate, which must be selected carefully. Conducting the test with a high C-rate will lead to a decreased capacity measurement in a CCCV discharge

test. This caused by the increased overpotential at lower SoC resulting in reaching the terminal voltage limit before the full capacity of the cell is realised. Since batteries exhibit an Arrhenius dependence on temperature, the temperature at which the CCCV test is conducted can also impact the capacity measurements. Conducting a test at higher temperatures would lead to improved ion mobility and solid state diffusion which would cause reduced internal resistance resulting in a greater measured capacity [68]. Conversely, conducting the CCCV test at a significantly lower temperature would lead to a lower capacity measurement due to the increased electrolyte viscosity and reduced ion transport properties [69] [70] .

To ensure the CCCV test used in this study provide a consistent and accurate estimation of the cell capacity, the test design accounts for the various stress factors that can impact the data. The CCCV test was conducted using a C/2 dis/charge current to ensure the cell was not cycled at a high C-rate and the constant voltage step was held until the current was below C/60. The thermal influences were accounted for by allowing the cell to fully relax before conducting the CCCV. This ensures that there are limited thermal gradients within the cell which could result from continuous cycling and the external temperature is controlled by conducting the CCCV tests in a thermal chamber under 25°C.

Galvanostatic Intermittent Titration Technique

Galvanostatic intermittent titration technique is conducted by dis/charging the cell in small SoC steps, with prolonged relaxation time between each change in SoC. Alternatively, potentiostatic intermittent titration technique can be applied which employs voltage-controlled steps rather than current dis/charge steps. For battery applications it is more common to see GITT because with this it is easier to set voltage limits and control the current and ensure the cell being tested is within safe operating limits. This technique is one of the most accurate methods of estimating the capacity due to the limited contribution from kinetic effects, plus the near thermal equilibrium, however it requires extended testing time. The OCV curve

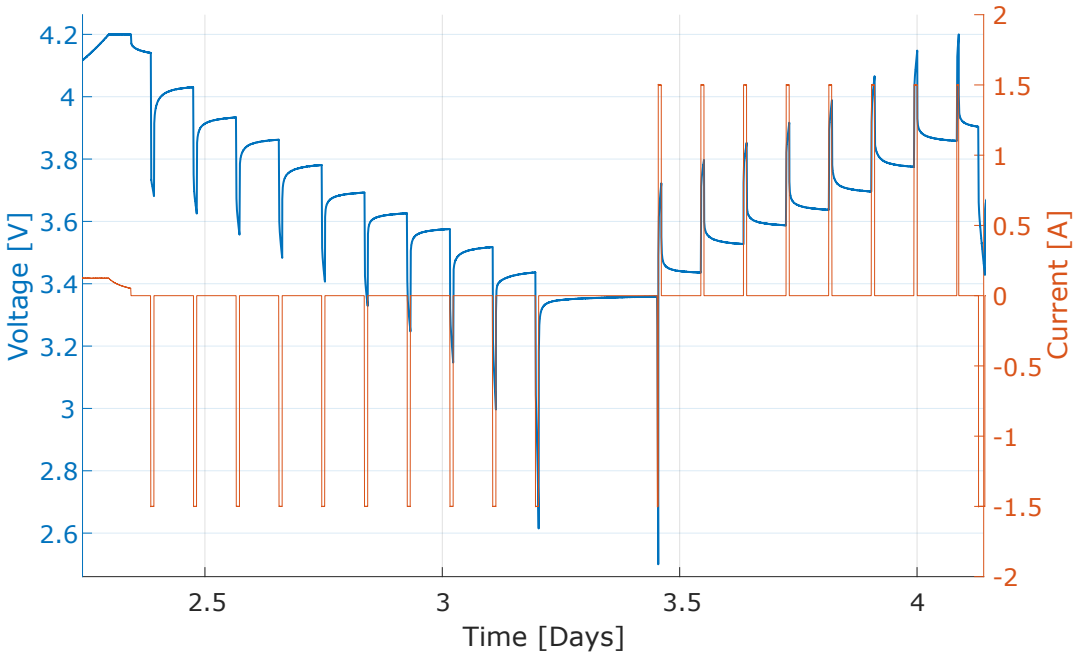

Fig. 2.6 Galvanostatic intermittent titration technique in steps of 10% SoC

can be constructed at each SoC step by measuring the potential at the end of each relaxation period. To ensure the cell voltage is not changing due to concentration gradients equilibrating, the relaxation period must be selected carefully. Depending on the cell chemistry, the optimum relaxation duration will vary. As discussed by Barai et al., GITT can be conducted by discharging the cell in steps of 10% SoC with a relaxation period of at least 1 hour. A 1 hour relaxation periods between discharge pulses is suggested to be acceptable for LFP batteries however in order to ensure electrochemical equilibrium is attained, most other chemistries may require a longer relaxation to ensure the voltage after relaxation is as close to the theoretical capacity as possible [66]. An example of the GITT data collected is shown in Fig. 2.6. The data collected using GITT can also be used to gain insights into the charge transfer resistance and solid state diffusion of lithium [71].

Pseudo Open Circuit Voltage Test

Open circuit voltage is the difference in potential between the positive and negative electrodes after an extended relaxation period when no external current is flowing. Due to overpotentials caused by transport, ohmic/ionic resistance, and kinetic effects during charging or discharging, it is difficult to attain true equilibrium of the electrode potentials. As mentioned in the constant current constant voltage section, this can be addressed by either incorporating a constant voltage step or by conducting a constant current dis/charge at a very low C-rate. This latter approach, called a pseudo OCV test, reduces the kinetic influences, lowers the electrode polarisation and limits the ohmic heat generation. The Butler-Volmer equation governing kinetics shows how a higher C-rate leads to greater overpotentials at lower SoCs, causing the cell to reach the lower voltage limit before the entire stored capacity can be extracted. To ensure an accurate estimation of cell capacity, it is common practice to use a C-rate of C/20 or lower for a pseudo-OCV test. This results in longer testing time compared to CCCV tests, however more accurate capacity data can be collected [66]. In our study a C/24 dis/charge C-rate was used to ensure that an accurate estimation of capacity is obtained and to ensure that the pseudo OCV data collected can be used for the analysis techniques discussed below.

Tracking Degradation by Analysing Open Circuit Voltage Data

Incremental capacity analysis (ICA) and differential voltage analysis (DVA) are non-invasive techniques that give useful insights into battery degradation by analysing open circuit voltage data. Incremental capacity analysis examines the changes in the derivative of charge with respect to OCV, as a function of OCV, as the cell ages. This allows changes in electrode-specific thermodynamics to be investigated. Differential voltage analysis provides similar insights to ICA from a different perspective by studying the derivative of OCV with respect to charge, but as a function of charge (or SOC). Using ICA and DVA derived from OCV data collected at low C-rates, three degradation modes can be identified: loss of lithium

inventory (LLI)—in other words loss of cyclable lithium—, loss of active material at the positive electrode (LAM_{pe}) and loss of active material at the negative electrode (LAM_{ne}) [72],[52] , [73]. The LAM can occur due to the loss of lithiated material at the anode/cathode or the loss of delithiated material at the electrodes.

The relationship between the half cell open circuit voltage curves, the LLI/LAM degradation modes and the resulting changes in the full cell OCV curve is presented in Fig. 2.7. Fig. 2.7 (a) presents the BoL OCV data collected from a fresh full cell and the half cells constructed in section 2.1.2. Ageing of the anode or cathode leads to the shifting and compression of the half cell OCV curves resulting in a modified active operating window. The solid lines in Fig. 2.7 (b)-(f) represent the fresh OCV data in Fig. 2.7 (a). Following the degradation mode simulations and studies conducted by Dubarry et al. and Birkl et al., the dashed lines are modified versions of the fresh OCV curves to provide a schematic representation of the changes in the anode/cathode OCV curves and subsequent degradation seen in the full OCV curve [1, 74].

In terms of half cell voltage curves, LLI shifts the negative electrode towards higher SoCs, causing the cell active window to decrease. The capacity lost due to LLI can therefore often be referred to as the electrode balancing capacity. The shift of the anode and the change in full cell OCV due to LLI is depicted in Fig. 2.7 (b) . LAM_{ne} or LAM_{pe} results from the negative or positive OCV being compressed with respect to capacity, with either the lower or upper SoC being maintained depending on whether the active material lost is lithiated or delithiated. This also leads to a smaller active window of operation, and hence a lower capacity of the cell. The loss of active material at the electrodes means the charge accepting material and the active surface area is decreased which increases the current density and impacts the charge transfer[74]. The loss of de/lithiated cathode or anode material and the subsequent changes to the full cell OCV is shown in Fig. 2.7 (c),(d),(e) and (f). Both ICA and DVA have their own unique advantages and can provide insight into the changes in the

half cell voltage curves and can be coupled with other analysis techniques to a gain greater understanding of degradation trends.

The staging of graphite in the negative electrode and the phase transitions of lithium metal oxide materials in the positive electrode can be identified using DVA from the plateaus in the OCV curve [56], [74]. Since DVA is plotted against capacity or SoC, i.e., dV/dQ against Q , changes in the DVA signature are an indication of changes in the cell capacity. By tracking the peak height and peak location in the DVA signatures of a cell, the degradation modes (LAM_{ne},LAM_{pe} and LLI) can be identified. The shift and changes in the peaks can be attributed to a loss of active material, while high SoC peaks shifting to lower SoC can indicate a growing imbalance between the two electrodes in the form of loss of lithium inventory [74]. DVA is advantageous as the changes in the signatures caused by degradation is studied with respect to capacity.

By conducting DVA on the half-cell pseudo OCV data, the influence of each electrode on the full cell DVA can be determined. The peaks in the full cell DVA signature corresponds to peaks in the half cell DVA signatures, allowing the identification of the influence of each electrode on the full cell [4], [75]. Attributing each peak in the full cell DVA signatures to an electrode, the influence of degradation on the cathode and anode can be monitored. A pseudo OCV test run at C/24 was conducted on each half cells described in section 2.1.2. The analysis of the OCV curves shown in Fig. 3.10 indicates that peaks P1 and P2 of the full cell DVA can be attributed to the anode, while the cathode governs the higher SoC voltages attributed to P3 and P4 in the full cell DVA.

Studying the DVA signatures also allows quantification of capacity loss attributed to each electrode and provides insight into the electrode balancing of the cell [76]. Keil et al. [76] suggest that there are three characteristic capacities that can be tracked as an NCA cell ages in order to determine the influence of LAM_{ne}, LAM_{pe} and electrode balancing. LAM_{ne} can be identified as the change in capacity between 0% SoC and P2, since all the features of

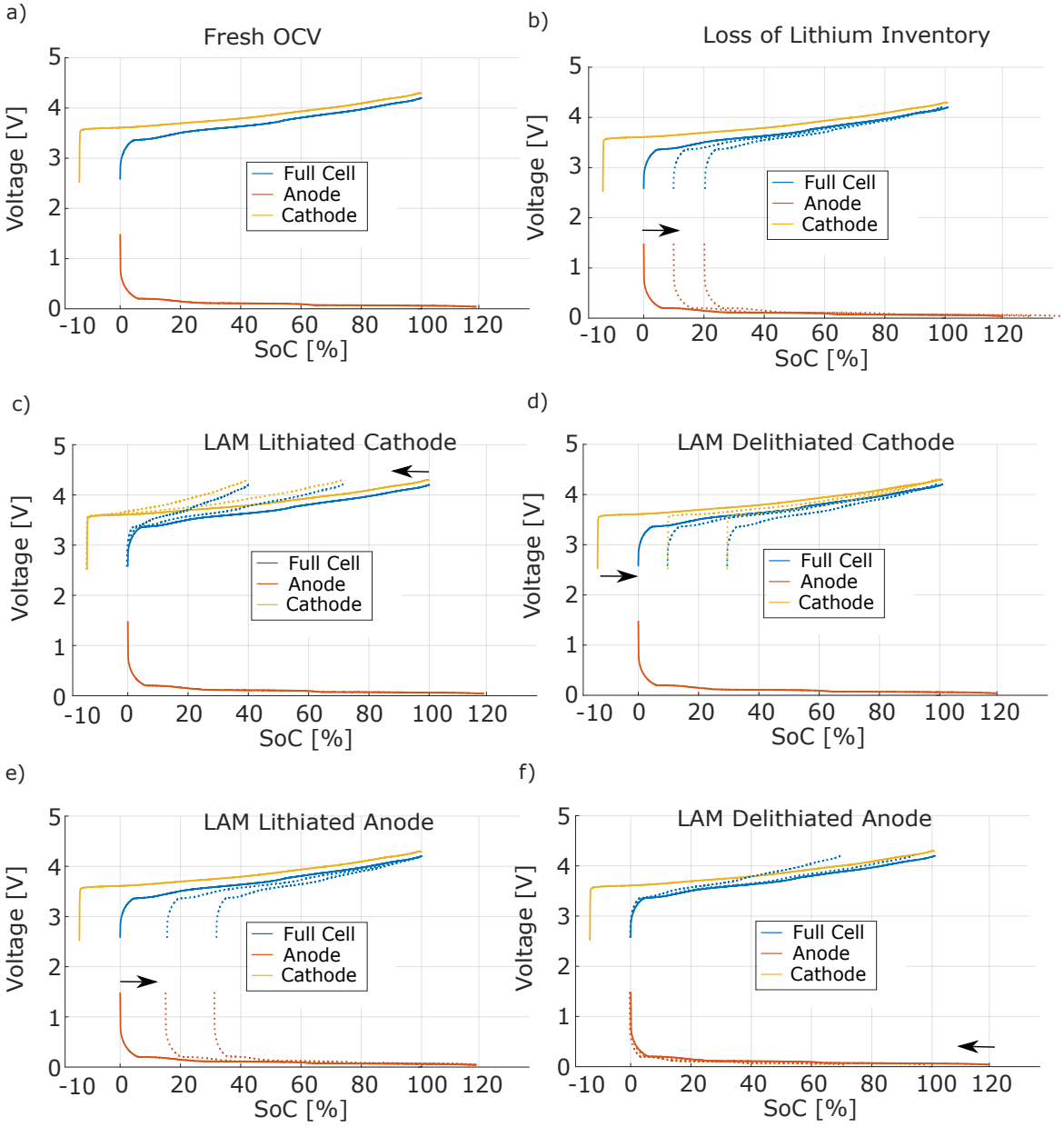

Fig. 2.7 The changes in half cell OCV curves caused by the influence of LLI and LAM and the resulting change in full cell OCV. Solid lines represent the OCV data collected from a fresh full cell and constructed half cells. The dashed lines are schematic representation of degraded OCV curves.

interest within this range are anode specific. Similarly, LAM_{pe} can be determined by the change in capacity between P3 and 100% SoC. Changes in the electrode balancing and loss of lithium inventory can be found by studying the capacity changes between P2 and 100% SoC. The capacity change in LAM_{ne},LAM_{pe} and the balancing as the cell ages can be tracked through Q_{NE}, Q_{PE} and Q_{BAL} as shown in Fig. 2.8

Incremental capacity analysis is the reciprocal of DVA and hence provides similar information. The degradation of a cell can be tracked by monitoring the changes in the ICA signature shape, with the change in peak height indicating loss of active material and a shift in peak location showing loss of lithium inventory. A crucial difference between the two analysis techniques is that ICA is referred to cell voltage, i.e., dQ/dV against V, which is an intrinsic property of a cell, while DVA is referred to capacity, which is a secondary, accumulative property which varies as the cell ages. Hence, ICA has the benefit of retaining a consistent reference against voltage as the cell ages.

Using modelling tools like the 'Alawa toolbox developed by Dubarry et al. [77], half-cell data can be used to simulate the impact of LLI and $LAM_{pe/ne}$ on the ICA/DVA signatures and open circuit voltage. The peak shifting and shrinking in an ICA/DVA signature obtained from the simulations for each degradation mode can be compared to those of the measured experimental degradation data to identify the degradation modes and degradation trends that are taking place as the cell ages [78].

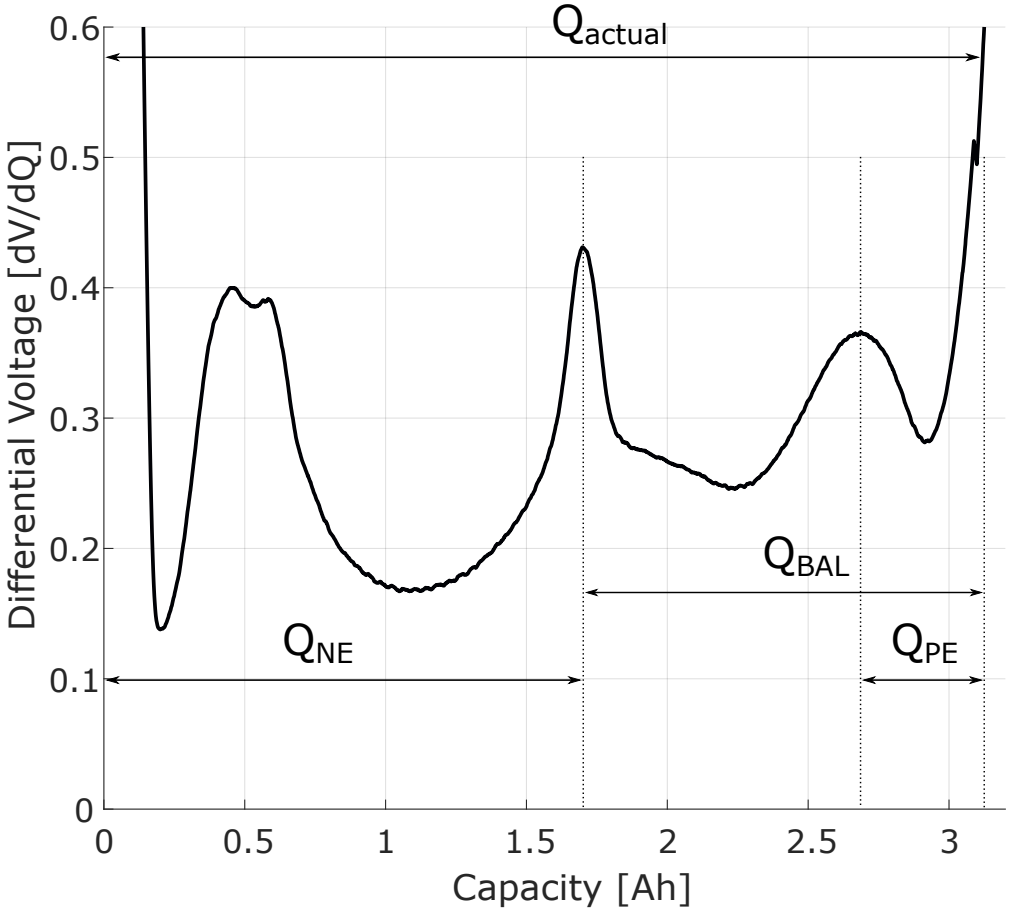

Fig. 2.8 Quantifying the capacity changes at the anode, cathode and cell balancing using DVA signatures

2.2.2 Resistance and Impedance Data Analysis

The power fade a cell experiences as it ages can be studied by collecting resistance and impedance data. The resistance can be estimated from the voltage drop when the cell is exposed to a sudden change in load current. The resistance data of a cell can be studied in the time domain using the pulse power characterisation (PPC) test, while the impedance in the frequency domain can be estimated using electrochemical impedance spectroscopy (EIS) , where cells are exposed to sinusoidal excitation. Using a PPC test can provide an estimation of resistance, however this resistance is a combination of ohmic resistance, charge

transfer resistance and polarisation resistance. The duration of pulse, the state of charge at which the pulse is applied and temperature under which the data is collected must be controlled carefully in order to ensure comparable resistance data is collected as the cells age. Electrochemical impedance spectroscopy can provide more specific information on the dynamic behaviour of the cell and can therefore isolate the different resistive influences.

Pulse Power Characterisation Test

Tracking the increase in cell resistance in the time domain can be done using a PPC test. Power pulse characterisation involves exposing a cell to a step change current pulse and measuring the voltage response of the cell. PPC allows the tracking of electrochemical influences such as charge transfer and diffusion that have higher time constraints. Due to the limited sampling frequency of most battery testers, PPC is not suitable to track changes in high frequency (i.e., pure ohmic) resistance. Selecting the duration of the current pulse is a crucial element of the PPC test. A longer duration between samples may yield an apparently greater resistance due to the change in surface concentration of lithium on the active mass leading to solid state diffusion. Most ageing studies use a current pulse I_{pulse} of 10 s duration, which is used in this study, along with the change in voltage over the 10 s pulse duration, to find the R_{DC} [79–81]. A schematic of the I_{pulse} and associated voltage response used to calculate R_{DC} is shown in Fig. 2.9.

$$R_{\mathrm{DC}} = \frac{V_{10s} - V_{0s}}{I_{pulse}} \tag{2.1}$$

The PPC test is sensitive to cell temperature and SoC, so the C-rate for the current pulse must be selected carefully to ensure the resistance data is consistent and that there is minimal to no drift in the cell SoC and temperature conditions [82]. Using a higher C-rate leads to changes in the average stoichiometry which in turn leads to changes in the cell OCV. Once the OCV changes, it is not possible to attribute the resistance calculated with a PPC test

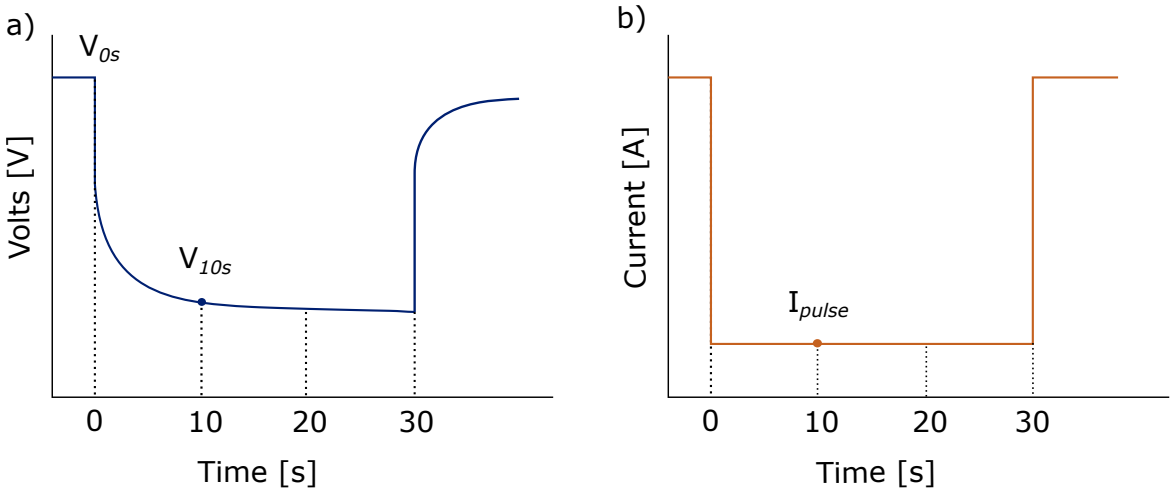

Fig. 2.9 (a)Voltage and (b) current response for power pulse characterisation

to a specific SoC. Cells at lower SoCs will have a greater resistance due to the decreased exchange current density. Conducting a charge current pulse on cells at higher SoC extremes will also lead to higher resistance.

Electrochemical Impedance Spectroscopy

Electrochemical impedance spectroscopy is a non-invasive technique used to gain insight into the dynamic characteristics of a lithium-ion cell in the frequency domain. Electrochemical impedance spectroscopy can be conducted galvanostatically, with a current excitation, or potentiostatically with a voltage excitation. Galvanostatic EIS is conducted by applying a small sinusoidal excitation current and measuring the induced voltage response. This is done at a range of different frequencies. Using galvanostatic EIS with an equal positive and negative current per period ensures the cell does not experience an overall average SoC drift. To obtain the EIS spectrum, batteries are tested at frequencies ranging from kilohertz to millihertz. For a sinusoidal current $i(t)$ with an amplitude of $\hat{I}$ and voltage $v(t)$ with an amplitude of $\hat{V}$, for a frequency f, the complex impedance $Z(f)$ computes as shown below. In these equations, $|\, Z(f)\,|$ provides the information about the amplitude ratio and ϕ about

the phase shift [83, 84].

$$i(t) = Re(\hat{I} \cdot e^{j(\omega t + \phi_i)}) \tag{2.2}$$

$$v(t) = Re(\hat{V} \cdot e^{j(\omega t + \phi_v)}) \tag{2.3}$$

$$Z(f) = \frac{V(f)}{I(f)} = \frac{\hat{V} \cdot e^{j(2\pi f t + \phi_v)}}{\hat{I} \cdot e^{j(2\pi f t + \phi_i)}} = \mid Z(f) \mid \cdot e^{j\phi} with \mid Z(f) \mid = \frac{\hat{V}}{\hat{I}} and \phi = \phi_v - \phi_i \tag{2.4}$$

Tracking Degradation with Electrochemical Impedance Spectroscopy

Electrochemical impedance spectroscopy spectra are usually shown on a Nyquist plot where the negative imaginary part of the impedance is plotted along the y-axis against the real part of the impedance across the x-axis. To interpret the spectrum, it can be divided into characteristic regions as shown in Fig. 2.10 which also shows the approximate frequencies at which the changes between regions takes place for a representative cell tested at the BoL.

The high frequency segment of the EIS spectrum when the imaginary part of the spectrum is positive represents the inductive behaviour of the cell. Physical properties such as the format of the electrodes and the position of the tabs impacts the cells' inductance. The arrangement of cables during the measurement can also impact this. The cylindrical format cell used here with spiral jelly roll electrodes leads to higher self-inductance compared to a pouch or coin cell with planar stacked electrodes. The inductance can also increase if the distance between the current collector and the tabs is increased.

The ohmic properties of the cell can be tracked by monitoring the intercept of the spectrum with the real axis. For the NCA cells used in this study, the ohmic resistance point occurs at close to 1 kHz excitation frequency. Due to the compensation of the inductive and capacitive phase shift at the frequency corresponding to that point, the imaginary part of the inductance cancels out and the cell behaves as a pure ohmic resistor. The conductivity

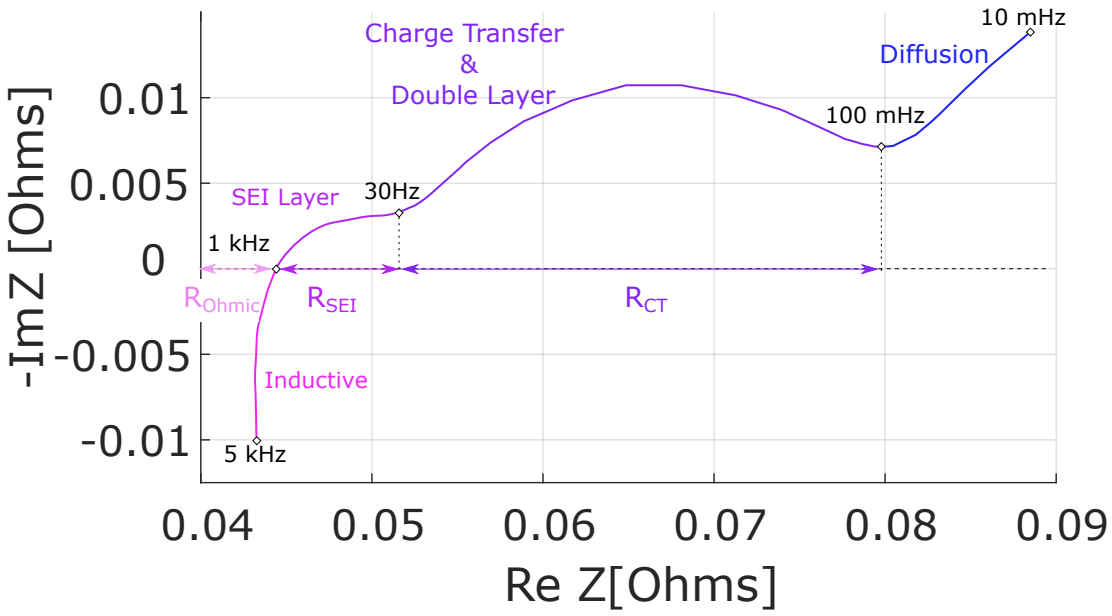

Fig. 2.10 EIS measurement presented in a Nyquist plot with the characteristic regions and frequencies indicated.

of the electrolyte is influenced by the concentration of the salts dissolved in it. This ohmic characteristic of the EIS spectrum can be used to track the electrolyte degradation as the cell ages. Changes in the contact resistance between the current collector and the active mass can also be studied using the ohmic characteristic point [26].

As frequency decreases, the ohmic characteristic point is commonly followed by two semi-circles that depict the electrochemical processes occurring at the electrode/electrolyte interface. The semicircle at higher frequency is thought to represent the presence of solid electrolyte interface on the negative electrode[84] . The semicircle at lower frequency represents the charge transfer resistance and the interfacial charge and double layer capacitance. Tracking changes in the charge transfer resistance can indicate the loss of active surface area

at the electrode which could be a result of degradation mechanisms such as the formation of electrode cracks leading to loss of electrical contact [85]. The final segment of the EIS spectrum at low frequency is the 'diffusion tail' which represents the solid state lithium ion diffusion through the electrodes .

At the beginning of life, the first (higher frequency) semicircle is small relative to the second and can hence be neglected. As the cell ages, the effect of SEI and particle to particle contact becomes more prominent and the two semi-circles become more distinguishable. Studies suggest that changes in the shape and location of the EIS signature can be used to track the degradation of characteristic resistances i.e., the ohmic resistance R_{Ohmic}, the SEI resistance R_{SEI} and the charge transfer resistance R_{CT}. The ohmic resistance in this study is estimated as the intercept of the EIS signature with the real axis [84]. The diameter of each semicircle or the cord length from the beginning to the end of the minor arc has been used in studies by Schuster et al. and Pastor-Fernandez et al. as a method to compare the change in resistance as the cell ages. In this study the characteristic resistances are tracked using the chord length method, where the distance between the beginning and end point of the SEI and charge transfer semicircles are compared as the cells age as shown in Fig. 2.10 [86, 87]. The changes in the Nyquist plot can also be analysed through equivalent circuit modelling and fitting, with the circuit elements representing the physical and chemical processes within the cell. Most commonly the equivalent circuit model to simulate a lithium-ion battery will consist of inductors, resistors, capacitors, a Warburg impedance, and constant phase elements. Using this model, the changes in the circuit element parameters can be tracked to gain insight into degradation trends [84, 88].

2.3 Reference Performance Tests

To understand the cell ageing in this study, degradation data was collected with periodic reference performance tests (RPT). To ensure the comparability of degradation data gathered

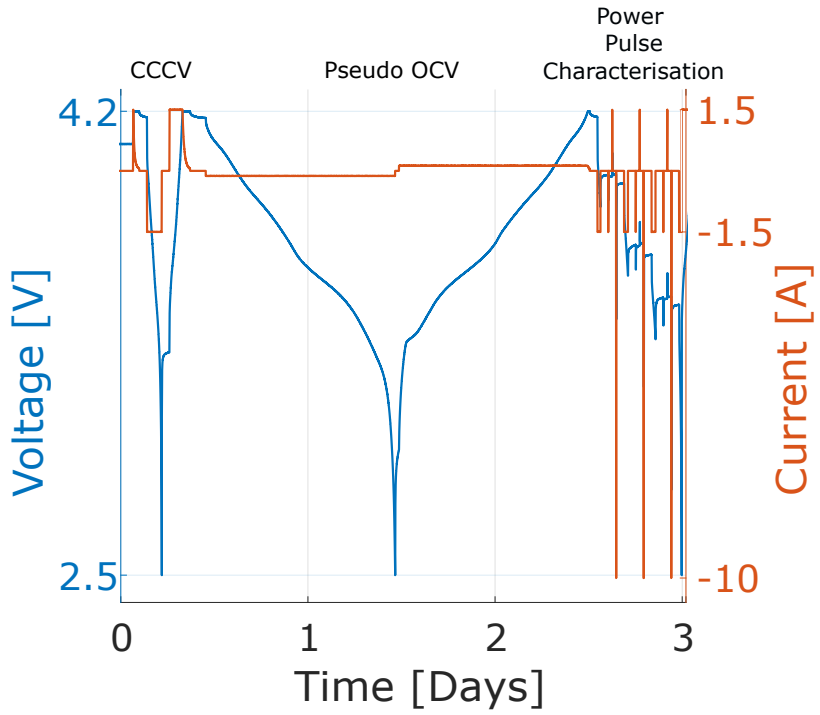

Fig. 2.11 Reference performance test procedure used for data collection

across all test groups, the RPTs were conducted every 48 cycles. Synchronising the RPTs with respect to cycles instead of calendar time ensures that in all cases the cells experience similar charge throughput between RPTs. This however means that the cells cycled at C/4 will take twice as long to complete 48 cycles before the RPT which means they will only experience half the RPTs in the same time period as the groups cycling at C/2. Hence, over the span of the whole test duration, groups 2 and 4 in experimental campaign 1 will experience half the RPTs that groups 1 and 3 experience however since all the groups in experimental campaign 2 are cycled with the same C/2, they will experience similar RPTs within the same duration. The RPTs have been designed to ensure that the cells under test were exposed to minimal additional degradation while gathering consistent data that can be used to study the ageing of the cell.

The RPT procedure used in this study is shown in Fig. 2.11. Each RPT started with a 3-hour relaxation period under open circuit conditions to ensure that cells were at thermal equilibrium. The cell voltage was reset to the maximum voltage limit of 4.2 V with CCCV

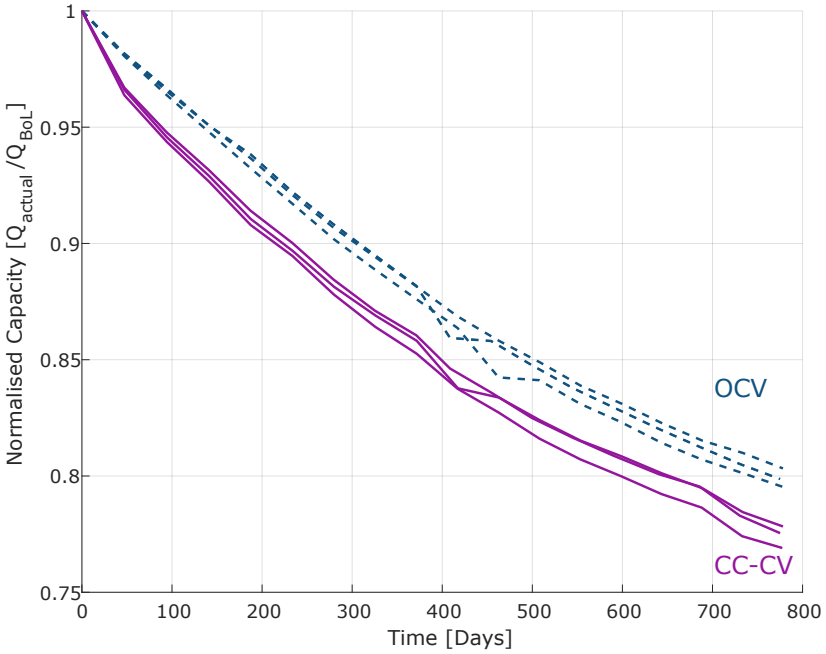

Fig. 2.12 Comparison of capacity fade data collected using a CCCV and pseudo OCV techniques

charging at a C-rate of C/2 in order to start capacity data collection. The capacity under load was estimated using a CCCV test. The discharge capacity was estimated by applying a constant current at a C-rate of C/2 (1.5 A) to the lower voltage limit of 2.5 V. The charge capacity data was collected using a C-rate of C/2 to charge the cell to the upper voltage limit which was held until the current was C/60 (0.05 A). After a 2 hour relaxation period to allow for thermal and electrochemical equilibration, charge and discharge pseudo OCV tests were conducted at C/24. The lower C-rate limits the cell internal overpotentials, ensuring that the capacity data collected is representative of the actual cell capacity. Fig. 2.12 highlights the difference in normalised capacity fade data for the same three cells collected in group 1 under CCCV and pseudo OCV conditions. The discharge OCV capacity data will be used throughout this study unless stated otherwise.

The pseudo OCV phase was followed by a PPC test to study the voltage response of the cell when exposed to current pulses and estimate the DC resistance. The PPC was conducted

at 80%, 50% and 20% SoC with 36-second pulses of C/2 (1.5 A) charge and discharge, and 3.33C (10 A) discharge at each SoC. The first 10 seconds of each current pulse and the voltage drop within the first 10 seconds is used to calculate the DC ohmic resistance using equation 2.1. As the cell ages, the SoC points relate to lower voltages, so setting a voltage condition to conduct the pulse test would result in incomparable resistance data. The SoC must be set as a percentage of the actual measured capacity to ensure the resistance data collected throughout the lifetime of the cell are comparable. The capacity used must be updated to account for the capacity fade due to degradation, hence a function within the test routine was used to reset the SoC at each pulse test. This determined the SoC according to the CCCV capacity data obtained in the first step of the RPT procedure and by determining the number of amp-hours passed between 2.5–4.2 V which was then saved as a variable. This variable was used to determine the length of time needed to discharge 20% or 30% of the prior-cycle capacity. The charge throughput the cell experiences during the pulses must also be accounted for when resetting the SoC. Fig. 2.13 shows the difference in resistance measured for three cells from group 1 using the three different current pulses at three different SoCs. The 1.5 A charge pulse shows a greater resistance as compared to the 1.5 A discharge pulse. The 10 A discharge pulse experiences a significantly lower resistance due to the higher C-rate. The resistance data at 20% SoC is also lower than the data collected at higher SoCs even though the reduced exchange current density would suggest that the resistance would increase at lower SoCs. A SoC lower than 20% was not used due to limitations with the minimum voltage cut off. In this study the resistance data shown will be taken from the 1.5 A discharge pulse at 50% SoC unless stated otherwise. The 10 A power pulse was taken into consideration when discharging to 50% and 20% SoC. The Maccor 4000 battery tester used for experimental campaign 2 has a current limit of 5 A which prohibits the ability to conduct the final 10 A discharge pulse, hence it was omitted from the PPC procedure in the second campaign.

The design of the RPTs ensures that valuable degradation data can be collected while minimising the full equivalent cycles and duration of the procedure as much as possible to limit the degradation caused by the RPTs. The cells would experience a loss of approximately 10 mAh in capacity during the RPTs. The degradation experienced as a result of the RPTs is assumed to have a negligible impact on isolating the extent of path dependence as the datasets being compared in chapter 3 (group 1 vs. 3 or group 2 vs. 4) and chapter 4 (group 7 vs. 8 or group 9 vs. 10) will have experienced the same number of RPTs within the same duration. The RPT test procedure is presented in Table A.2.

At beginning of life (BoL) , middle of life (MoL) and end of life (EoL) , some additional characterisation tests were incorporated alongside the RPT procedure in order to obtain an extended data set to compare the condition of the cells as they aged. The extended RPT incorporates galvanostatic intermittent titration technique (GITT) at BoL and EoL and electrochemical impedance spectroscopy (EIS) at BoL, MoL and EoL. The MoL dataset for the first experimental campaign was collected after 384 days at the 9^{th} RPT for groups 1 and 3 and after the 5thth RPT for groups 2 and 4. Middle of life data was not collected for experimental campaign 2. The GITT test was conducted to full charge (4.2 V) and full discharge (2.5 V) at C/2 in 10% SoC intervals based on the capacity of the most recent CCCV test with 2 hour relaxation periods before each SoC reset. To ensure the SoC steps were accurate, a similar technique to the PPC test was used where the steps were set as a function of the capacity obtained from the most recent CCCV test. Galvanostatic EIS was conducted with a 100 mA excitation amplitude within the frequency range of 5 kHz to 10 mHz, with a resolution of 6 points per decade. EIS was performed at the same SoCs, 80%, 50% and 20%, as the PPC test to allow some comparability. The test procedure for the capacity reset and EIS conditions is shown in Table. A.3.

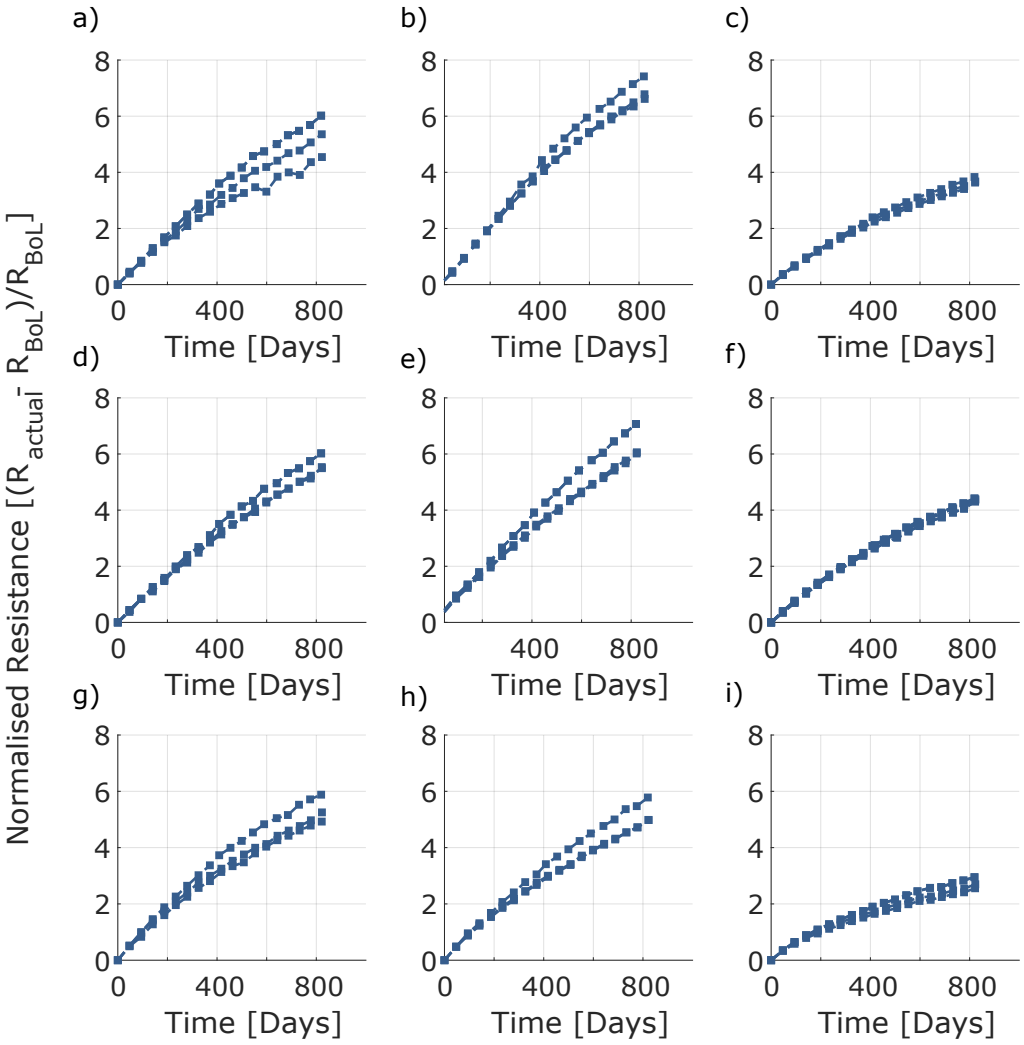

Fig. 2.13 Comparison of DC resistance data (a),(b),(c) collected at 80% SoC with 1.5 A discharge, 1.5 A charge and 10 A discharge pulse respectively; (d),(e),(f) collected at 50% SoC with 1.5 A discharge, 1.5 A charge and 10 A discharge pulse respectively; (g),(h),(i) collected at 20% SoC with 1.5 A discharge, 1.5 A charge and 10 A discharge pulse respectively

Chapter 3

Experimental Campaign 1

3.1 Objective

This chapter presents and discusses data collected during a long-term ageing study conducted to isolate the influence of path dependent degradation on battery ageing. Four groups of three cells each were subjected to combined load profiles which consisted of fixed periods of calendar and cyclic ageing in different orders. This enabled studying of the impact that the order of ageing modes has on degradation. When collecting degradation data in a laboratory environment, it is common to accelerate the ageing to gather a significant amount of degradation data within a short period of time. Most accelerated ageing studies focus on one mode of ageing per cell, either calendar or cyclic ageing. Ageing can be accelerated by exposing the cells to external stress factors such as extreme temperatures, high SoCs, high C-rates, etc [43, 86, 41] . There are a multitude of degradation mechanisms that occur simultaneously within a cell that are encouraged by different stress factors. By accelerating the ageing through external stress factors, degradation mechanisms are encouraged which may not take place under normal use conditions, and the interaction between the mechanisms may also be influenced. There is a clear trade-off between time efficiency of data collection and quality of realism of degradation data. To ensure data collected in this study isolated

the influence of path dependence, the tests were controlled to minimise the influence of stress factors. These tests were hence conducted at temperatures reflective of a well-managed battery system, with conservative C-rates used to cycle the cells and avoiding calendar ageing at the maximum voltage limit to reduce the influence of accelerated ageing.

Empirical models are commonly used to predict the lifetime of a cell by using calendar and cyclic degradation data collected under controlled test bench conditions. Most empirical models assume that calendar and cyclic ageing are independent and cumulative. This chapter aims to provide insight into the influence of path dependent degradation and the conditions that encourage path dependence, and to present the data required to understand the (in)accuracy of the cumulative assumption in empirical models of cell lifetime predictions.

3.2 Profile Design

All four groups of cells used in this study were subjected to a 1:5 ratio of cyclic to calendar ageing periods, which were arranged in different orders. The 1:5 ratio means that cells are exposed to either 1 day or 2 days of continuous cycling and 5 or 10 days of calendar ageing. The longer duration of calendar ageing ensures that the influence of calendar ageing in present in the degradation data collected. Since the experiments are conducted under 25 °C, the degradation is not accelerated. As seen in other studies, calendar ageing cells under ambient temperature does not result in significant degradation and hence it was decided to calendar age the cells for a longer duration than cycling [89]. The cells were exposed to a shorter duration of cyclic ageing as the degradation caused by continuous cycling for 1 or 2 days would have a significant impact on the rate of degradation. Three cells were tested under each condition and the cell selection is shown in Fig. 2.1. Cells in groups 1 and 2 were periodically exposed to one day of cycling followed by five days of calendar ageing. Cells in groups 3 and 4 were periodically exposed to two days of cycling followed by 10 days of calendar ageing ensuring that the same ratio of cyclic and calendar ageing was maintained

for all groups of cells. To probe whether C-rate influences path dependence, the cycling for groups 1 and 3 was conducted at a C-rate of C/2, while groups 2 and 4 were cycled at C/4. An overview of the groups, the cyclic/calendar duration and the cycling C-rate is shown in Fig. 3.1 (a). The combined load-profile conditions are presented schematically in Fig. 3.1 (b) and the current load profiles are presented in Fig. 3.1 (c),(d).

Cyclic ageing in this experimental campaign was conducted by applying constant current charge and discharge cycles. All cells were cycled between 0% and 100% state of charge (SoC), i.e., 2.5-4.2 V. Constant current cycling was selected instead of a dynamic drive cycle so as to expose the cells to the simplest possible continuous cycling profile, with equal time spent at all SoCs. Dynamic drive cycles are usually a realistic representation of EV driving and tend to incorporate factors such as regenerative braking, which produce high-power spikes that can introduce uncontrollable stress factors specific to the drive cycle chosen. Using a dynamic drive cycle would hence lead to difficulties in isolating the impact of cyclic ageing in the combined load profile on path dependence. The selection of drive cycles will also influence the degradation data collected, e.g., an urban drive cycle with a vehicle experiencing frequent braking due to traffic would result in more frequent power peaks leading to encouraged degradation, while a highway drive cycle would experience higher average discharge C-rates which will encourage different ageing trends. Keil et al. compare commonly used American and European drive cycles which clearly shows the difference in discharged capacity due to the cycling conditions and capacity recovered due to regenerative braking conditions [46].A symmetrical dis/charge constant current profile was hence used for cycling the cells with a C-rate of C/2 (groups 1 and 3) or C/4 (groups 2 and 4) to ensure all stress factors were controlled as much as possible. A C-rate of C/2 was selected for cycling groups 1 and 3 which is the maximum charge current (1.5A) as suggested in the cells' specification sheet. To maintain a symmetrical constant current cycling profile, a C/2 discharge was used for groups 1 and 3. To investigate the impact of C-rate of path

dependent degradation, groups 2 and 4 were cycled with a symmetrical constant current profile at a lower C-rate of C/4. Pushing the discharge to the maximum discharge current of 10 A as specified in the datasheet and creating an unsymmetrical cycling profile with either 1.5 A or 0.75 A charge and 10A discharge was avoided as an unsymmetrical profile may have led to increased temperatures due to discharging at higher C-rates. By introducing the additional stress of a high C-rate discharge, the rate of degradation of the cell would have been encouraged which may have influenced the impact of path dependent degradation. Constant current cycling is beneficial for maintaining a simplistic cycling profile which allows for the stress factors to be accounted for however using CC cycling at higher C-rates, such as C/2, can lead to the termination of dis/charge before reaching 100% SoC. Due to the increase in polarisation resistance as the C-rate increases, and since the termination condition of the CC dis/charge is a voltage condition, the voltage condition may be reached before a homogeneous lithiation of the electrodes is achieved [23]. Not reaching a fully homogeneous state can result in not reaching 100% SoC and not dis/charging to the cells full capacity. Over multiple CC cycles this can lead to a drift in the operating window within which the cell is cycled meaning that the cell will be cycled within a smaller SoC window which may reduce the rate of degradation since degradation is encouraged at SoC extremes. For the C/2 cycling conditions in this experimental campaign, a drift in the operating SoC window could mean that although groups 1 and 3 start cycling between an SoC window of 0% to 100%, the longer continuous cycling condition of 2 days for group 3 may lead to cycling through a smaller SoC window by the end of cycling as compared to group 1. Due to this drift, the degradation for the cells in group 3 may be slightly underestimated since the cells are not being cycled to the SoC extremes while the degradation in group 1 would be encouraged in comparison as they would experience less drift due to the shorter continuous cycling duration.

All calendar ageing periods were performed under open circuit conditions at 90% SoC based on actual capacity. As the cells aged, the SoC for each cycle was re-normalised by the

capacity achieved in the prior cycle. More specifically, the number of ampere-hours passed between 2.5-4.2 V was saved as a variable that was updated after a charge or discharge step. This variable was used to determine the end condition required to discharge 10% of the prior-cycle capacity. The longer duration and the relatively high SoC for calendar ageing in the combined profiles were selected to promote degradation without unduly accelerating calendar ageing by pushing the cell to the maximum voltage limit. The EoL condition for the tests was specified as a loss of more than 20% in the pseudo OCV measured capacity. The test procedures designed to expose the cells to the combined load profiles are presented in appendix 1, tables A.5, A.6, A.7 and A.8.

3.3 Results

The influence of path dependence can be studied by comparing results from groups 1 and 3, or groups 2 and 4, as these pairs experienced the same amounts and conditions of calendar and cyclic ageing, but in different orders. On the other hand, comparing the degradation data for groups 1 vs. 2 or 3 vs. 4 provides some insight into the impact of C-rate on degradation. The normalized discharge pseudo OCV data and normalised resistance data collected from all four groups of cells are shown in Fig. 3.2. Fig. 3.2(a) and (c) are plotted against time while data in Fig. 3.2(b) and (d) are plotted with respect to full equivalent cycles (FEC) , where FEC is defined as the total charge/discharge throughput divided by twice the initial capacity. The time that the data is plotted against does not include the time spent during RPTs, similarly the FEC data ignores the throughput from the RPT tests. Although groups 2 and 4 were exposed to the load profiles for the same durations as groups 1 and 3, the lower C-rates for cycling in the case of the former meant they experienced half the number of RPTs, as shown in the degradation data plotted against FEC.

The capacity data shown in Fig. 3.2 (a)-(b) was normalized by the measured capacity at BoL, i.e., as Q_{actual}/Q_{BoL}. There was a divergence in ageing behaviour between groups 1 and

a)

	C/2	C/4
1 day Cycling 5 days Calendar	1	2
2 days Cycling 10 days Calendar	3	4

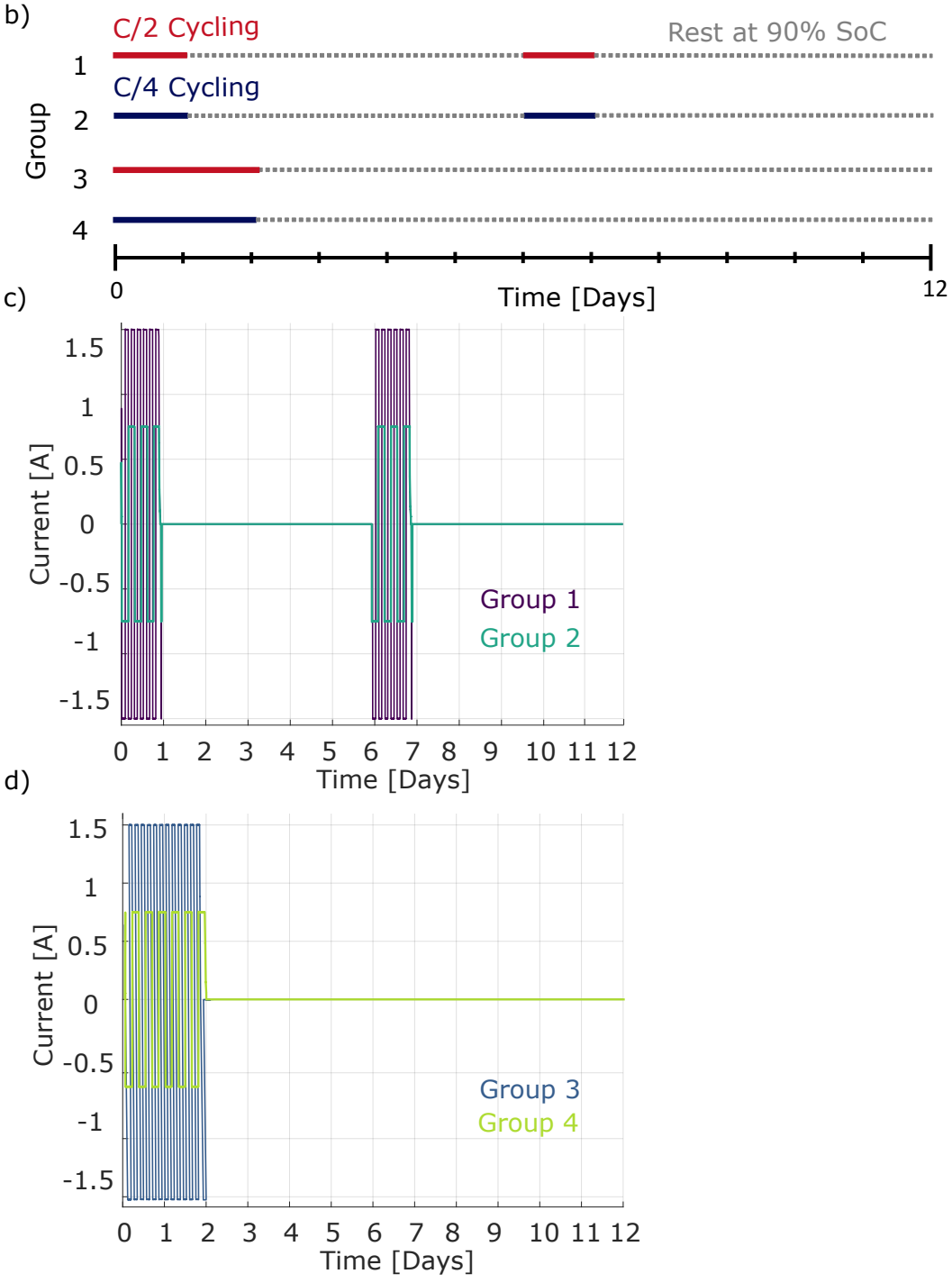

Fig. 3.1 (a) Overview of combined CC cycling at C/2 and C/4 and 90% SoC calendar ageing load profiles for groups 1-4 (b) schematic representation of combined profiles for groups 1-4 (c) the current profile for groups 1 and 2, (d) the current profile for groups 3 and 4

3, with the latter experiencing a higher rate of capacity fade. Group 3 incurred an average of 21.8% capacity loss by the end of the experiment, while group 1 lost 19.5% on average at the end of the test. A cell in group 1 experiences a slight increase in capacity after 480 days which can be seen with respect to time and FEC. The cause of this increase could be due to a brief channel shutdown during the cyclic ageing period prior to this RPT which may resulted in some capacity recovery due to the cell being under rest while the channel was being reset. The difference in degradation paths is especially clear in Fig. 3.2(b) where the capacity fade is plotted against FEC. On the other hand, the rate of capacity fade for groups 2 and 4 is similar, with group 2 experiencing an average of 15.2% capacity loss over the experimental campaign, compared to 14.8% for group 4. The cells cycled at a lower C-rate experienced a lower rate of degradation with respect to time. However, with respect to FEC, groups 2 and 4 follow a similar degradation trend to that of group 3.

The normalised instantaneous DC resistance (R_{DC}) is shown in Fig. 3.2 (c)-(d), expressed as a fractional change relative to the DC resistance measured at BoL, i.e., as $(R_{\text{actual}} - R_{\text{BoL}})/R_{\text{BoL}}$ at 50% SoC with a 1.5 A discharge pulse. The trends seen in the resistance data follow the trends seen in the capacity data, however the relative rate of resistance increase is greater than the rate of capacity fade. The resistance of group 3 increases by an average of 5.68 times the initial resistance while group 1 increases by 4.49 times. Group 3 experiences a higher rate of resistance increase than group 1, whereas groups 2 and 4 show similar rates of increase. Similar to the capacity data, the divergence in the resistance increases between groups 1 and 3 is especially prominent when plotted with respect to FEC. Groups 2 and 4 experience a slightly higher rate of resistance increases than group 3 vs. FEC but follow a similar rate of increase to group 1 with respect to time. The normalised R_{DC} data at all three SoCs, and with all three pulse currents used in the pulse power characterisation test, is presented in Fig. 3.3 where (a), (b), (c) show the data collected at 80% SoC with a 10 second pulse of 1.5 A discharge , 1.5 A charge and 10 A discharge pulse respectively.

Similarly, Fig. 3.3 (d),(e),(f) were collected at 50% SoC and Fig. 3.3 (g),(h),(i) were collected at 20% SoC. Group 3 experiences a greater rate of resistance increase than group 1 across all three current pulses used at 80% and 50% SoC. At 20% SoC, group 1 experiences a greater rate of power fade.

The Nyquist plots in Fig. 3.4 present the EIS data collected for groups 1 and 3 at the BoL, MoL, EoL at 20% SoC (a),(d),(g); 50% SoC (b),(e),(h) and 80% SoC (c),(f),(i). The Nyquist plots shows the difference in the rate of degradation between groups 1 and 3, as the cells age, with group 3 experiencing a greater change in impedance compared to group 1. The impedance spectra comparing groups 2 and 4 in Fig. 3.5 show a similar degradation path for groups 2 and 4. This supports the results given in the R_{DC} data, showing the influence of path dependence on power fade at higher C-rates.

The surface temperature data of each cell was collected every second throughout the duration of the experiment using a thermocouple secured at the same location for each cell. The thermocouples were calibrated prior to the commencing the experiments. A histogram of the surface temperature data presented in Fig. 3.6 with the average cell temperature indicated by the dashed black line. The figure plots the temperatures experienced for a representative cell in each group respectively during cyclic vs. calendar ageing, allowing the thermal stress experienced under each mode of ageing to be studied individually. This omits the data collected during RPTs, as the temperatures experienced during RPT data collection across all cells were similar. The temperatures for all groups during calendar ageing were similar, with the cells in groups 1,2 and 3 spending most of the time during relaxation between 24 °C and 24.5 °C while group 4 spent most calendar ageing between 24.5°C and 25°C. The temperature during cyclic ageing is similar for groups 2 and 4 with most time spent between 26°C and 26.5°C. Group 3 cycles at a slightly higher temperature compared to group 1. Group 1 was most frequently cycled at 25 °C to 25.5 °C, while cells in group 3 were most frequently cycled at 25.5 °C to 26 °C.

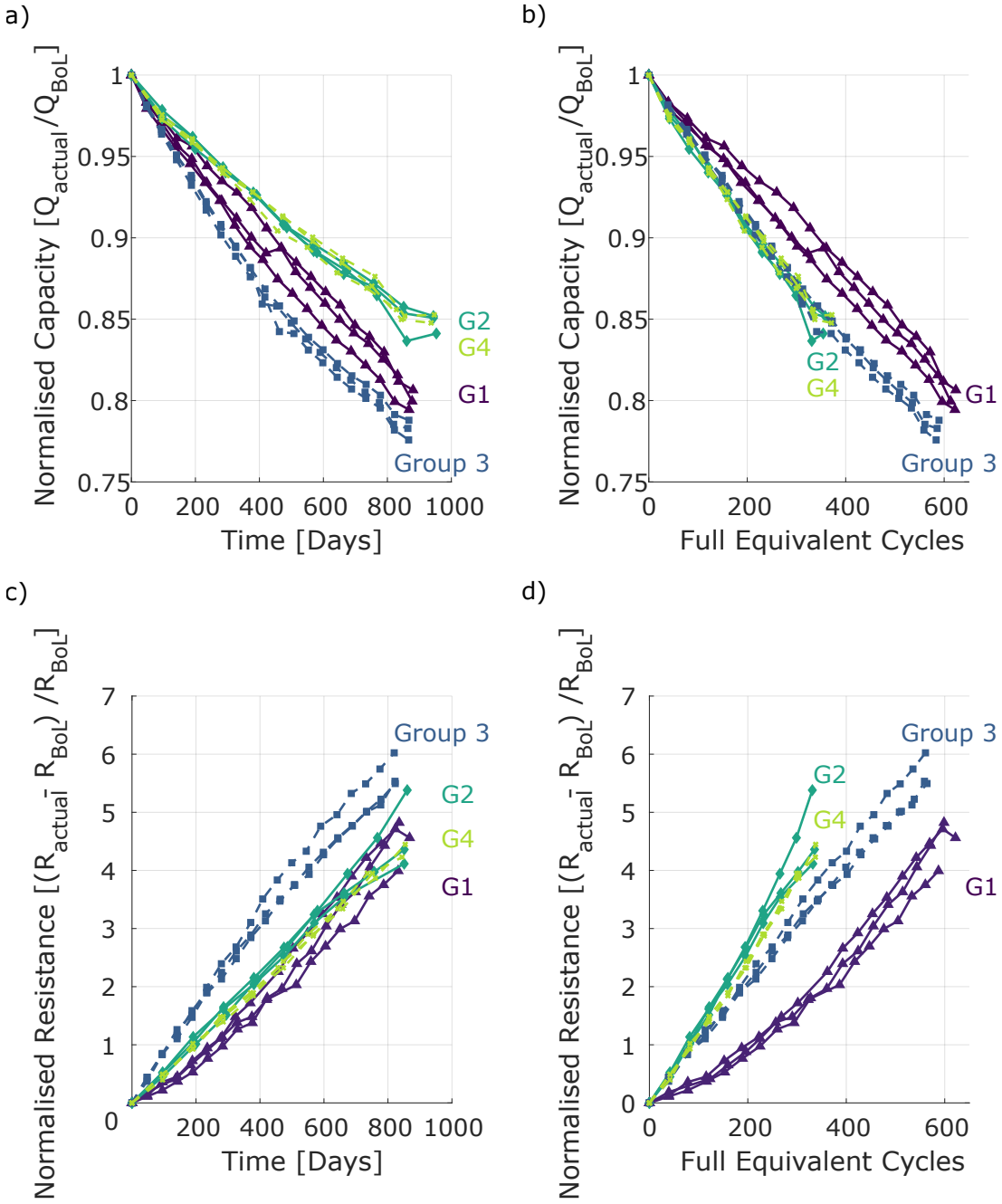

Fig. 3.2 Normalised pseudo OCV capacity fade for groups 1 to 4 in (a)time and (b)full equivalent cycles; Normalised R_{DC} increased in (c)time and (d)full equivalent cycles

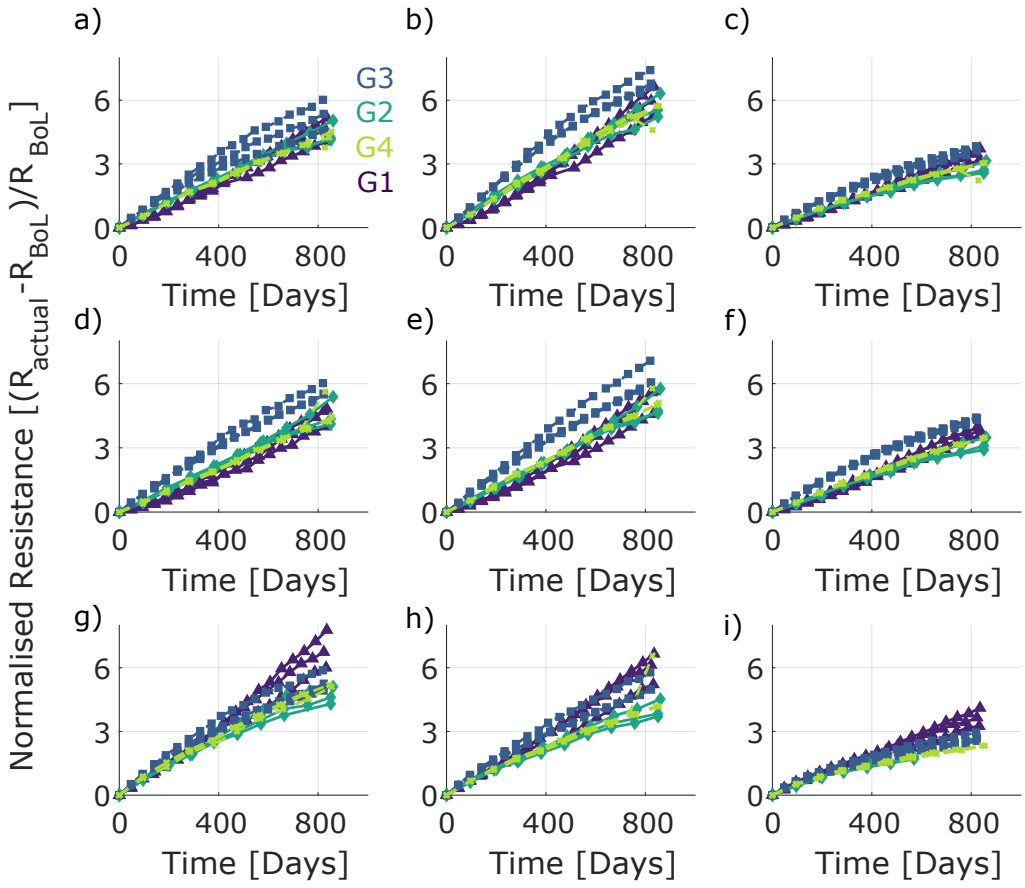

Fig. 3.3 Normalised DC resistance (a),(b),(c) taken at 80% SoC with 1.5A discharge, 1.5A charge and 10A discharge pulse respectively; (d),(e),(f) taken at 50% SoC with 1.5A discharge, 1.5A charge and 10A discharge pulse respectively; (g),(h),(i) taken at 20% SoC with 1.5A discharge, 1.5A charge and 10A discharge pulse respectively

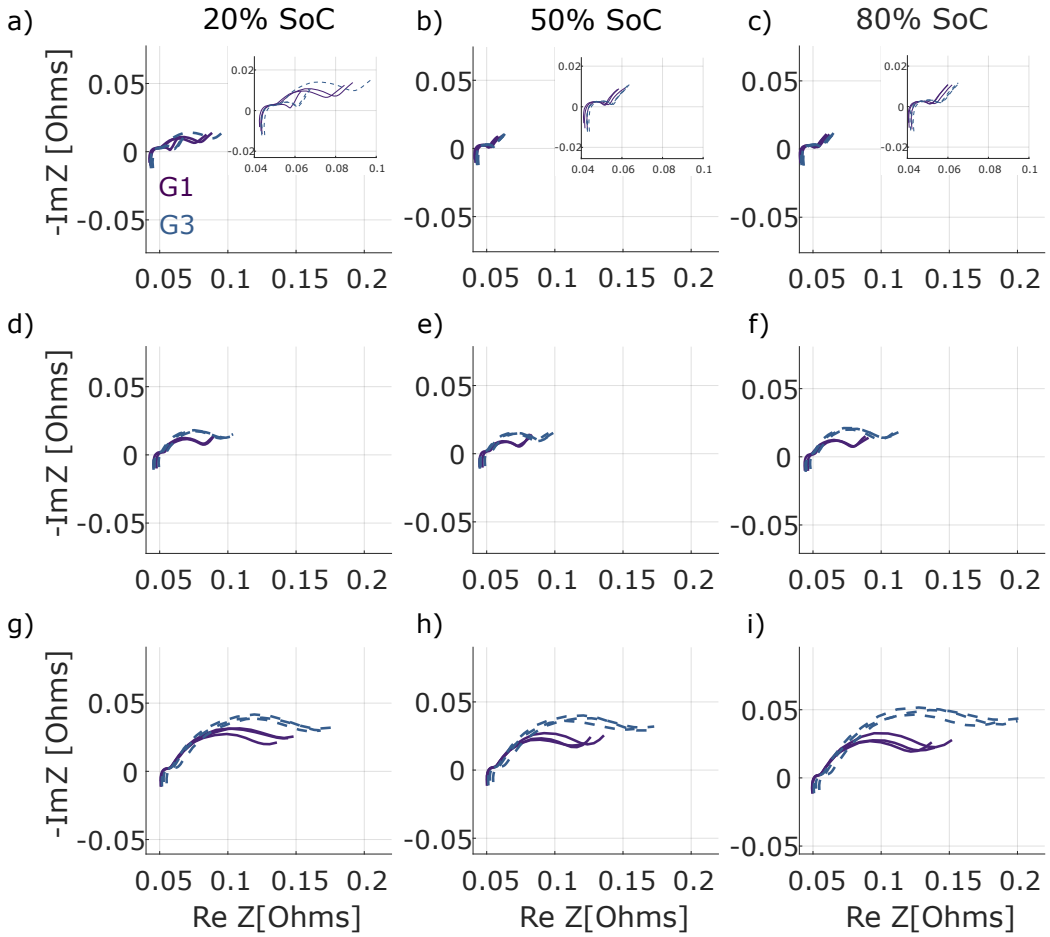

Fig. 3.4 Impedance spectra for groups 1 and 3 at BoL at (a)20% SoC, (b) 50% SoC, (c) 80% SoC; MoL at (d) 20% SoC, (e) 50% SoC, (e) 80% SoC and EoL at (g)20% SoC (h) 50% SoC (i) 80% SoC

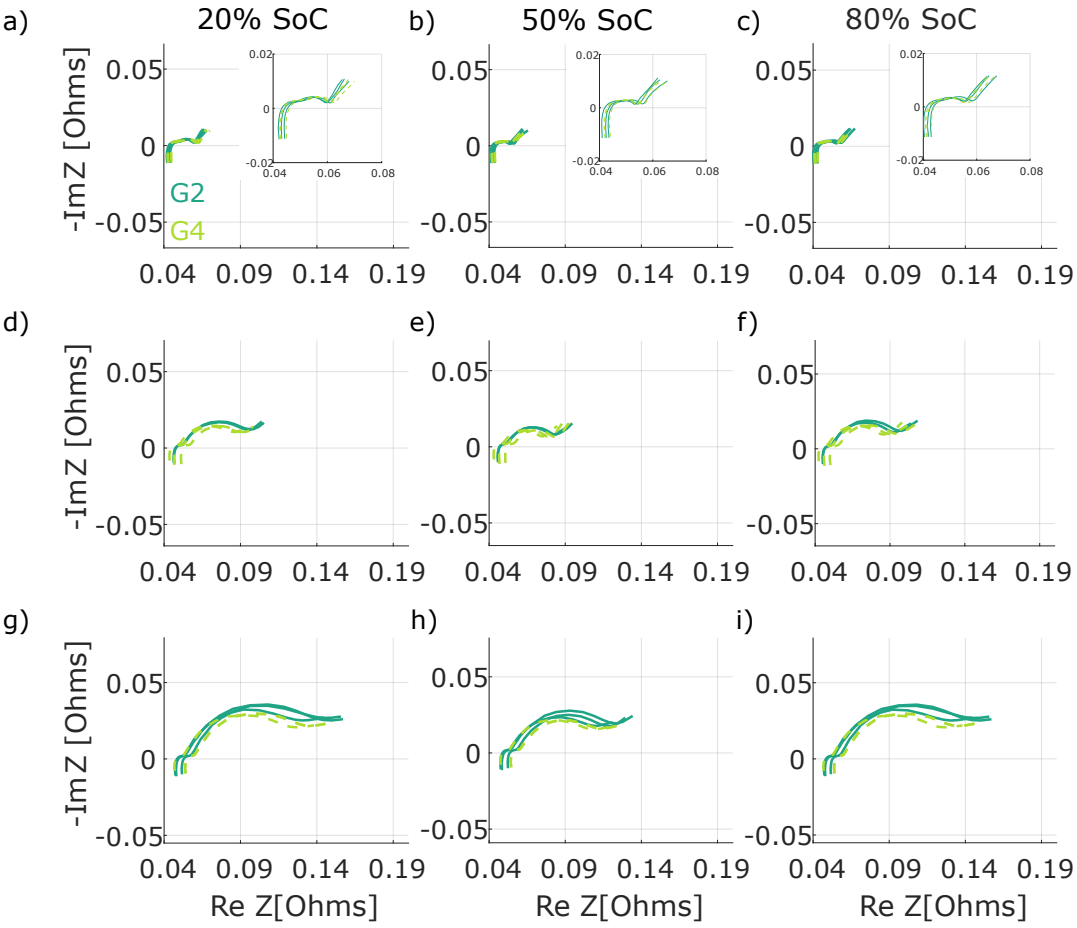

Fig. 3.5 Impedance spectra for groups 2 and 4 at BoL at (a)20% SoC, (b) 50% SoC, (c) 80% SoC; MoL at (d) 20% SoC, (e) 50% SoC, (e) 80% SoC and EoL at (g)20% SoC (h) 50% SoC (i) 80% SoC

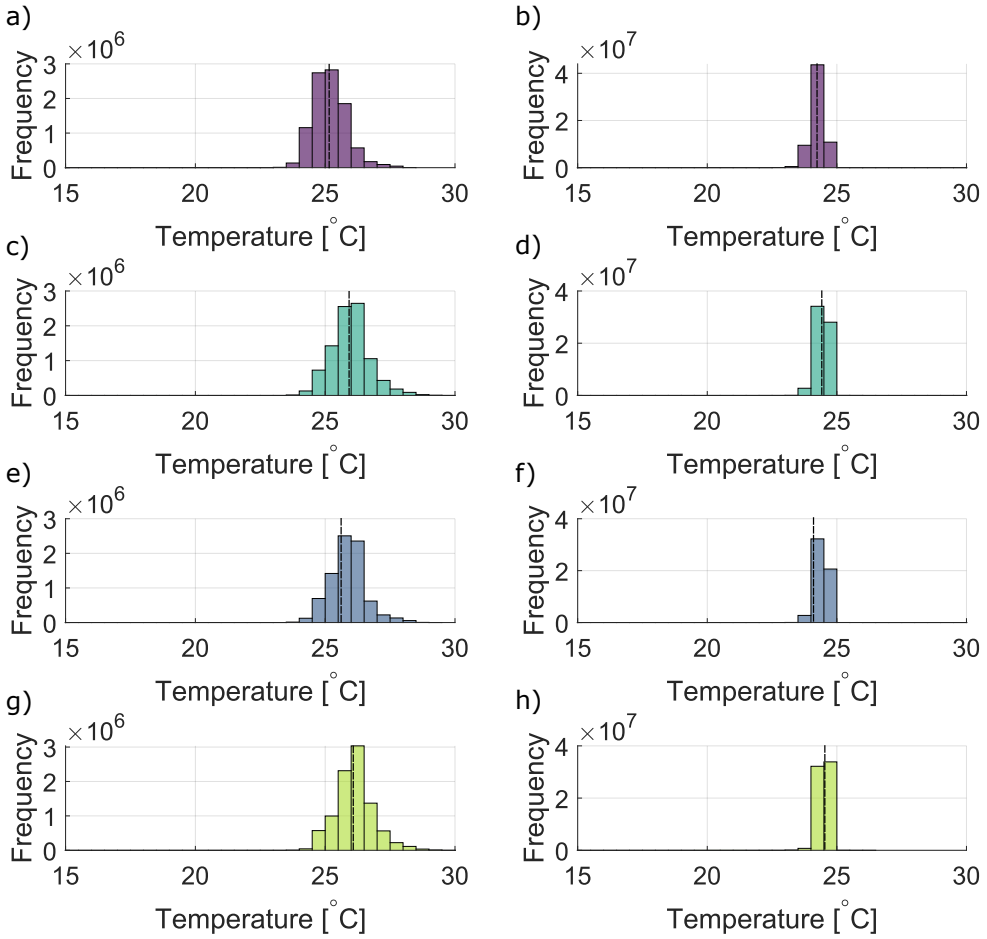

Fig. 3.6 Histogram of temperature for group 1 during (a) cyclic ageing, (b) calendar ageing; group 2 during (c) cyclic ageing, (d) calendar ageing; group 3 (e) cyclic ageing, (f) calendar ageing; group 4 (g) cyclic ageing and (h) calendar ageing

3.4 Analysis and Discussion

The data presented in Fig. 3.2 shows there is little or no difference in the degradation trajectories of cells tested at C/4 (groups 2 and 4), but a discernible difference in those of cells tested at C/2 (groups 1 and 3). The greater path dependence seen between the cells cycled at C/2 could indicate that path dependence is C-rate dependent. This section aims to explore the reasons behind the difference in degradation rates.

Cycling and calendar ageing at temperature extremes have been shown to encourage ageing [27, 41, 90]. Low temperatures can encourage degradation mechanisms such as lithium plating while higher temperatures can promote SEI layer growth [39, 91]. Internal thermal gradients can be encouraged by cycling at high C-rates or for longer durations. This means that cells in groups 3 and 4 could be experiencing greater relative internal temperatures due to the 2 days of continuous cycling which may result in greater rates of degradation. This is especially true for cells in group 3 that are cycled at C/2 resulting in a greater rate of degradation compared to group 1. Group 1 spends more time cycling around 25 °C to 25.5 °C while group 3 spends more time at around 26 °C to 26.5 °C as shown in Fig. 3.6. There is a 0.5 °C difference between the temperatures that groups 1 and 3 spend most time at during cyclic ageing. This shows that the longer continuous cycling duration associated with group 3 does lead to an increased cell temperature, however the 0.5 °C difference between the groups does not justify temperature as a significant factor impacting the rate of degradation. The temperature data for groups 2 and 4 during cycling indicate that both groups cycle at similar temperatures. Comparing the thermal data during calendar ageing shows cells in groups 1, 2 and 3 most frequently calendar age between 24 °C and 24.5 °C while group 4 spends the most time while calendar ageing between 24.5 °C and 25 °C. Overall, the temperature variations seen between the groups during cycling and calendar ageing are insignificant and it is assumed that these differences would not noticeably encourage different rates of degradation.

3.4.1 Capacity Fade Analysis and Discussion

The most significant divergence in capacity data was seen between groups 1 and 3. As seen in Fig. 2.1 and table 2.2, there is a difference in the average initial capacity with the cells in group 1 having an average initial capacity of 3.07 Ah and group 3 having 3.04 Ah. Since group 1 has a higher average initial capacity than group 3, it could be explained that the initial difference of 0.03 Ah in the average capacity has resulted in group 1 experiencing a longer lifetime. However, groups 2 and 4 had a more significant difference in the initial average capacity of 0.09 Ah and still follow a similar rate of degradation. This could indicate that the initial average capacity does not have enough significance to justify the difference in the rate of degradation between groups 1 and 3 and that the difference between groups 1 and 3 could be attributed to path dependence. The unnormalized data for charge and discharge OCV data with respect to both time and FEC is presented in Fig. B.1 and shows a similar trend with group 3 experiencing a greater rate of capacity fade as compared to group 1. A point to note in Fig. B.1 is that the average initial capacity for group 3 is greater than group 1 which contradicts the initial capacity data used for the cell selection criteria. This is due to a CCCV test being used for the cell selection while the raw data in Fig. B.1 is the dis/charge OCV data. As seen in Fig. 2.12, the OCV capacity estimation is assumed to be more accurate as it limits the impact of polarisation resistance. The unnormalized capacity data hence shows that cells in group 3 had a higher overall initial capacity and still degraded at a greater rate compared to the cells in group 1 which had a lower initial OCV capacity. This confirms that there is an influence apart from the initial capacity selection that is encouraging the divergence between groups 1 and 3.

The path dependence in the capacity fade data was more prominent in Fig. 3.2(b) which isolates the influence of cyclic ageing by studying the charge throughput. The cells in group 3 were cycled for a longer continuous period of time compared to group 1, which could lead to the difference in degradation rate with respect to FEC. The prolonged continuous

mechanical stress at the electrodes brought on by repeated de/intercalation may have resulted in a higher rate of degradation. Studies of the volume expansion of the electrode material have shown that during cycling the graphite electrode can undergo a 10% change in volume, while the NCA electrode experiences a 4.5% change in volume [92]. This leads to increased mechanical stress, especially at the anode, and consequently could lead to degradation mechanisms such as particle cracking and loss of electrical contact which, in turn, would lead to capacity fade due to loss of active material. The divergence with respect to FEC suggests that it is the CC cycling condition that is encouraging the divergence.

Fig. 3.2(a) incorporates the influence that calendar ageing has on capacity fade. The capacity against time plot indicates that periods of calendar ageing could reduce the impact of path dependence as the divergence between groups 1 and 3 is less prominent. The shorter but more frequent relaxation periods in group 1 that interrupt the continuous cycling periods seem to reduce the rate of degradation perhaps by allowing the lithium distribution to homogenise through the electrodes after intercalation. It was shown by Rashid et al. that at the end of a full charge, there is a large variation in the concentration gradients, and it takes an hour of relaxation for the concentration of lithium through the electrodes to become uniform. Relaxation longer than an hour leads to marginal changes in the concentration across the electrode [93]. The more frequent calendar ageing periods in group 1, will allow the lithium to homogenise through the electrode leading to less stress as compared to group 3. Studies have shown that relaxation periods also allow for capacity recovery from the anode overhang region. Since the cells in group 1 experienced shorter but more frequent calendar ageing periods, this may have allowed for capacity to have been recovered from the overhang region more frequently than compared to group 3 which experienced less frequent but longer rest periods [47, 94, 95]. The cells in all four groups were calendar aged at 90% SoC, however their SoC was reset before every calendar ageing period using an updated value of capacity as the cell aged, as described in 3.2. Since the relaxation voltage is a function of capacity,

the corresponding voltage would be lower for cells that have experienced more capacity fade. The cells in group 1 experienced more frequent calendar ageing resets to a higher voltage compared to group 3, due to the lower rate of degradation experienced by group 1. Since group 1 was therefore held at a higher voltage more frequently than group 3, the degradation experienced by group 1 is slightly greater than if it were calendar aged at the same voltage as group 3. The capacity recovery from the anode overhang region may also have been limited in group 1 due to the higher voltage. This means that the rate of degradation for group 1 may have been encouraged by this phenomenon, leading to a greater rate of degradation, suggesting that the divergence between groups 1 and 3 with respect to time may underestimate the path dependent degradation. An underestimation may have also been made due to the nature of the continuous CC cycling as discussed earlier in section 3.2. The drift in the SoC window within which the cell is cycled caused by an increase in the polarisation resistance. For groups 1 and 3, this means that the cells in group 1 will be cycled through a larger SoC window while the cells in group 3 will be cycled through a smaller SoC window by the end of the 2 days of continuous cycling. Since the cells in group 3 are not pushed to the SoC extremes, the rate of degradation seen would be less than if the cells were to be cycled within the same SoC window as group 1. This means that due to the calendar and cycling conditions selected in this profile design, the extent of divergence seen between groups 1 and 3 could be underestimated.

Comparing the capacity fade of groups 2 and 4 that were cycled at C/4 indicates that both groups follow very similar degradation trends with respect to time and FEC. Their rate of degradation is not influenced by the continuous cycling or the frequent calendar ageing breaks as seen for groups 1 and 3. This indicates that path dependence is rate dependent, with divergence increasing at higher C-rates. The lack of path dependence seen between groups 2 and 4 could be due to the lower C-rates allowing a more homogenous lithiation

of the electrodes This would lead to a more uniform mechanical stress for the cells during cycling and reduce the impact that relaxation periods have on degradation for both groups.

The difference between groups 1 and 2, or 3 and 4, highlights the impact that different C-rates of cycling can have on capacity fade, as they experience the same load profiles at different C-rates (groups 2 and 4 at C/4 vs. groups 1 and 3 at C/2). On average, groups 1 and 2 experience a difference of 4.78% in capacity fade while groups 3 and 4 experience a difference of 6.99% with respect to time. This was expected, since these cells only experienced half the number of full equivalent cycles as compared to the cells in groups 1 and 3, however the greater difference between groups 3 and 4 indicates that the duration of continuous cycling at higher C-rate has a significant impact on the rate of capacity fade.

The capacity data with respect to full equivalent cycles shows groups 2 and 4 experiencing a higher rate of capacity fade than group 1. Groups 2, 3 and 4 all follow a similar trajectory of capacity fade with respect to FEC. This could be because groups 2 and 4, which cycled for the same duration but at a lower C-rate, spent longer periods of time at voltage extremes compared to groups 1 and 3 – an electrochemical stressor known to accelerate degradation [32] [96] [47]. The cells in group 1 spends 1 day of continuous cycling at C/2 while group 2 spends 1 day at C/4. This means that within the same duration, the cells in group 2 experience half the FECs which indicates that the cells spend longer at the voltage extremes. Groups 2 and 4 follow a similar trajectory to groups 3 with respect to FEC. With respect to cycling, group 3 experiences a longer continuous duration of cycling which could encourage degradation due to the mechanical stress the cells would experience. The cells in groups 2 and 4 could be degrading at a higher rate due to being held at SoC extremes for a longer duration. Group 1 shows less degradation with respect to FEC as it experiences less mechanical stress due to cycling and spends less time at SoC extremes during cycling. This shows that it is important to consider the combined input of degradation factors that depend on time spent in a certain state (e.g., voltage) as well as C-rate.

3.4.2 Resistance Increase Analysis and Discussion

Trends in the resistance data shown in Fig. 3.2(c)-(d) are similar to the capacity fade data. In relative normalised terms though the rate of resistance increase is higher than the rate of capacity loss with respect to both time and cycling.

The unnormalized resistance data shown in Fig. B.3 shows that group 1 has a greater average initial resistance compared to group 3 however as the cells age, the power fade in group 3 is greater than group 1. This increase in the resistance can impact the voltage window within which the cells are cycled causing the cell to hit the voltage limits before the SoC limits have been reached. Given that the resistance for group 3 is greater than group 1, the cells in group 3 will cycle through a smaller voltage window than group 1. Cycling through a smaller voltage window will reduce the rate of degradation as the cells will not be pushed to the voltage extremes which would encourage degradation. Comparing the SoC window for group 1 with group 3 will provide some insight into the influence that the resistance can have on the early termination of dis/charge and hence the impact on the SoC window. At the end of initial cycling and before the second RPT (i.e., when the difference would be most apparent), there was a difference of 0.23% SoC, with group 1 cycling through a larger SoC window than group 3. As the cells aged, the difference between the cycling SoC windows increased to a difference of 3.15% SoC with group 1 maintaining a larger SoC window. Despite the smaller cycling window however, group 3 still degraded more significantly than the cells in group 1. Since the cells cycled at C/4 have longer to for the lithium to homogenise through the electrode during cycling, the polarisation resistance will be limited which will encourage the cells to cycle through the full SoC window. Comparing the SoC windows after initial cycling and cycling towards the end of test for groups 2 and 4 showed that there was an insignificant difference in the SoC cycling window.

A significant influence of path dependence was seen in the rate of resistance increase (or power fade), between groups 1 and 3 with respect to time with the cells in group

3 experiencing an average increase of 5.68 times their initial resistance while group 1 increases by 4.49 times their initial resistance. The divergence could be a product of the longer continuous cycling encouraging mechanical degradation mechanisms such as particle cracking, graphite exfoliation and structural disordering. Relatively, the divergence in resistance increases between groups 1 and 3 is more significant than the divergence in the capacity fade data suggesting the path dependence could have a greater influence on power fade than capacity fade. The resistance data following similar trends to the capacity data could indicate that the degradation is a result of mechanical stress at the electrodes [1].

Groups 2 and 4 experienced similar rates of resistance increase. This supports the path dependence trends seen in the capacity data and confirms that path dependence is rate dependent. The cells cycled at C/4 had a lower rate of degradation with respect to time and followed the degradation trends experienced by the cells in group 1. With respect to FEC however, the cells cycled at a lower C-rate experienced a resistance increase greater than that experienced by group 3. This indicates that holding the cells at a higher voltage for longer periods of time due to the lower cycling C-rate had a greater effect on power fade than capacity fade.

The difference in the resistance increases between groups 1 and 2 with respect to time is not pronounced even though group 2 experienced half the full equivalent cycles that group 1 experienced. With respect to FEC however, the difference in resistance increases between groups 1 and 2 caused by the different C-rates during cycling is significant. The difference between groups 3 and 4 that experienced a longer duration of continuous cycling and calendar aging is more significant with respect to time, similar to that of the capacity fade data. With respect to FEC, group 4 degrades at a higher rate than group 3.

Changes in the characteristic resistances of the cells can be tracked with EIS using the Nyquist plots presented in Fig. 3.4 and Fig. 3.5 as described in section 2.2.2. Changes in the ohmic resistance (R_{Ohmic}) can be studied by the shift in the intercept of the EIS

spectrum with the x-axis. Changes in the chord length of the first semicircle can be used to estimate the changes in the SEI layer resistance (R_{SEI}) while the chord length of the second semicircle can be used to track changes in charge transfer resistance (R_{CT}) [97, 87]. These three characteristic resistances taken at 50% SoC at the BoL, MoL and EoL are shown in Fig. 3.7 with respect to time and FEC. The analysis shows a similar increase in R_{Ohmic} between all four groups, however there is a slight difference between groups 1 and 3 in the increase of R_{SEI} and a more noticeable divergence between the two groups in R_{CT}. The similar degradation trends for R_{Ohmic} indicates that resistance increase due to the degradation of the current collectors, binder and electrolyte is similar for all groups [98]. The slight divergence in R_{SEI} between groups 1 and 3 could indicate that there is a slight difference in the SEI layer formation growth rate, which could lead to group 3 experiencing a slightly higher rate of loss of lithium inventory. Group 3 experiences a greater increase in charge transfer resistance which follows the trend seen in the R_{DC}. The difference in charge transfer resistance could be caused by loss of active material or loss of electrical contact at the electrode which would result in a higher current density due to the reduced active material. A similar result is seen in a study by Ovejas et al. during cycling at 25 °C that resulted in a greater increase in charge transfer resistance than SEI resistance [85]. It was suggested that the increase in R_{CT} was due to microcracks forming and the electrical isolation of active material [85]. The charge transfer data is collected at lower frequencies which are similar to the pulse test conducted to collect the R_{DC} due to the limited sampling frequency of the battery tester. This makes the trends seen in R_{DC} and R_{CT} comparable and explains why they exhibit a similar divergence. Groups 2 and 4 follow similar resistance trends across all three characteristic resistances.

3.4.3 Incremental Capacity Analysis and Differential Voltage Analysis

ICA and DVA analyses were conducted using the pseudo OCV data collected from the RPTs to gain insight into the degradation mechanisms associated with path dependence. Tracking

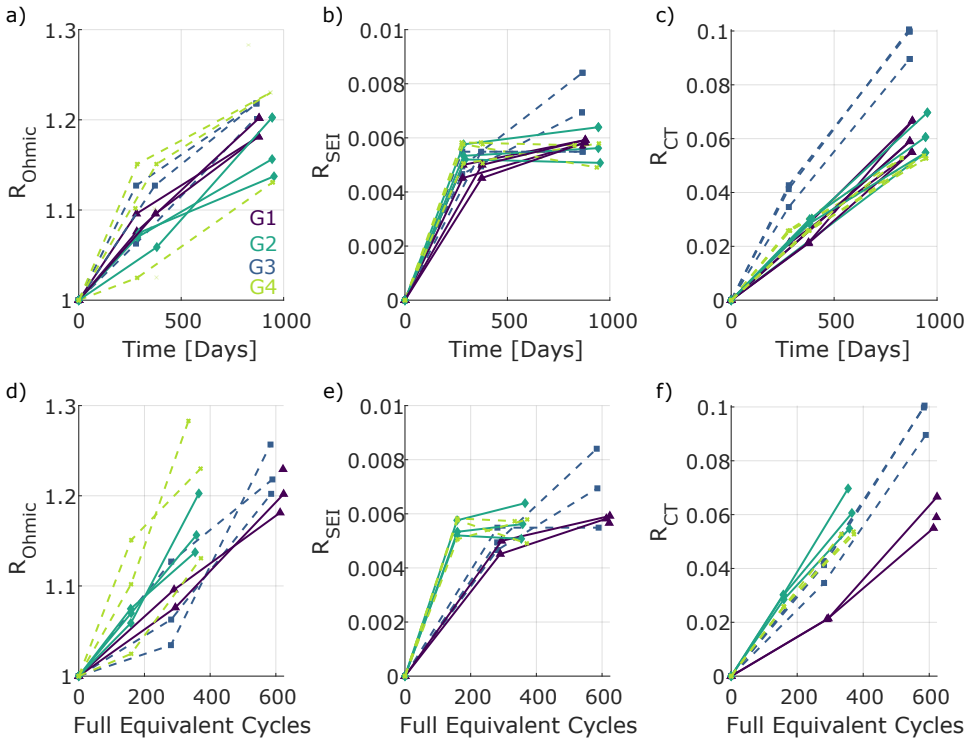

Fig. 3.7 Characterisation of EIS resistances as the cells age in (a), (b), (c) time and (d), (e), (f) full equivalent cycles

the shifting of features of interest in the ICA/DVA signatures can be used to estimate changes in lithium inventory. Shrinking and shifting of the features of interest can provide separate estimates of the loss of active material at the positive electrode and negative electrode [72] [52] [73].

Fig. 3.8 shows the progression of ICA signatures of a representative cell from each of groups 1, 2, 3 and 4. The cell that experienced the least degradation in all groups was selected to ensure the comparison between the groups is not exaggerated by the influence of any unintentional acceleration of ageing. The features of interest are denoted by numbers P1-P4, the direction of ageing indicated by the arrow, and the thick blue signature corresponds to the MoL ICA signature at the 7^{th} RPT after approximately 240 FECs. The thick blue signature facilitates the comparison between groups as a function of FEC, since groups 2 and 4 experienced half the RPTs compared to groups 1 and 3 due to the difference in C-rates. Time-based comparisons are made using the EoL signatures. The BoL ICA signatures shown as the purple line for all groups demonstrate similar peak heights and positions. The ICA signatures of groups 2 and 4 show similar peak shrinking and shifting. Peaks 1, 2 and 3 maintain their positions and the peak height gradually reduces while P4 moves towards lower voltages as the peak diminishes at a similar rate in both groups. Comparing groups 1 and 3 shows that group 3 experiences a higher rate of change in peak heights compared to group 1. Comparing P2, P3 and P4 highlights that not only do the peaks in group 3 shrink faster but they also shift to lower voltages. The shrinking of the peaks can be attributed to loss of active material, while peak shifting is due to the loss of lithium inventory. Groups 2 and 4 experience loss of active material and lithium inventory at similar rates while it is the rate of loss of active material that is leading to path dependent degradation between groups 1 and 3.

To examine the difference in ICA signatures between groups 1 and 3 as the cells age, Fig. 3.9 shows the difference in signatures at BoL, MoL and EoL . There is little difference at the beginning of life, but as the cells age a significant difference between the two groups emerges.

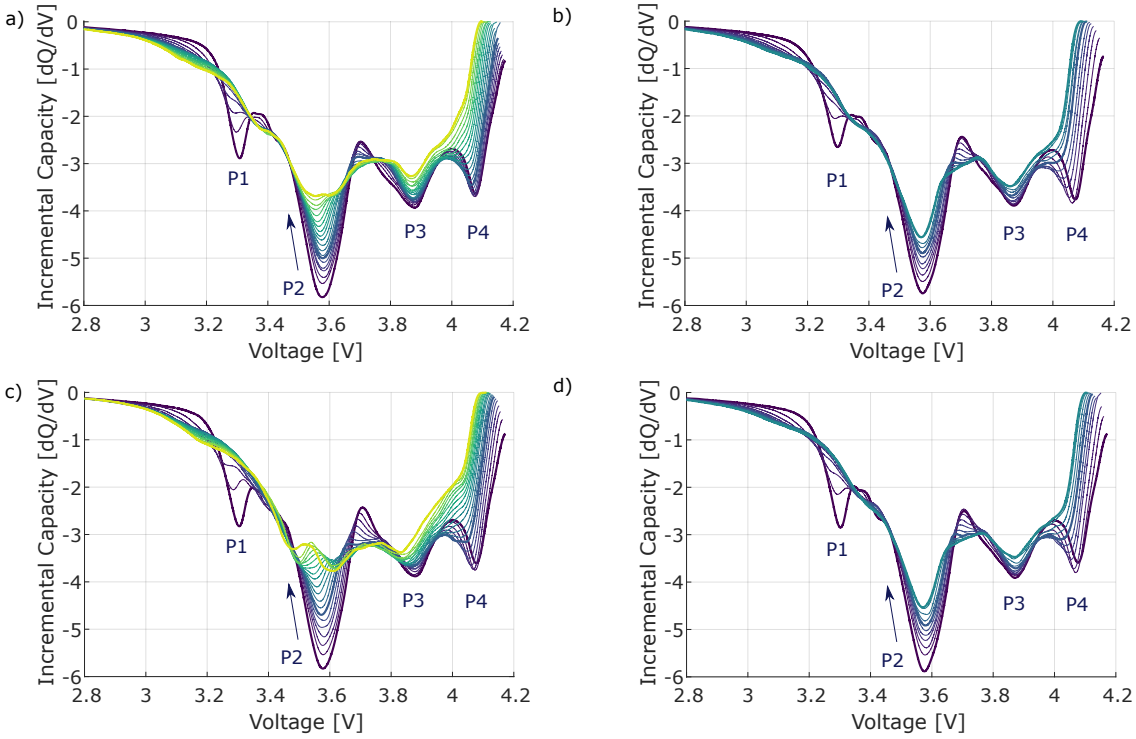

Fig. 3.8 progression of ICA signatures for (a) group 1, (b) group 2, (c) group 3 and (d) group 4 with arrow indicating the direction of ageing and the thick blue line indicating the 7^{th}

From the BoL to MoL, there is a significant difference in the shrinking of P1 and P2 due to loss of active material. As the cell progresses to the EoL, the influence of peak shifting and changes at P3 and P4 also become evident. However, it is not possible to determine from the ICA data alone at which electrode the loss of active material is occurring.

Half-cell data is required to identify whether the difference in rate of active material loss is occurring at the anode or the cathode. Half-cell data and DVA were used to attribute changes respectively to the anode or the cathode [4] [75]. DVA was conducted on the pseudo OCV data collected from a pristine 18650 cell and the pseudo OCV data collected from the half-cells constructed from a pristine 18650 cell as described in section 2.1.2 . Half-cell data was normalized by the active area of electrode material in the coin cells, to produce a SoC measure that could be meaningfully compared to the SoC of the 18650 cells. The results

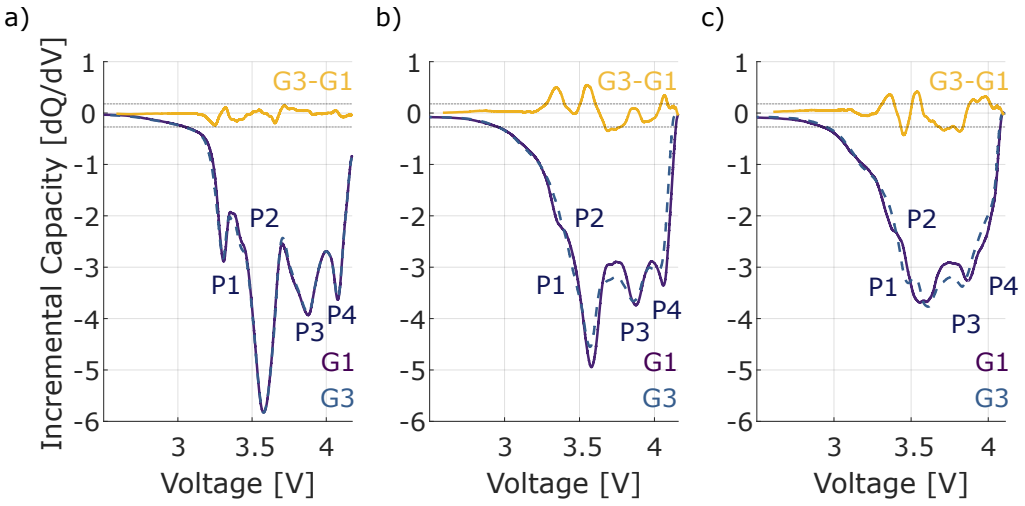

Fig. 3.9 Difference in G1 and G3 ICA signatures at (a) BoL, (b) MoL and (c) EoL

presented in Fig. 3.10 indicate that peaks P1 and P2 of the full-cell DVA can be attributed to the anode, while the cathode governs the higher SoC voltages attributed to P3 and P4.

The difference in ICA signatures in Fig. 3.9 shows that between BoL and EoL, peaks P1 and P2 experienced the most significant difference, and these are dominated by the anode according to the half-cell data. As the cells age, the difference in P4 also becomes evident and is a cathode peak. Therefore, the loss of active material at the negative electrode likely plays a significant role in path dependence. Comparing the ICA and full cell DVA signatures in Fig. 3.11 with simulated signatures for a cell of the same chemistry by Dubarry et al. [74] confirms that the difference in the rate of degradation could be due to differing rates of loss of lithiated material at the negative electrode.

Full-cell DVA signatures of a representative cell from each of groups 1, 2, 3 and 4 are shown in Fig. 3.11. The signatures show that the groups cycled at C/4 both experienced the same degradation modes, at similar rates, while the cells cycled at C/2 exhibit a difference in ageing trajectories between each other. Similar to the ICA plots, the 7^{th} signature is represented by the thick blue line, which makes it easier to compare the four sets of DVA signatures with respect to full equivalent cycles. Comparing the signatures for groups 1 and 3, it is clear that the rate of peak shrinking/shifting is greater in group 3, especially at P1 and

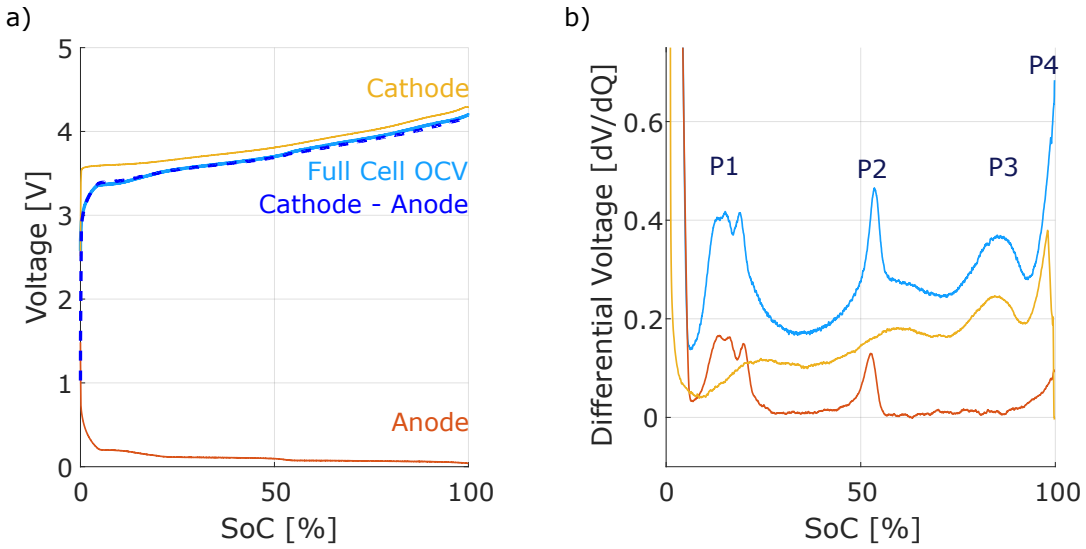

Fig. 3.10 (a) Pseudo OCV curves for a pristine full cell, half-cells constructed from pristine cell material, and the difference between the half-cell pseudo OCV curves. (b) DVA signatures of full cell, cathode, and anode

P2. With P1 and P2 being attributed to the anode, this provides confirmation that there is a difference in anode degradation between the two groups which is due to the rate of loss of active material. A slight difference in the peak shrink at P3 can be seen in response to cathode degradation and a difference in the rate of peak shift at P4 due to the loss of lithium inventory which could result in a change in electrode balancing.

The DVA signatures can be used to quantify the capacity loss attributed to each electrode, while also giving insight into the cell's electrode balancing as explained in section 2.2.1 [76]. Keil et al. [76] suggest that there are characteristic capacities that can be estimated from the DVA signature as shown in Fig. 2.8 as the cell ages, reflecting the change in electrode balancing, and the loss of active material at the electrodes. Fig. 3.12 shows the changes in these characteristic capacities as the cells age. It confirms that the anode capacity (Q LAM_{ne}) experiences the most significant difference in electrode degradation between groups 1 and 3. The cathode capacity (Q LAM_{pe}) shows some slight differences which were picked up in the ICA/DVA signatures but does not seem to be a driving force for the divergence in ageing behaviour in response to the load profiles used. There are some slight differences

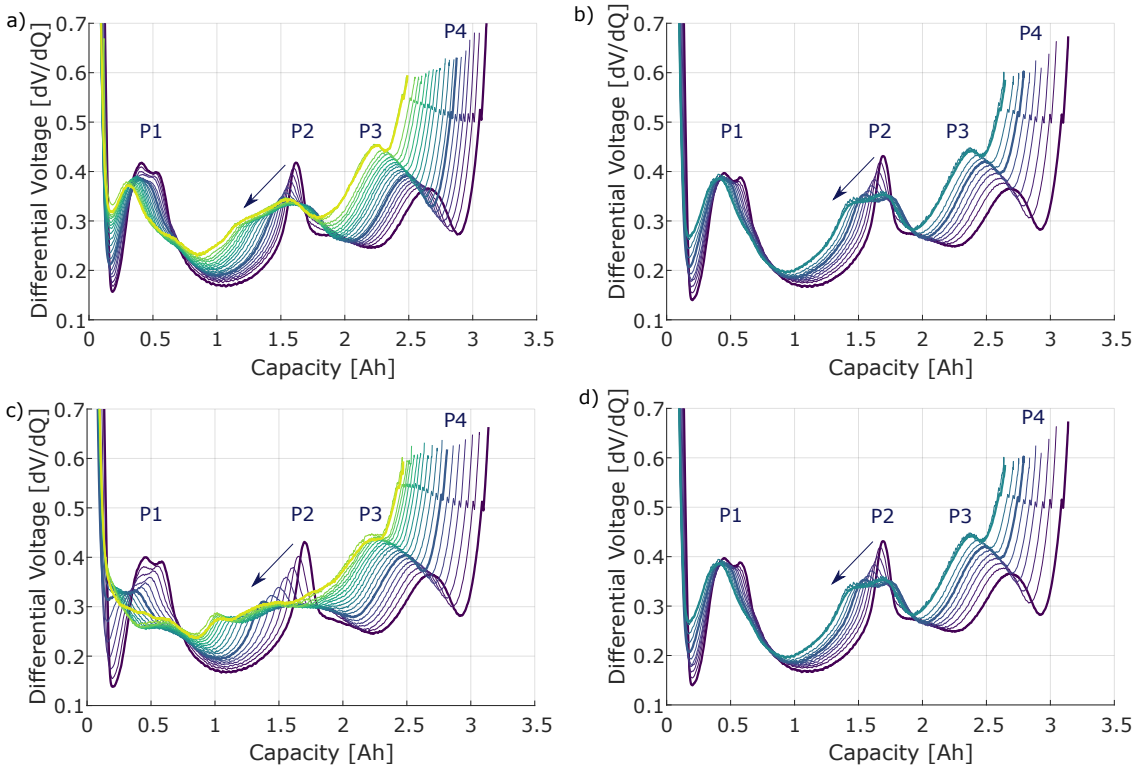

Fig. 3.11 Progression of DVA signatures as the cell ages for (a) Group 1, (b) Group 2, (c) Group 3 and (d) Group 4 with arrow indicating ageing and the thick blue line indicating MoL

in electrode balancing also ($Q_{balance}$) . This is because there will be some underlying loss of lithium inventory due to SEI layer formation and other lithium consuming degradation mechanisms leading to changes in $Q_{balance}$. The shifting and shrinking of the electrode half cells with respect to the full cell due to loss of lithiated active material at the electrodes will also be reflected in $Q_{balance}$.

The peak analysis for groups 2 and 4 confirms that the electrodes aged in a similar fashion in these cells and do not show any indication of being influenced by path dependence. Comparing the cells cycled at different rates can provide insight into the influence of C-rate on cell degradation. It is crucial to note that Fig. 2.8 (b) and (d) have half the data points that Fig. 2.8 (a) and (c), due to the lower C-rates used. The cells cycled at C/2 experienced a greater loss of active material at the anode compared those cycled at C/4 as seen in P1 and P2 of the DVA signatures as well as the quantified capacity characteristics. There is also a noticeable difference in the change in the balancing capacity with the cells cycled at C/4 seeing a steady decrease which could be attributed to loss of lithium inventory. The higher rate of LLI at C/4 could be due to longer time spent at voltage extremes leading to side reactions such as SEI formation which is supported by the R_{SEI} data from the Nyquist plots in Fig. 3.7.

3.4.4 Post-mortem Study

A post-mortem tear-down study was conducted on the cells exposed to the combined profiles in order to visually inspect the impact that the degradation had on the electrodes. The cells were fully discharged using a C/24 CC discharge protocol to ensure the anodes were fully delithiated and were opened in an argon filled glove box following the methodology outlined by Waldmann et al. [99]. Fig. 3.14 shows the extracted electrodes for a fresh cell and a representative cell from each of the groups, 1 to 4. Both the anode (top electrode) and cathode (bottom electrode) are shown for each segment of the electrode from the skin (the outermost

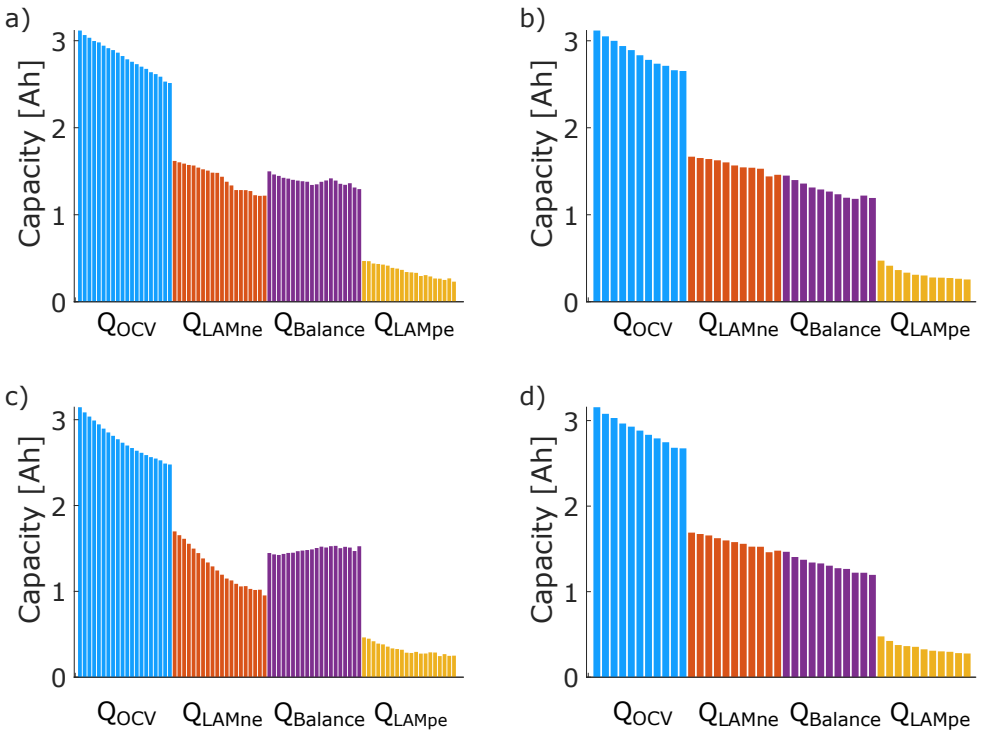

Fig. 3.12 DVA peak analysis for (a) Group 1, (b) Group 2, (c) Group 3 and (d) Group 4 with the progression in time shown from left to right within each sub-metric

layers of the cell) to the core of the cell. All 5 sets of electrodes show some material cracking at the core of the electrode due to being tightly wound. Significant areas of electrode material separation from the current collector are indicated by blue circles and of lithiated electrode material are indicated by red brackets.

Comparing groups 2 and 4 shows that visually both the electrodes have been affected in a similar fashion. The anodes have experienced some active material detachment from the current collector, especially at the core and halfway segments. This could be due to mechanical stress and the brittle nature of graphite. The delithiation of the anode material is homogeneous indicated by the even grey/black colour of the anode material. The cathodes for groups 2 and 4 have experienced a similar extent of cathode active material cracking and separation.

The cathodes for groups 1 and 3 exhibit similar trends in material separation from the current collector and the existing material separation is minimal. The anodes for groups 1 and 3 on the other hand show some significant differences. Both groups show signs of active material separation and material cracking. Group 1 shows signs of active material stress at the core leading to material separation. Group 3's anode shows significant signs of stress with more graphite delamination occurring at the skin and halfway segments. The separation of the active anode material from the current collector could be a result of concentration gradients causing structural stress within the graphite particles [100]. Ahmed et al. found that delamination at the anode increased with high C-rates, and it was suggested that this could be due to local thermal issues, or the metallic lithium reacting with the binder and destroying its adhesive properties[101]. The anodes in both groups also shows some inhomogeneity in lithium distribution. As the lithium intercalates through the active anode material, the colour of the graphite goes from grey to deep blue to copper to gold as the concentration of lithium increases as shown in Fig. 3.13 [102, 103]. In the group 1 anode, some patches of deeper blue material can be seen at the skin of the cell indicating that there could be some

lithiated material still present in the anode despite the slow discharge to 0% SoC. This could account for some of the loss of lithium inventory, and the cause for the trapped lithium could be due to the loss of electrical contact resulting in the loss of active material at the anode. Inspecting the group 3 anode shows a significant amount of trapped lithiated material is present in the form of deep blue patches throughout the electrode but more significantly at the skin and halfway segments similar to the uneven lithiation seen by Cannarella et al. [28]. This confirms the suggestion that loss of active material identified in the ICA/DVA analysis could be attributed to the anode and may be caused by loss of electrical contact, particle cracking and delamination of active material from the current collector as a result of mechanical stress.

To investigate the impact of trapped lithiated material in the anode, another cell from each of groups 1 and 3 was partially discharged to 20% SoC and then opened to study the lithiation of the anode. The cells were opened in an argon filled glovebox and were visually inspected. Fig. 3.15(a) shows both sides of the anode and cathode for group 1 and Fig. 3.15(b) shows the same for the group 3 cell. The anode in group 1 has a deep blue horizontal band through the middle of the electrode on both sides that indicates partial lithiation. The reddish copper-coloured regions at the core indicate that the graphite is at an even higher lithiation state [104] which is indicated on the images by the blue bracket. The copper-coloured region of higher lithiation at the core of the anode surrounds a patch of unlithiated graphite which clearly shows the inhomogeneous lithium distribution in the anode and may indicate some loss of electrical contact or electrolyte contact. The unlithiated region being surrounded by a lithiated border could indicate some additional stress is being experienced in that region which may have led to loss of electrical contact. The rest of the anode, both front and back, exhibit some patches of higher lithium concentration at the skin of the cell, however this is not as significant as the inhomogeneity at the core. Both sides of the cathode look similar

to the pristine cathode in Fig. 3.14(a) apart from some material separating from the current collector at the core which could be due to the unwinding of the jelly roll.

Studying the anode in group 3 shows there is more lithiated active material present compared to group 1. Even though the cells were discharged to the same voltage, the higher resistance of group 3 may have caused the cell to hit the cut off limit earlier. There is a thick horizontal band of copper coloured lithiated graphite in the middle of the anode front. Within the copper band there is a thin section that is gold (indicated by a yellow bracket) which is especially prominent at the skin, indicating fully lithiated graphite towards the skin of the cell. The back of the anode shows some larger regions of partially lithiated graphite with a fully lithiated stripe of gold through the middle. The back of that anode shows clear patches of unlithiated graphite dotted through the partially/fully lithiated regions from the skin to the core of the cell. Similar to the post-mortem conducted at 0% SoC, this confirms the inhomogeneous lithiation of the anode and the potential loss of active anode material due to loss of electrical contact. The cathode shows some slight separation of the active material from the current collector at the core however the condition of the flipped cathode is similar to that seen in the group 1 cell.

3.5 Summary

To investigate degradation path dependence and its influence on battery state of health, an experimental study was conducted using combined calendar and cyclic ageing profiles designed to isolate path dependent aging. Four groups of cells were subjected to the same ratio of calendar to cyclic ageing and the same overall duration under both aging conditions. The order of the two ageing modes and the C-rate of the cycling was varied between groups.

Capacity data collected during reference performance tests with the pseudo-OCV technique revealed a significant divergence in the degradation paths between groups 1 and 3 (at C/2), whereas groups 2 and 4 (at C/4) showed very little difference in their degradation

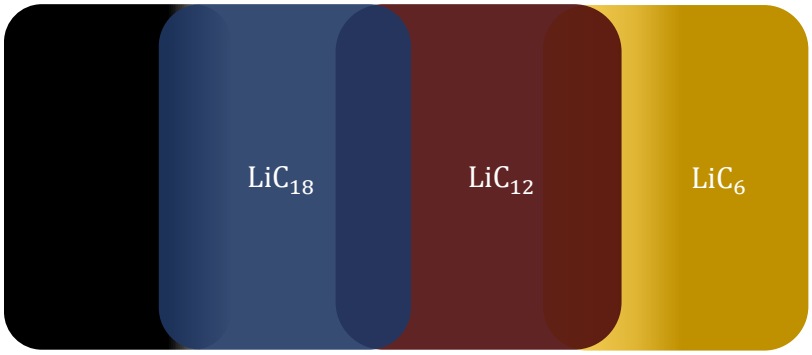

Fig. 3.13 Colour changes of graphite during lithiation

rates. Resistance data supported the interpretation of the capacity-fade data, displaying similar trends. Characterising the EIS data indicates that there is no divergence between the groups for the rate of pure R_{Ohmic} increased. The R_{SEI} increase shows some slight divergence between groups 1 and 3, however R_{CT} showed significant divergence between groups 1 and 3, with group 3 experiencing a higher rate of resistance increase which supports the R_{DC} data. Solely from the capacity and resistance data, we can conclude that the order in which a cell is exposed to calendar or cyclic ageing can impact the rate of degradation. The extent of divergence due to path dependence is subject to the stress factors that the cell is exposed to. The greater divergence between cells cycled at C/2 as compared to C/4 suggests the path dependence is rate dependent. When expressed as a fractional change relative to initial values, path dependence appeared to influence the increase of resistance more strongly than the decrease in capacity meaning that the power capabilities of a cell may be more influenced by path dependence than the cell lifetime, at least according to the cells and profiles tested here. Comparing the data with respect to time versus FEC highlights the significant positive

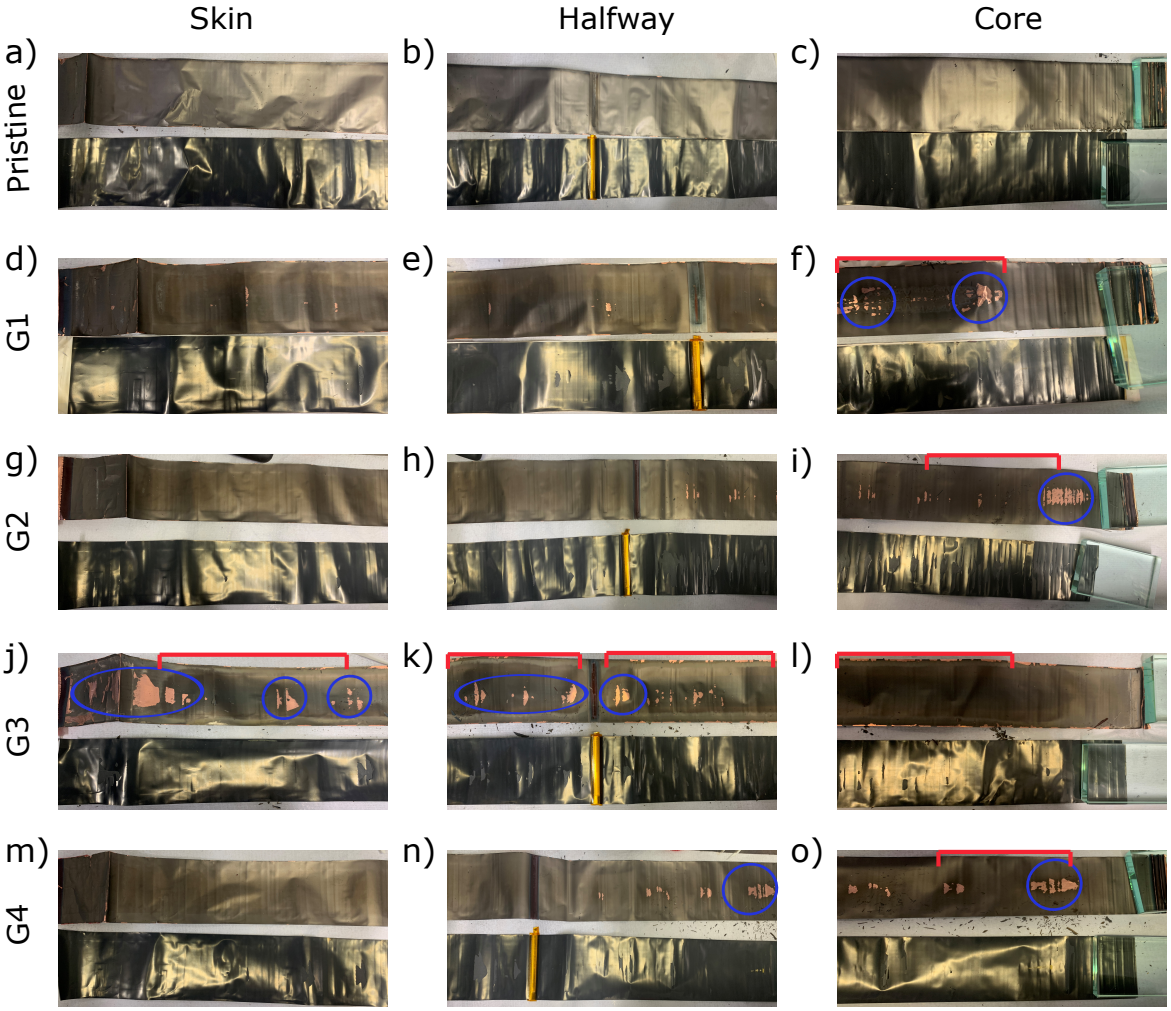

Fig. 3.14 Extracted anode (top) and cathode (bottom) for post-mortem analysis of a pristine cell (a), (b), (c); group 1 cell (d), (e), (f); group 2 cell (g), (h), (i); group 3 cell (j), (k), (l); group 4 cell (m), (n), (o).

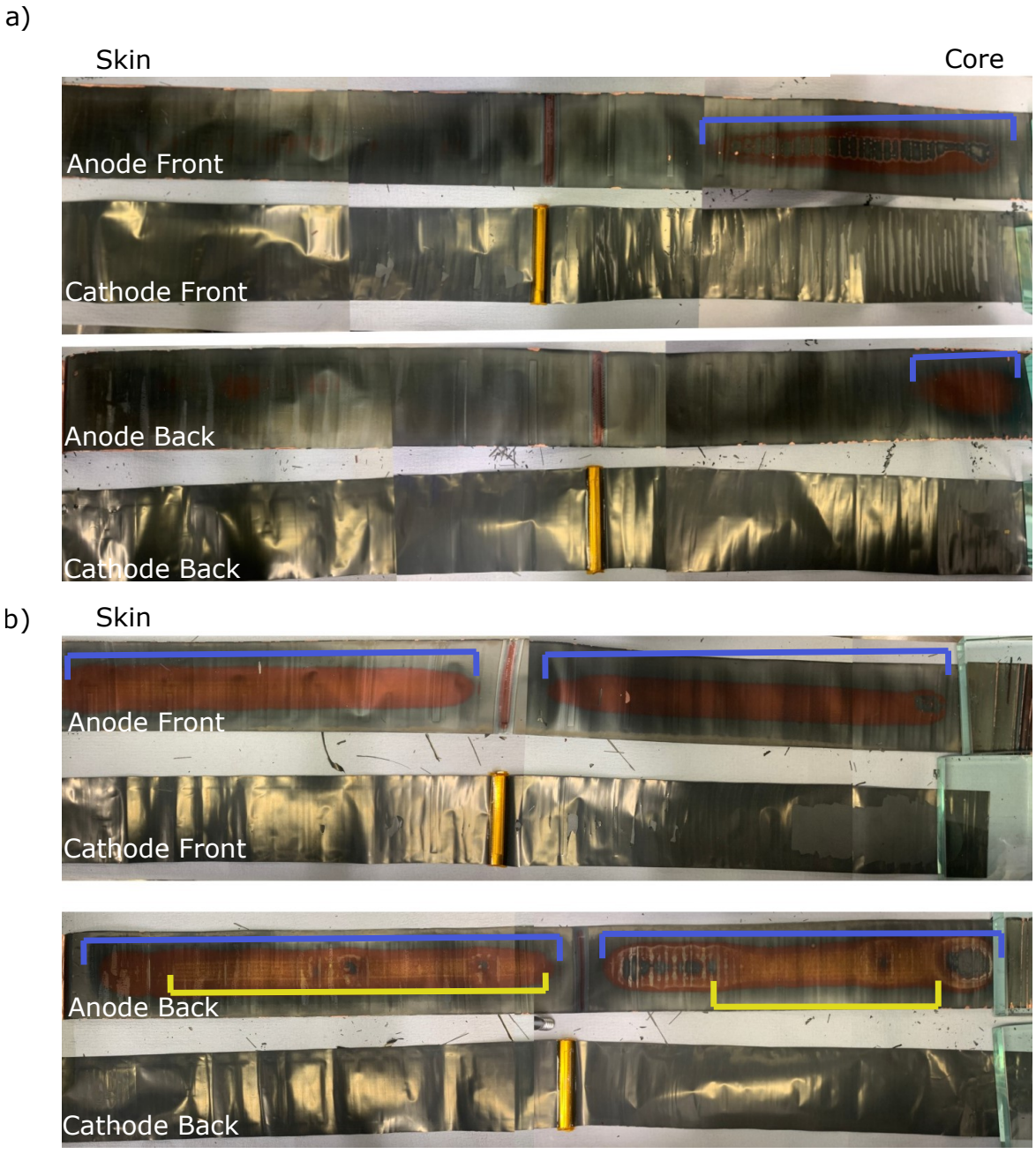

Fig. 3.15 Both sides of electrodes extracted from a partially discharged cell from (a) group 1 and (b) group 3

impact that frequent, short relaxation periods can have on cell lifetime and divergence in degradation trends.

The ICA and DVA data comparing groups 2 and 4 confirmed that the cells cycled at the lower rate experienced similar degradation mechanisms and degraded at similar rates. The IC/DV analysis conducted on groups 1 and 3 showed that the features of interest change at different rates. The group 3 signatures showed the features of interest shrinking and shifting at a greater rate than group 1. The impact of ageing on the individual electrodes was studied by comparing DVA of the aged cells to similar data gathered from half-cells. The difference in ICA/DVA signatures between groups of cells aged at C/2 suggests that path-dependent degradation is most prominently a product of the difference in the rate of loss of active material at the anode. This was further confirmed by quantifying the characteristic capacities obtained from the full cell DVA signatures, which also showed that the greatest difference in characteristic capacity loss occurs at the negative electrode.

Conducting a visual inspection of the electrodes showed that both electrodes in groups 2 and 4 exhibited similar stress patterns. The anode for groups 2 and 4 showed similar signs of deterioration at the core and halfway segments while the cathode shows little indication of ageing. The cathodes for groups 1 and 3 also showed very slight signs of deterioration at the core. The anodes for groups 1 and 3 showed some significant differences in the structural integrity of the graphite coating which was extremely brittle in group 3. This could be due to the mechanical stress of the volume changes during de/intercalation. Although the cells were fully discharged, sections in the group 3 anode were still partially lithiated which could indicate that there is trapped lithiated material due to the loss of electrical contact. Inspecting the partially lithiated anode confirms that group 3 experiences less homogeneity of lithium distribution through the anode, with patches of unlithiated graphite which could be due to loss of electrical contact. This confirms that the difference in the rate of degradation seen between groups 1 and 3 could be due to the loss of active material at the anode. The partial lithiation

of the LAM_{ne} along with the expected SEI formation could account for the difference in the balancing capacity between groups 1 and 3 seen in the quantification of the DVA signatures.

From this experimental campaign, it was identified that the order of calendar and cyclic ageing can impact the rate of degradation. The extent of this divergence is rate dependent with cycling at higher c-rates encouraging the difference in the rate of cell degradation. The difference in the rate of degradation impacts the rate of power fade more than the rate of capacity fade under the designed load profiles. This indicates that path dependence has a greater influence on the cell performance than the cell lifetime under the specified load profiles. The divergence between the groups is encouraged by the CC cycling leading to increased mechanical stress at the electrodes which results in the loss of active material at the negative electrode due to mechanisms such as particle cracking and loss of electrical contact. The frequency of OCV relaxation periods has a significant influence on the rate of degradation. The shorter but more frequent calendar ageing allows for improved lithium distribution which limits the stress through the electrode and reduces the rate of degradation. The difference in degradation caused by the frequency and duration of relaxation periods during cycling highlights the inaccuracy of assuming calendar and cycling ageing can be cumulative. By incorporating the understanding of path dependence into lifetime degradation models, the accuracy of lifetime predictions and warranties for Li-ion batteries in EVs as well as other applications such as grid storage could be improved.

Chapter 4

Experimental Campaign 2

4.1 Objective

A second experimental campaign was conducted to further explore path dependence and to examine some of the choices made in the design of experimental campaign 1 that could have influenced the path dependence that was observed. The first issue that was addressed was the selection of cells, as described in section 2.1.1 and Fig. 2.2. In experimental campaign 1, cells of similar initial capacities were grouped together, which led to some groups having a higher average capacity than others. The normalised degradation data shows that groups 2 and 4 had similar degradation trends, even though the differences in average initial capacity were largest within those two groups. This indicates that the cell screening used in the first campaign likely did not have a significant impact on the exploration of path dependence, which is to be expected [67]. To ensure that the initial cell selection within each group does not unduly influence the rate of degradation, especially when cycling at higher C-rates, the cells in experimental campaign 2 were selected differently. Instead of clustering their initial capacities, a mix of a lower, mid, and higher initial capacity cells within a specified range as described in section 2.1.1 was selected for each test group to ensure that the average initial capacity was similar for all four groups of cells tested.

The second design choice made in experimental campaign 1 was the use of constant current cycling. The results from experimental campaign 1 showed that C/2 constant current cycling, i.e., the highest rate that was tested, produced a divergence in degradation rates between groups. It was identified that one of the causes for the difference in degradation rate could be the inhomogeneous lithiation of the anode, leading to increased stress resulting in a different rate of loss of active material at the anode between groups 1 and 3. To understand the influence of constant current cycling used in experimental campaign 1, the second experimental campaign incorporated constant current constant voltage cycling instead. Using CCCV cycling can encourage degradation in cells since they spend longer at higher potentials. However, the constant voltage step ensures that the lithium distribution in the electrodes is homogeneous by the end of the charge or discharge, and the cell reaches equilibrium at the maximum voltage limit. Using CCCV also guarantees that the cell is cycled through the whole voltage window and there is no drift in cycling end conditions due to resistive influences. Even though CCCV cycling may encourage ageing with respect to FEC, within a period of time cells cycled exposed to CCCV cycling will experience fewer cycles than those with CC cycling, which could result is less degradation. Since the greatest divergence between test groups in the first campaign was observed between the two groups cycled at C/2, the tests in this campaign were all run with a C-rate of C/2.

The final condition to address in this second campaign is the reset of state of charge at the beginning of each calendar ageing period. The calendar ageing condition in the first experimental campaign was set to 90% SoC. The 90% SoC condition was updated according to the most recent capacity test data before each calendar ageing period so as to ensure all the cells under test were calendar aged at the same SoC. However, as the cells aged the corresponding open circuit voltage at 90% SoC changed, which led to the cells calendar ageing at slightly different open circuit voltages as their capacity trajectories diverged. Because of this effect, since group 3 experienced a more rapid rate of capacity fade, the

cells in groups 3 were set to an increasingly lower voltage during calendar aging compared to the cells in group 1. By the EoL, there was a difference of 24.3 mV between calendar ageing conditions. Calendar ageing studies have shown that degradation is accelerated in cells that are calendar aged at higher voltages. This could mean that the rate of degradation in group 3 was slightly underestimated in later life. Nonetheless, this is not significant enough to invalidate previous results—despite being calendar aged under less stress, group 3 still experienced a greater rate of capacity fade overall, indicating that the influence of path dependence may even have been underestimated. To understand the influence that this calendar aging condition may have on path dependence, two groups of cells in the second campaign were chosen to be calendar aged instead at the maximum voltage limit (4.2 V), providing a comparison versus the other two groups in this second campaign, which were held at 90% SoC (i.e., using the same method as the first campaign).

4.2 Profile Design

Following a similar procedure to the first experimental campaign, all four groups were subjected to the same 1:5 ratio of cyclic to calendar ageing periods but in different orders. Cells in group 7 were exposed to one day of CCCV cycling followed by five days of calendar ageing at 90% SoC, while cells in group 8 were exposed to 2 days of CCCV cycling followed by 10 days of calendar ageing at 90% SoC. The SoC in both these groups was reset with the same method as previously described for the first campaign. Cells in groups 9 and 10 experienced the same cycling conditions as groups 7 and 8, respectively. However, the calendar ageing for groups 9 and 10 was conducted by setting the cells to 4.2 V with a C/2 CCCV charge after they had been cycled. All calendar ageing was conducted under open circuit conditions. The CCCV cycling for all groups in this campaign was conducted between 2.5 V (0% SoC) and 4.2 V (100% SoC) with a C-rate of C/2 during the constant current phase, and the CV phase continuing until the current dropped to 0.05 A. Similar to the first

experimental campaign, a symmetrical C-rate for charge and discharge was used to limit any uncontrollable stress factors that may lead to difficulty in isolating the influence of path dependent degradation. An overview of the groups and the two calendar ageing conditions is shown in Fig. 4.1(a). A schematic of the combined load-profile conditions and the current profiles for groups 7-10 are presented in Fig. 4.1 (b),(c),(d).

4.3 Results

Comparing the results of groups 7 and 8 provides some insight into the influence of path dependence under CCCV cycling conditions, while maintaining the same calendar condition (90% SoC) used in the initial campaign. The discharge pseudo OCV capacity data presented in Fig. 4.2 shows that group 7 experienced an average capacity loss of 14.3% while group 8 experienced an average loss of 16.1%, suggesting that path dependence likely has some influence for the cells exposed to CCCV cycling as a function of time. The capacity fade for groups 7 and 8 with respect to FEC also follow the same trends, with little divergence in degradation between the two groups. The instantaneous DC resistance data for groups 7 and 8 in Fig. 4.2(c) and (d) were collected at 50% SoC with a 1.5 A discharge pulse and further confirm this, following a similar trend to the capacity data. Group 8 experienced a slightly higher rate of resistance increase in time compared to group 7 but followed the same degradation trends in terms of FEC.

Groups 9 and 10 incorporated both CCCV cycling and calendar ageing at the same maximum voltage limit. The capacity fade shows some divergence with respect to time, with group 9 experiencing an average capacity fade of 14.5% and group 10 experiencing 17.4%. However, these groups follow similar degradation trends in terms of full equivalent cycles. The resistance data also shows a similar divergence between groups 9 and 10 with respect to time but not with respect to FEC. The rate of capacity fade and resistance fade decreases suddenly at the second RPT (approx. 100 days/ 100 FECs) for all three cells in

a)

	90% SoC	100% SoC
1 day Cycling 5 days Calendar	7	9
2 days Cycling 10 days Calendar	8	10

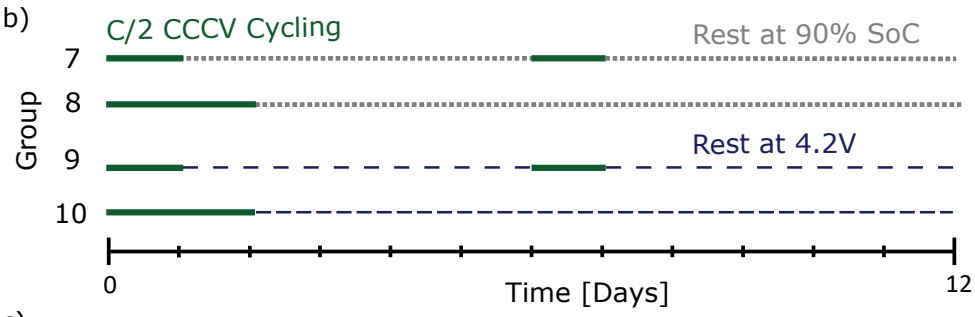

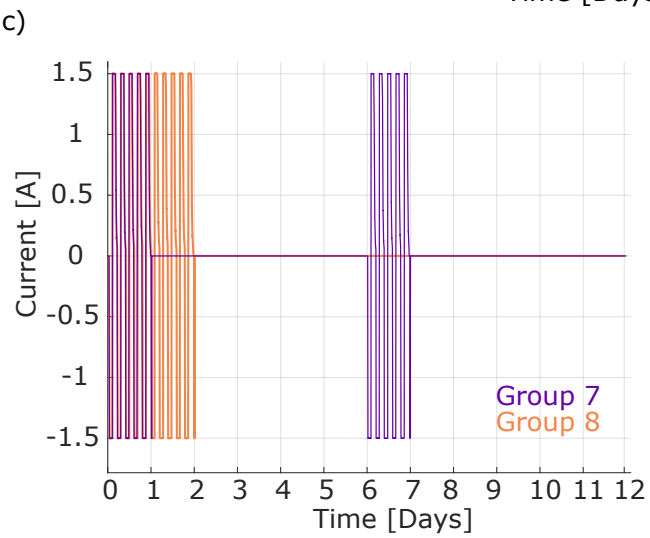

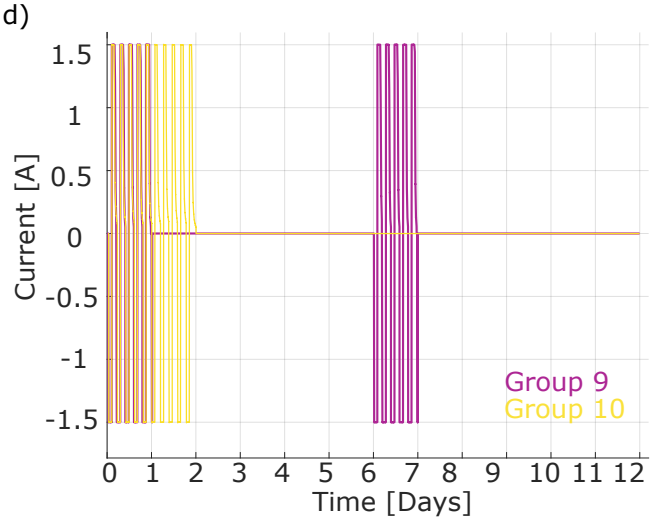

Fig. 4.1 (a) Overview of the combined CCCV cycling and calendar ageing at 90% SoC or 100% SoC shown for groups 7-10 (b) schematically for groups 7-10 (c) the current profile for groups 7 and 8, (d) the current profile for groups 9 and 10

group 9. After studying the data collected before and after this RPT, there was no clear cause identified that could result in this change in the rate of degradation.

Comparing the normalised resistance and capacity data indicates that the cells experienced a greater power fade than capacity fade in relative terms, similar to the data seen in the first experimental campaign. The equipment used to conduct the second experimental campaign had a lower current limit of ± 5 A compared to the ± 10 A current limit of the tester used in the first experimental campaign. Due to this limitation, the pulse power characterisation test conducted in this campaign was limited to the 1.5 A charge and discharge pulse at 80%,50% and 20% SoC; the 10 A discharge pulse was omitted.

Due to Covid-19 restrictions while running this experimental campaign, it was not possible to access to some equipment, hence the testing for cells in groups 7, 8 and 9 were stopped earlier than the cells in group 10. These limitations also meant that the EIS tests for groups 7, 8 and 9 were conducted after a prolonged calendar ageing period of around 5 months. The Nyquist plots in Fig. 4.3 show the EIS data collected across the various states of charge at the beginning of life and at the end of life. The BoL data in Fig. 4.3(a), (b), (c)shows all cells having similar EIS signatures at 20% , 50% and 80% SoC, respectively. As the cells age, a slight divergence can be noted between groups 7 and 8, with the latter ageing at a higher rate. The EIS data for groups 8 and 9 follow similar trends as the cells age. These observations follow the degradation trends seen already in the capacity and resistance data. Due to the cells in group 10 being under test for longer than those in groups 7, 8 and 9, it is not possible to directly compare the end of life EIS data, as they were not collected under similar health conditions. Temperature data was collected every second throughout testing, using thermocouples attached to the surface as described in chapter 2. The temperature during calendar and cyclic ageing is shown in Fig. 4.4 and this enables the thermal data collected under each ageing condition to be studied individually, with each interval accounting for 0.5 °C. Similar to the thermal data presented in the first campaign, the RPT temperature data

has been omitted since during RPTs the thermal variations were assumed to be comparable across all cells. The thermal data during calendar ageing show that group 7 is most frequently resting between 21.5 °C and 22 °C, groups 8 and 9 are most frequently resting between 22.5 °C and 23°C, while group 10 calendar ages at a slightly higher temperature of 24 °C to 24.5 °C. Group 10 was conducted in a separate thermal chamber which could indicate why there is a difference between the thermal data collected compared to groups 7, 8 and 9. A study conducted by Preger et al. exposes the same NCA 18650 cell used in this study to various temperatures. Comparing the difference in the degradation data collected for cells tested under 25 °C and 35°C indicates that a difference of 10 °C results in a small difference in the rate of degradation [105]. From this it can be assumed that the difference caused by testing group 10 cells in a different chamber and the difference of 2 °C between groups would not lead have a significant impact on the rate of degradation. Comparing the temperature data collected during cycling for groups 7 and 8 shows that group 7 cycles most frequently at a significantly lower temperature of 23°C to 23.5°C compared to group 8 which is most frequently between 25 °C and 25.5°C. The higher temperature experienced by group 8 could be a result of the longer continuous cycling duration. A similar trend is seen when comparing the cycling temperature of groups 9 and 10. Group 9 is most frequently between 24.5 °C and 25 °C during cycling while group 10 is most frequently at 26 °C to 26.5°C. The difference in temperature due to the different calendar ageing conditions could be leading to the difference in cyclic ageing temperatures between groups 7 and 9.

4.4 Analysis and Discussion

The capacity and resistance data collected indicate that by changing the constant current cycling to CCCV cycling, and changing the calendar aging conditions, the influence of path dependent degradation has changed significantly compared to the previous campaign.

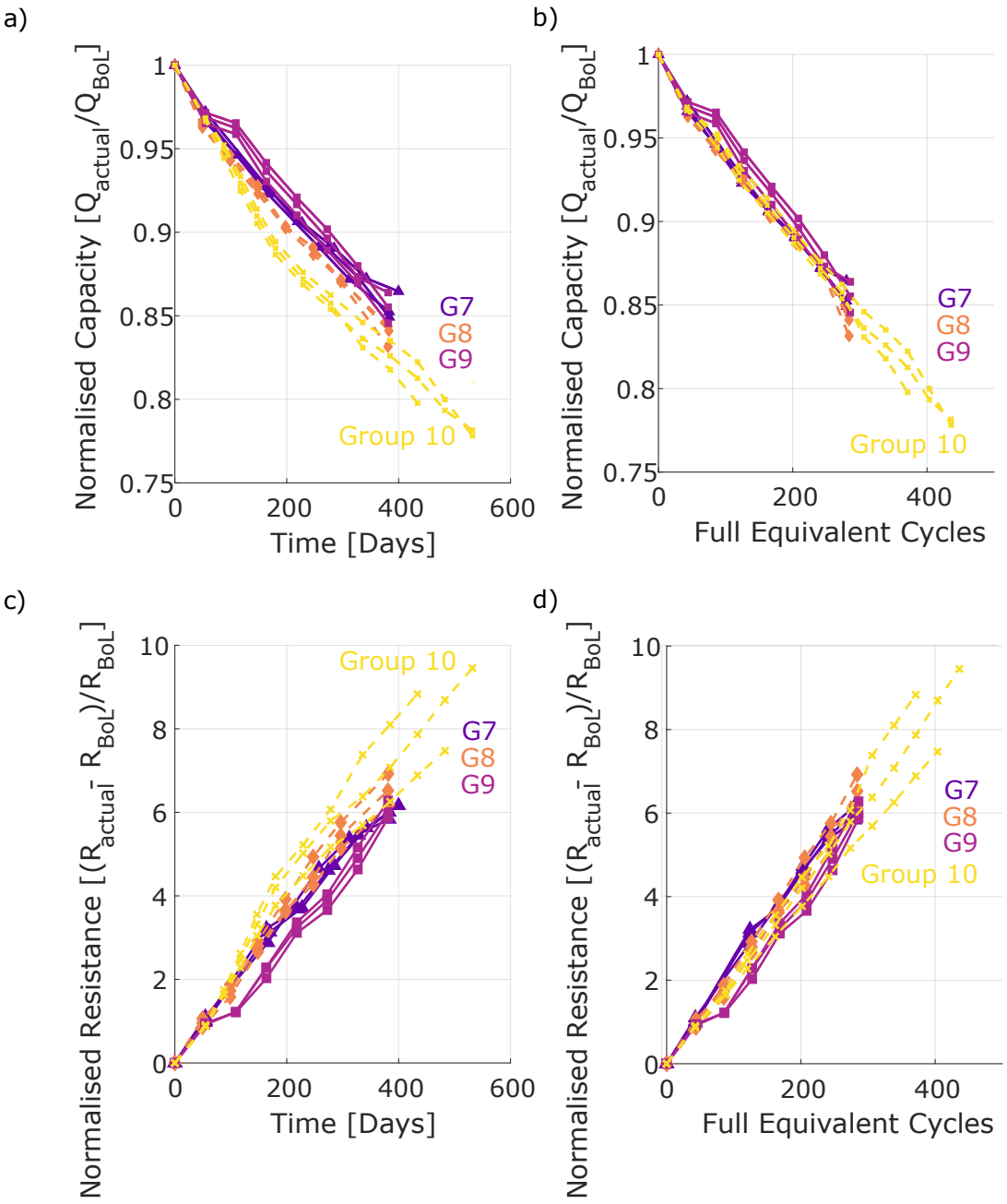

Fig. 4.2 Normalised pseudo OCV capacity data for groups 7 to 10 with respect to (a) time and (b) full equivalent cycles; Normalised resistance data with respect to (c) time and (d) full equivalent cycles

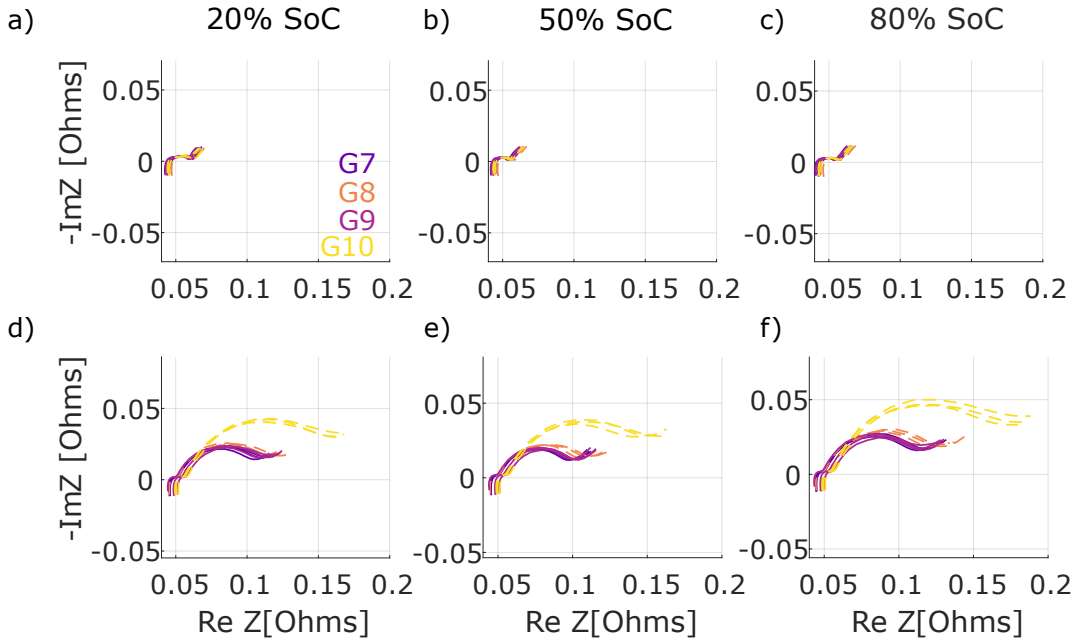

Fig. 4.3 Nyquist plots of EIS data for groups 7 to 10 collected at the BoL at (a) 20% SoC, (b) 50% SoC, (c) 80% SoC and at EoL at (d) 20% SoC, (e) 50% SoC and (f) 80% SoC

The temperature data presented in Fig 4.4 show that groups 8 and 10 that were cycled continuously for a longer period of time are around 2 to 3 degrees warmer in general than the groups that were exposed CCCV cycling interspersed with calendar aging. The different thermal chamber in which the cells in group 10 were cycled could also have influenced the difference in temperature however this difference would have had minimal impact on degradation. The longer continuous duration of cycling could be leading to an increase in internal temperature of the cell. The cycling temperature in general is lower than that seen in experimental campaign 1. This could be due to the constant voltage step acting as a relaxation period minimising heating that would have occurred during continuous CC cycling. A similar trend is seen in the calendar ageing temperature data, with cells from the groups exposed to shorter continuous durations of calendar ageing being 1 to 2 degrees cooler than the cells held at calendar ageing for 10 days. This could be due to the temperature at the end of the continuous cycling period preceding the calendar ageing period being higher, and hence the cells start calendar ageing at a higher temperature. Groups 7 and 9 experience

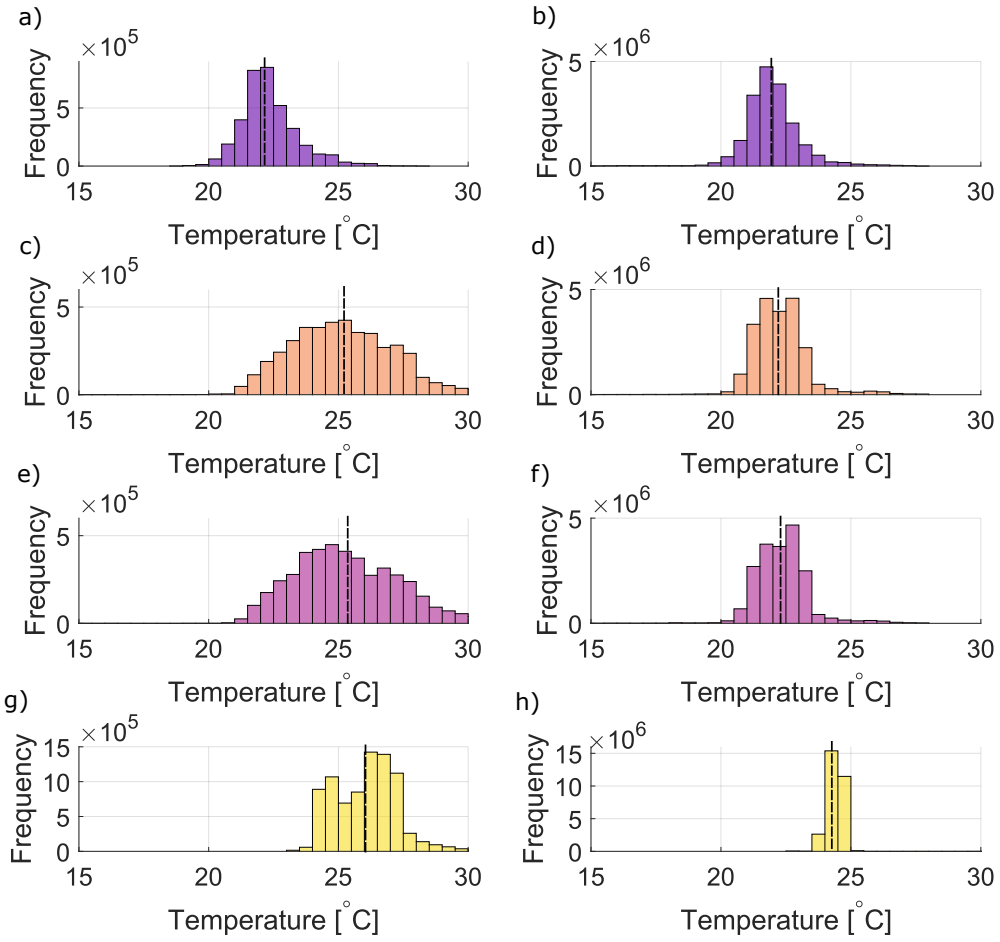

Fig. 4.4 Histogram of temperature for group 7 during (a) cyclic aging, (b) calendar aging; group 8 during (c) cyclic aging, (d) calendar aging; group 9 (e) cyclic aging, (f) calendar aging; group 10 (g) cyclic ageing and (h) calendar aging

similar temperatures and the difference between groups 8 and 10 could be due to the different thermal chamber.

4.4.1 Capacity Fade Analysis and Discussion

The slight divergence with respect to time between the capacity fade data collected for groups 7 and 8 suggests that the cycling with CCCV does not exhibit much path dependence under the conditions tested here, especially since the calendar aging conditions were maintained at 90% SoC. The additional constant voltage step during cycling reduces the concentration gradients within the electrodes (and electrolyte) and improves the homogeneity of the lithium distribution. By limiting the concentration gradients, the mechanical stress caused by rapid intercalation and deintercalation is reduced, which can reduce electrode cracking and passivation layer growth on the electrode surfaces. The impact that the constant voltage step has on the rate of degradation during cycling can be seen in the data plotted with respect to FEC, clarifying that the divergence is not a product of the changed cycling condition under these specific load profiles.

Groups 9 and 10 show a more significant divergence with each other compared to groups 7 and 8 with respect to time. Since the only difference between groups 7 and 8, and groups 9 and 10, is the calendar ageing condition, the influence of path dependence could be encouraged by the 4.2 V calendar ageing condition imposed in groups 9 and 10. This is confirmed by the insignificant divergence seen with respect to FEC. Group 10 experiences longer continuous cycling and spends longer continuous time at a higher potential compared to group 9 which could have encouraged more degradation. Breaking up the continuous time spent at high potentials in group 9 by cycling the cell allows for the cell to be brought to a lower potential which can reduce the rate of SEI formation. The divergence seen with respect to time and not FEC indicates that the difference in the rate of degradation could be a product of the calendar ageing conditions and the cycling conditions when there is no current applied

on the cell. Since group 10 spends a longer continuous duration cycling, the cell is held at 4.2V during the CV step more frequently during the 2 days cycling as compared to group 9 which may also encourage degradation. Since changing the calendar ageing condition from 90% SoC to 4.2 V led to apparent path dependence, this could mean that the divergence seen in the first experimental campaign was perhaps underestimated due to the 90% SoC calendar ageing condition.

Comparing groups 7 and 9, or groups 8 and 10, shows the influence of changing the calendar ageing condition from 90% SoC to 4.2V. With respect to time there is a slight difference in degradation between groups 7 and 9. The divergence between groups 8 and 10 however, suggests that the cells being held at 4.2V for a longer continuous period of calendar ageing results in more rapid degradation compared with those held at 90% SoC. SEI formation may be encouraged by being held at a higher temperature for a longer continuous duration which could cause degradation mechanisms such as pore clogging and material cracking. The divergence exhibited in the data with respect to time instead of FEC indicates that for these combined profiles, the calendar ageing condition may be causing the path dependence, while the CCCV cycling is reducing the influence of path dependence.

4.4.2 Resistance Increase Analysis and Discussion

The resistance data follows the trends seen in the capacity data. There is no significant divergence between all four groups with respect to FEC, however there is some divergence with respect to time. Similar to the capacity data, there is a slight divergence between groups 7 and 8, but a more significant divergence between groups 9 and 10. As already discussed, this could be a product of the cell being cycled for longer continuous periods of time and/or left at a higher voltage for a longer continuous time during calendar ageing which could encourage degradation mechanisms such as SEI formation, binder decomposition or graphite exfoliation. It is interesting to note that for experimental campaign 1, the divergence in the

resistance was greater than the divergence in capacity however, when the ageing conditions are changed in this campaign, the capacity shows a greater influence of path dependent degradation.

Analysing the EIS data and fitting the characteristic resistances, albeit only at beginning of life and end of life, shows that there is no divergence between the four groups in R_{Ohmic} with respect to time or to FEC. Although the EoL conditions for group 10 is not comparable with groups 7,8 and 9, the trends of the characteristic resistance increase are studied. Groups 7, 8 and 9 experience a similar increase in R_{SEI}. However, group 10 diverges from group 9, especially with respect to FEC. Group 10 , experiences a lower increase in R_{SEI} as compared to group 9, even though group 10 experiences a greater increase in R_{DC}. The extended calendar ageing period at a high voltage before the EIS was conducted for groups 7, 8 and 9 may have resulted in additional SEI formation. However, the R_{SEI} as a function of FEC suggests that the difference in R_{SEI} increase is perhaps a function of the cycling condition. A divergence can also be seen in R_{CT} between groups 9 and 10, with group 10 experiencing a higher rate of resistance increase than group 9, corroborating the resistance data collected using the power pulse tests. The divergence in R_{CT} between groups 9 and 10 could suggest that the influence of loss of active material at the electrodes could be leading to reduced active surface area and the difference in the rate of R_{CT} similar to what was seen for experimental campaign 1.

4.4.3 Quantifying Degradation with ICA and DVA

Comparing the ICA signatures for a representative cell from groups 9 and 10 indicates the signatures for both cells are similar at the BoL as seen in Fig. 4.6 (a) with the difference between the signatures shown in blue. The signatures for the groups at the EoL presented in Fig. 4.6 (b) shows the slight difference between groups 9 and 10. The most noticeable difference between the two signatures forms at P2. This is similar to the trends seen in

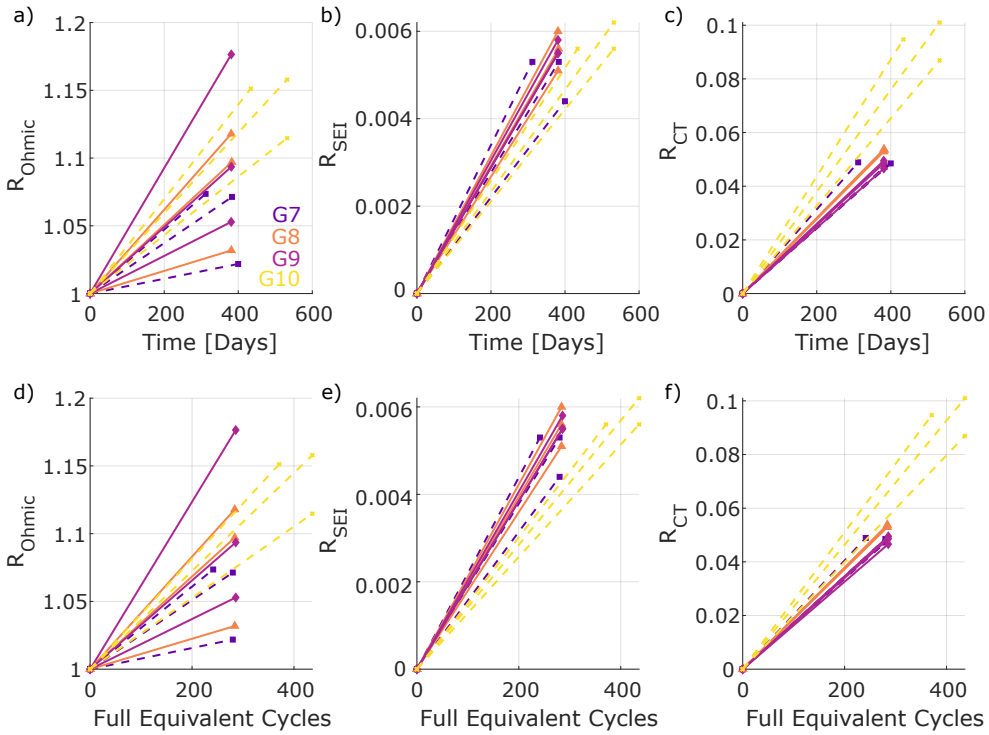

Fig. 4.5 Tracking the changes in characteristic resistances versus time (a), (b), (c) and versus FEC (d), (e), (f)

experimental campaign 1 where the most significant difference occurred at P2 which was attributed to the loss of active material at the anode.

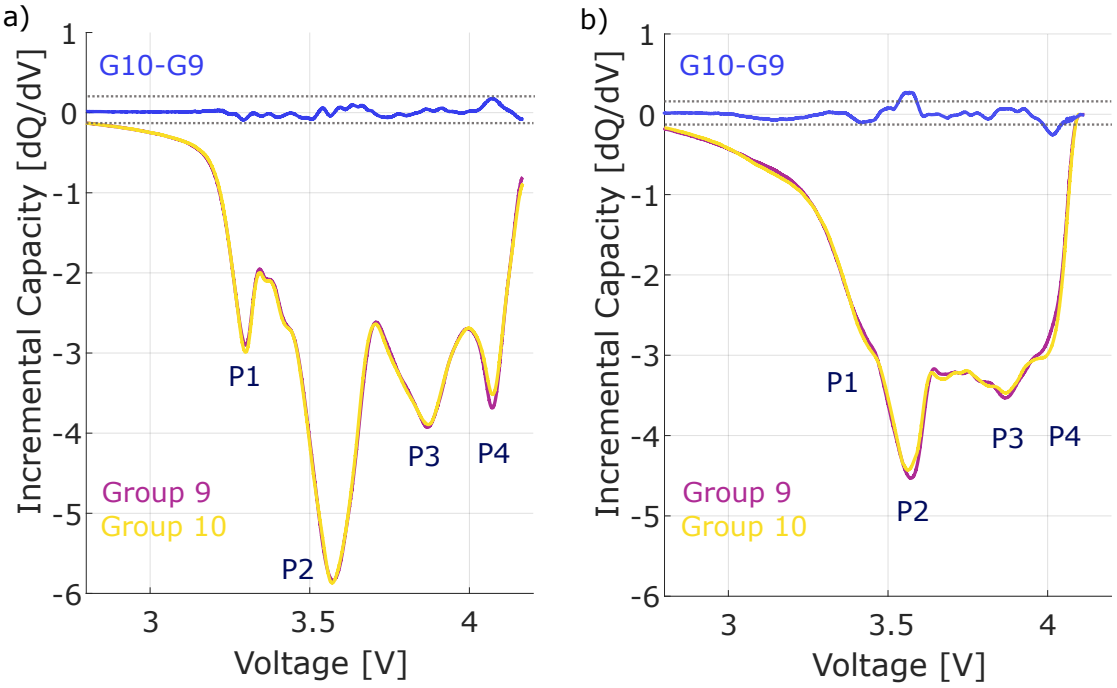

Fig. 4.6 Comparing ICA signatures at (a) BoL and (b) EoL for groups 9 and 10

Differential voltage analysis was conducted on the cell that experienced the least degradation of each of the four groups, as presented in Fig. 4.7, in order to gain insight into the relevant degradation modes. Since the cells used in this campaign are the same cells used in the first experimental campaign, the attribution of the electrode DVA peaks to the full cell DVA peaks is the same as shown in Fig. 3.10. Peaks 1 and 2 are anode dominated and peaks 3 and 4 are cathode dominated. The progression of time is indicated by the arrow from the BoL to the end of test.

The DVA signatures for groups 7 and 8 shown in Fig. 4.7(a) and (b) experience a similar rate of shift and shrink across all four peaks, as might be expected from the capacity data. There is a slight difference between P1 and P2 with group 8 experiencing a greater shrink indicating that the cells in group 8 experience a slightly greater rate of loss of active material

at the anode. The cathode peaks experience a similar rate of shrinking suggesting the loss of cathode material is not a dominating factor leading to the slight divergence.

Since the testing of groups 7, 8 and 9 were suspended before group 10, the thick pink DVA signature shown for group 10 corresponds to the EoL signatures in groups 7,8 and 9. Hence, in order to make a fair comparison and study the difference in DVA signatures of groups 9 and 10, the pink signatures need to be compared. Comparing groups 9 and 10 indicates that P1 and P2 experience a greater shrink in group 10 compared to those in group 9 showing that the divergence could be attributed to loss of active material at the anode, similar to what was seen for groups 1 and 3 in the first experimental campaign. The cathode dominated peaks and the shifting of the peaks due to the loss of lithium inventory are similar for both groups.

Quantifying the characteristic capacities from the DVA signatures as shown in Fig. 4.8, using the same method as previously described and demonstrated for groups 1-4, illustrates these differences more clearly. The lighter bars in Fig. 4.8(d) represent the RPTs that took place after the last RPT of groups 7,8 and 9. The comparison between groups 7 and 8 shows that they experienced similar degradation modes, with group 8 experiencing a marginally more rapid loss of active material at the anode while group 8 experienced a slightly greater loss of lithium inventory ($Q_{Balance}$) than group 7. The mechanism being loss of lithium inventory is supported by the greater average R_{SEI} increase for group 8 seen in Fig. 4.5.

Comparing the capacity loss of groups 9 versus 10 indicates that group 10 experienced a higher rate of active material loss at the anode, while group 9 experienced a larger change in the balancing capacity indicating a difference in the loss of lithium inventory. The more rapid decrease in balancing capacity is supported by the greater R_{SEI} increase for group 9 seen in Fig. 4.5(b) which could account for loss of lithium inventory, and the loss of active material in group 10 could perhaps be attributed to the increased R_{CT} seen in Fig. 4.5(c) .

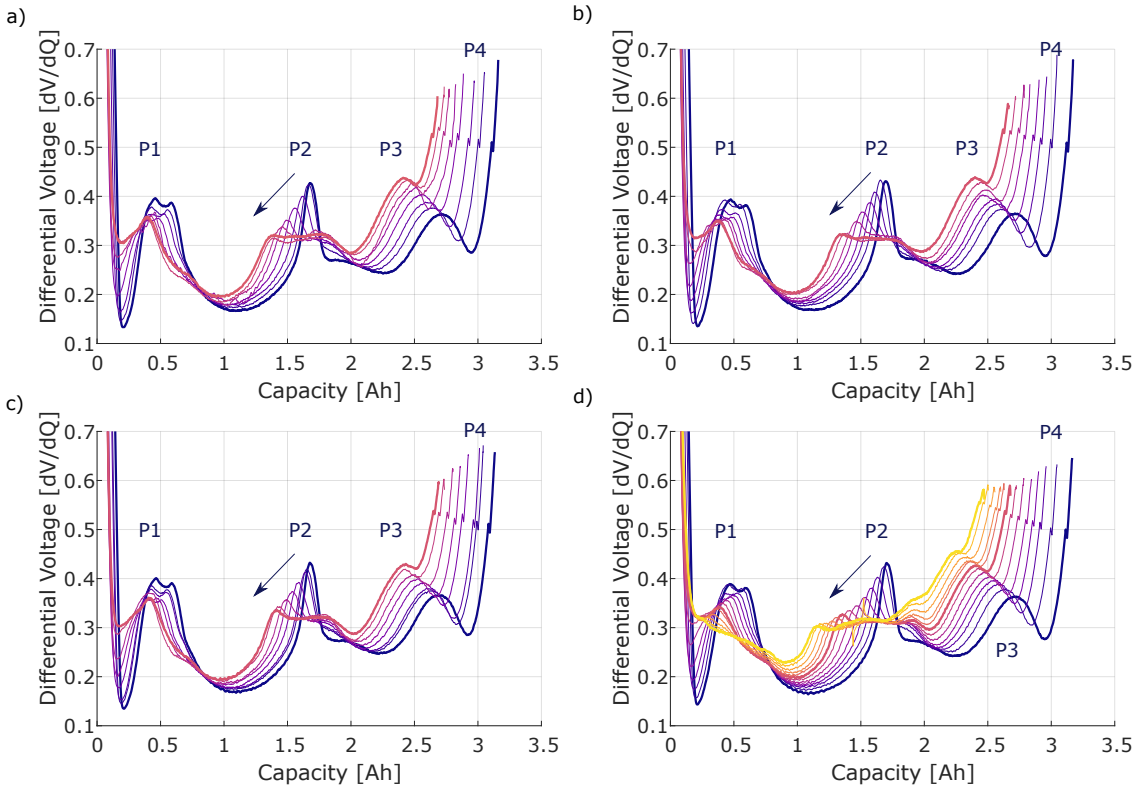

Fig. 4.7 Progression of DVA signatures as the cell ages for (a) Group 7, (b) Group 8, (c) Group 9 and (d) Group 10 with the thick pink line in group 10 corresponding with the last RPT in groups 7, 8 and 9. The arrow indicates the progression of ageing

The overall differences in the DVA signatures suggest that the most dominant degradation mode accounting for the divergence could be the loss of active material at the negative electrode with some slight influences of loss of cyclable lithium caused by SEI formation, similar to what was determined to experimental campaign 1.

4.4.4 Impact of cycling and calendar ageing conditions on path dependence

To illustrate the difference in degradation caused by the different cycling and calendar ageing conditions, Fig. 4.9 overlays the capacity and resistance data from both experimental campaigns and Fig. 4.10 tracks the mean trajectory of each group with the variance in each group indicated by the shaded regions.

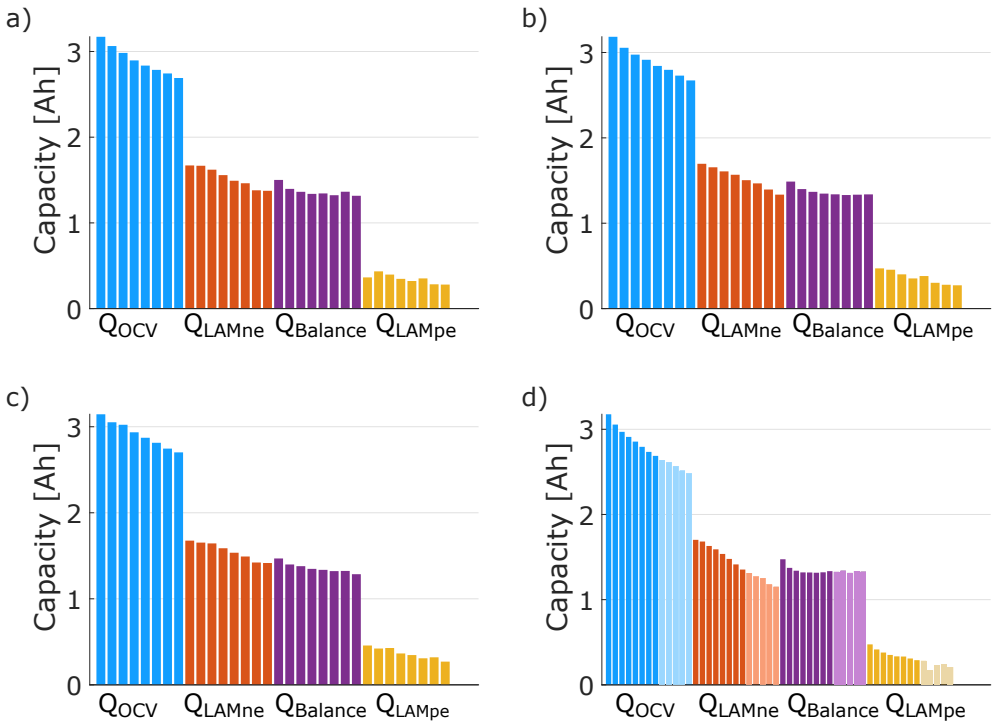

Fig. 4.8 Peak analysis to quantify the changes in electrode balancing and electrode capacity for (a) group 7, (b) group 8, (c) group 9 and (d) group 10 with the lighter bars in (d) representing the RPTs that took place after the final RPT of groups 7 to 9. The progression of time is from left to right.

With respect to time, Fig. 4.9(a), the cells exposed to the lower C-rate (i.e., C/4) during cycling exhibited the lowest rate of capacity fade, which is a result of fewer cycles taking place within a given period of time, and lower stress due to less intensive concentration gradients. However, in terms of FEC/charge throughput, shown in Fig. 4.9(b), constant current cycling even at low C-rates led to a higher rate of relative degradation per cycle—similar to cycling with CC at double the C-rate (i.e., C/2) for a longer continuous duration, and close to CCCV cycling at the higher C-rate. This could be a result of the cells that were cycled at lower C-rates spending longer at voltage extremes. A similar trend is also seen in the R_{DC} resistance data for groups 2 and 4, with the resistance increase falling between the second experimental campaign results and group 3 with respect to FEC, while following the degradation trends of group 1 with respect to time.

An aspect of the C/2 CC cycling (i.e., groups 1 and 3) is the build-up of concentration gradients within the cells, which could cause polarisation, leading to the cut-off voltage limit being reached before the lithium is fully extracted from the electrodes. Since group 3 was CC cycled for a longer continuous duration of time, there was concern that due to the lack of CV "reset" step, a drift in the cycling window would appear over time which would result in the cell cycling through a smaller voltage window, or individual electrodes being pushed beyond their voltage limits. However, a smaller cycling window between the maximum and minimum cut off voltage would lead to less degradation experienced by the cells in group 3. The close agreement of results of the C/4 CC cycled cells (groups 2 and 4) provides some confidence that drift in the cycling window caused by continuous CC cycling may not be a significant issue, at least for the cycling lengths used here, since cycling at a lower C-rate ensures that the cycles through all SoCs of the full voltage window. This is further confirmed by the close correspondence in capacity fade between group 3 and the CCCV cycled cells (i.e., groups 7-10) with respect to FEC, which indicates that group 3 experienced a similar full cycling window compared to the CCCV cycling where the latter

held cells at their maximum cell voltage limit ensuring their internal voltage drops did not trigger a premature suspension of charging. The influence of a smaller cycling window, if any, for group 3 is negligible and does not have a significant impact on the path dependent trends seen between groups 1 and 3.

It is evident that the cells exposed to CCCV cycling (groups 7-10) experienced a higher rate of capacity and especially power fade compared to the cells exposed to CC cycling (groups 1-4). This is expected because the cells exposed to CCCV cycling were held at higher potentials for longer and this increases degradation rate, which can be seen with respect to both time and FECs. Comparing the degradation experienced by groups 1 vs. 7 or groups 3 vs. 8 highlights the different degradation rates as a result of the different cycling conditions (i.e., where the only difference is the switch from CC cycling to CCCV cycling).

The most significant influence of path dependence is seen in comparing between groups 1 and 3 and between groups 9 and 10. The divergence between groups 1 and 3 is greater with respect to full equivalent cycles while the slight difference in degradation between groups 9 and 10 can only be seen with respect to time. This indicates that the length of continuous cycling influences path dependence during CC cycling, while the time spent at 4.2 V is a key factor influencing path dependence when the cells are exposed to CCCV cycling. This confirms that the continuous CC cycling in the load profiles designed for the first campaign illustrated path dependence, which could be due to increased concentration gradients through the electrodes and increased mechanical stress caused by the high C-rates. The CCCV cycling limits the overall lithium inhomogeneity making path dependence less obvious. The increased degradation during calendar aging at 4.2 V, and longer duration spent at 4.2 V during the constant voltage step, however, has a greater impact on path dependence compared to using a 90% SoC setting for the calendar aging portion. This could be due to the longer duration spent at higher voltages encouraging degradation mechanisms such as SEI formation. The difference between groups 1 and 3 with respect to time is more pronounced

in the resistance data while the difference between groups 9 and 10 is more prominent in the capacity data. This is seen in Fig. 4.10 where the mean trajectory of each group is shown along with the variation within each group indicated by the shaded area. This could suggest that the difference in LAM_{ne} in groups 1 and 3 is due to a mechanical effect such as particle cracking and loss of electrical contact, while the difference between groups 9 and 10 is more of an electrochemical effect caused by LLI due to SEI formation resulting in pore clogging leading to differences in LAM_{ne}.

Across both experimental campaigns, the degradation data shows the positive impact that shorter, more frequent calendar ageing periods have during cycling, limiting degradation by allowing the cell time to relax. Groups 1 and 9 experienced less degradation than their comparable partner groups 3 and 10, respectively. Increasing the frequency of open circuit relaxation periods, irrespective of the exact calendar ageing condition, could significantly increase the lifetime of a cell by allowing for capacity recovery and even lithium distribution through the electrodes.

4.5 Summary

The second campaign was conducted in order to gain insight into the influence of path dependence in relation to CCCV cycling and more extreme calendar aging conditions, and to explore experimental design decisions made in the first experimental campaign.

Another aspect addressed with experimental campaign 2 was the cell selection. The cells in the first campaign were grouped based on having similar capacities which led to groups having significantly different initial average capacities. With group 1 having a higher average initial capacity compared to group 3, one of the factors that required clarification was whether the divergence seen in the degradation data was a product of the initial cell selection, specifically whether group 3 aged more rapidly due to the lower initial capacity of the cells. However, this was seen not to be the case—the most significant difference between initial

average capacity due to cell selection was between groups 2 and 4 in the initial campaign however, the degradation trends experienced by the two groups when normalised were not impacted by this. On the other hand, the degradation data collected in experimental campaign 2, that ensured the initial average capacity of all groups was similar, still experienced some divergence between groups, indicating that the initial selection criteria did indeed not seem to lead to different degradation trends when the data were normalised.

Combined load profiles were designed to study the impact of incorporating a CV step during charging, while maintaining the same calendar condition as before, of 90% SoC. The degradation data showed that there was little divergence between the group that was exposed to longer continuous CCCV cycling compared to having calendar ageing breaks during cycling. This indicates that the CC cycling condition in the first campaign is an important factor encouraging path dependence. The CV step during cycling in campaign 2 allowed the cell to relax and the lithium distribution in the electrode to homogenise. This perhaps reduced the mechanical stress, limiting the impact of microcracks or rapid volume changes leading to the loss of active material. However, even with cycling conditions that encouraged homogeneity and aimed to reduce any influence of incomparable cycling conditions, there were still signs of path dependence between groups 9 and 10.

As another comparison, the calendar ageing condition was changed from 90% SoC to the maximum voltage limit of 4.2 V to ensure all cells were experiencing the same calendar ageing stress. Increasing the calendar ageing stress resulted in a divergence between groups 9 and 10 with respect to time. The small path dependant influence seen with respect to time, and not versus FEC, could suggest that the calendar ageing condition is encouraging path dependence. The longer continuous CCCV cycling period and the longer calendar duration at 4.2 V could be encouraging degradation, leading to a higher rate of capacity and power fade in time. The 4.2 V calendar condition encouraging the divergence between groups 9 and

10, suggests that the path dependence seen in the first experimental campaign may have been less severe with respect to time.

The characteristic resistances fitted to the EIS data indicate some divergence in R_{SEI} and R_{CT} between groups 9 and 10, with a similar but less significant trend seen for groups 7 and 8. Groups 7, 8 and 9 experienced a greater rate of SEI formation while group 10 experienced a greater charge transfer resistance increase. Conducting DVA on the OCV curves and quantifying the characteristic capacities confirmed that groups 7 and 9 experienced a more significant change in their balancing capacity (i.e., lost lithium inventory), while the more rapid degradation of groups 8 and 10 could be attributed to a difference in the rate of capacity loss at the anode due to loss of active material.

The results from the DVA quantification supports the EIS characterisation, suggesting that not only is path dependence influenced by loss of active material at the anode in the case of CC cycling, but incorporating CCCV cycling ageing influences the rate of SEI formation. Overall, the incorporation of CCCV cycling reduces the influence of path dependent degradation and calendar ageing at higher SoCs encourages the divergence. The significant impact of path dependence seen between groups 9 and 10 is a result of loss of active material at the anode which is similar to that seen in experimental campaign 1 between groups 1 and 3. The loss of active material at the anode would lead to a reduction in active surface area of the electrode which would increase the current density and can be seen in the difference in charge transfer resistance between groups 9 and 10. It is interesting to note that in experimental campaign 1, it was the power fade that was most significantly impacted by path dependent degradation while in experimental campaign 2, the influence of path dependence is more visible in the capacity data. This shows that not only the order of ageing but also the condition of calendar/cyclic ageing can encourage different degradation mechanisms. The trend of more frequent calendar ageing periods to break up the continuous cycling resulting in improved cell lifetime seen in experimental campaign 1 also holds in experimental campaign 2 when

different cyclic and calendar conditions are incorporated. Increasing the frequency of open circuit calendar ageing can improve cell lifetime as seen for groups 1 and 3 in campaign 1 and in groups 9 and 10 in campaign 2. This confirms the suggestion that the degradation mechanisms caused by calendar and cyclic ageing can encourage and influence each other, leading to different degradation trends.

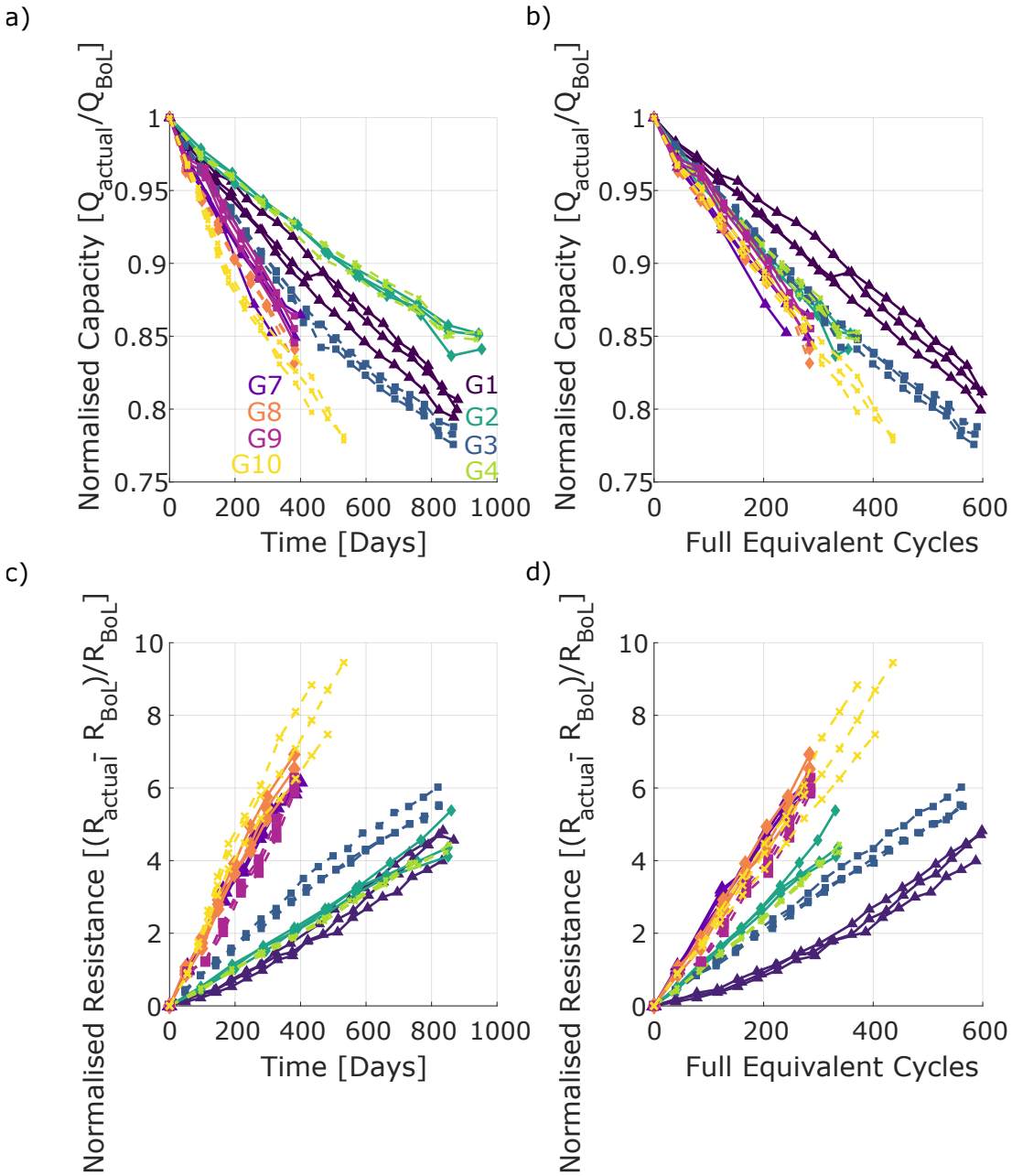

Fig. 4.9 Normalised capacity data for groups 1 to 4, and 7 to 10, versus (a) time and (b) full equivalent cycles; Normalised resistance data for groups 1 to 4, and 7 to 10, versus (a) time and (b) full equivalent cycles

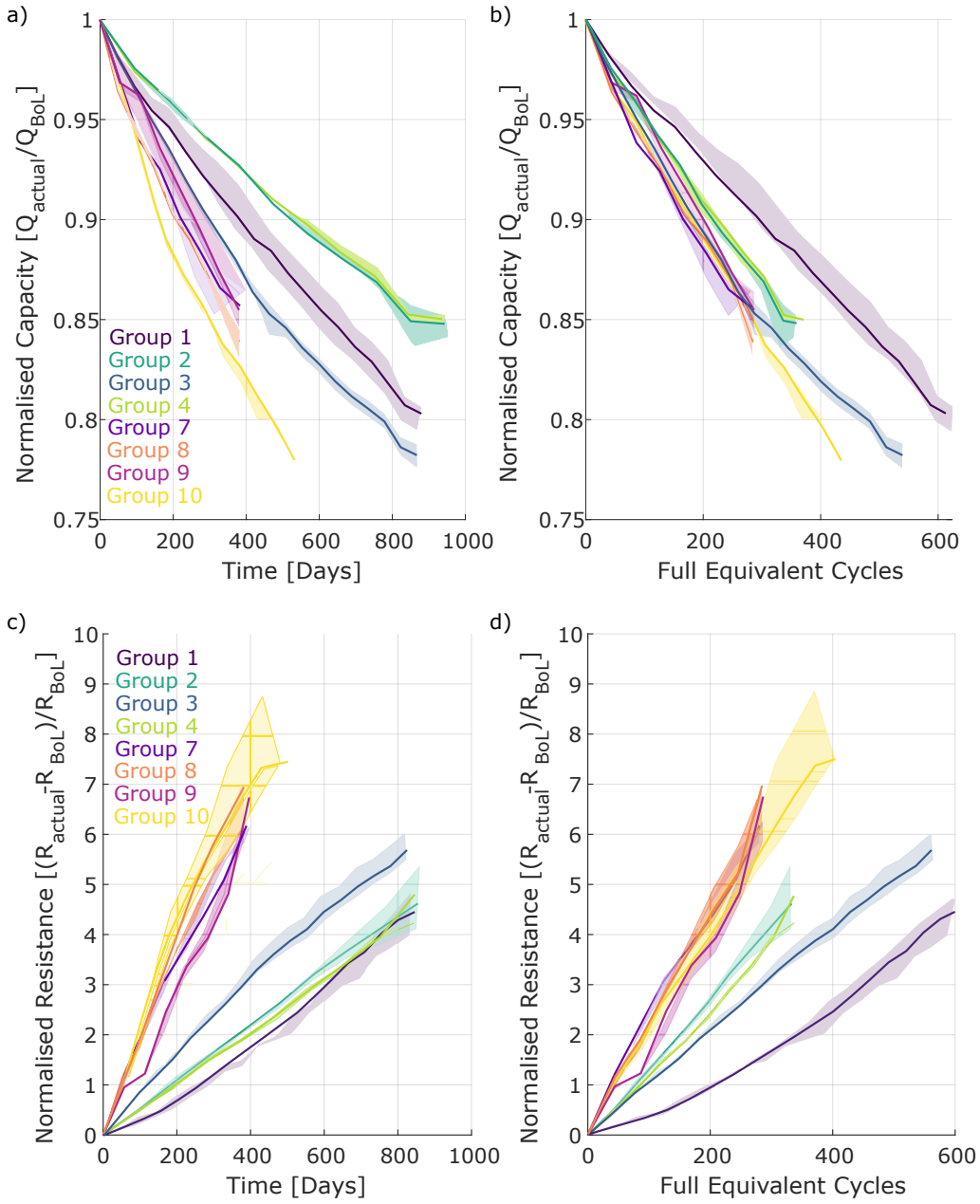

Fig. 4.10 Mean capacity (a),(b) and resistance (c),(d) trajectory of each group with the variation indicated by shading.

Chapter 5

Exploration of the separation of calendar and cyclic ageing in empirical models

It is common for empirical models of battery ageing to assume that calendar and cyclic ageing may be measured separately, and then their impacts added together to 'synthesize' an ageing response for any given 'combined' usage profile [6, 60, 4]. The work of this thesis calls this assumption into question. To investigate this further, here a study is introduced that compares lifetime predictions made under this assumption—that calendar and cyclic ageing are separable—versus actual lifetime measurements from the path dependence experiments discussed previously. In order to facilitate this, two additional datasets were recorded: continuous CC cycling ageing, and continuous calendar ageing (with periodic RPTs). The conditions used in these new tests were the same as those used in the combined profiles implemented in experimental campaigns 1 and 2. Then the cumulative degradation impact of calendar and cyclic ageing of cells exposed to continuous ageing in one mode (calendar or cycling) was compared to the degradation experienced by cells exposed to combined load profiles consisting of a mixture of calendar and cyclic ageing.

5.1 Superimposition of CC Cycling and 90% SoC calendar ageing

In experimental campaign 1, as discussed in section 3.3, the most significant divergence in ageing was experienced between groups 1 and 3, which were both tested at C/2 with CC cycling. Therefore, this chapter focuses on comparing the measured degradation of these two groups with the estimated degradation predicted by assuming that calendar and cyclic ageing can be separated. To conduct the study, an additional group of 3 cells, termed group 5 here, was subjected to continuous constant current cycling with a C-rate of C/2. This ensures that the continuous cycling condition is comparable to the cycling type using within groups 1 and 3. Also, a single cell was calendar aged at 90% SoC, i.e., at the same calendar ageing conditions as used within groups 1 and 3. A single cell was tested under calendar ageing conditions due to equipment limitations, this cell is termed group 6 in this work. Reference performance tests were conducted at a similar frequency to those of groups 1 and 3 to ensure degradation was not being accelerated due to frequent data collection.

The normalised capacity and resistance data collected from the cells experiencing continuous constant current cycling (group 5) are presented in Fig. 5.1(a)-(c) and the degradation data collected from the cell exposed to calendar ageing conditions (group 6) are given in Fig. 5.1(b)-(d). Due to the accelerated nature of the ageing of the cells exposed to continuous cycling, the cells lost an average of 68% of their capacity within less than 300 days or approximately 3264 FEC, while the cell exposed to calendar ageing at 90% SoC lost only 5% of its capacity after being aged for more than 3 years.

The resistance data, collected at 50% SoC with 1.5 A discharge pulse, for continuous calendar and cyclic ageing respectively, follows similar trends to the capacity fade data. However, in relative terms, the increase in resistance is significantly greater than the capacity fade, similar to the data in Fig. 3.2. Due to the rapid degradation of the cells exposed to

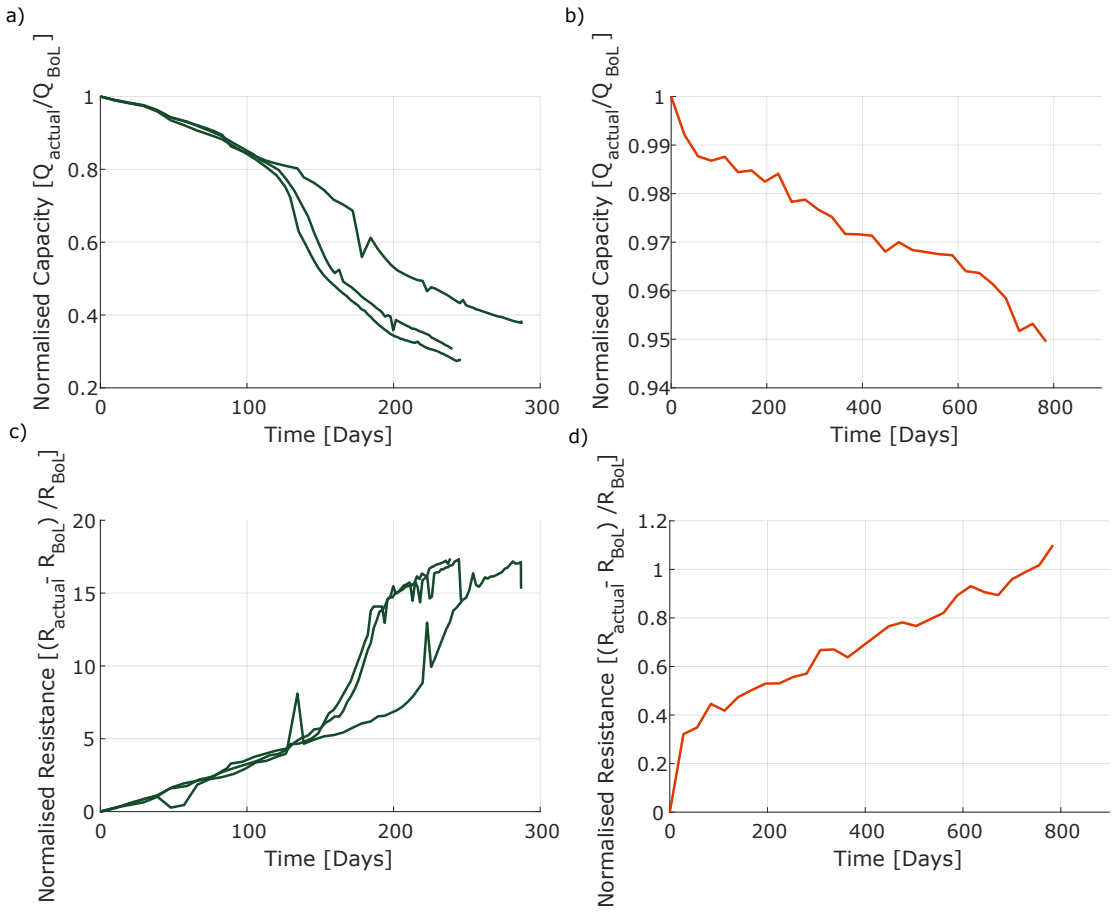

Fig. 5.1 (a) Normalised capacity fade data for 3 cells exposed to continuous cycling, versus time, (b) Normalised capacity fade of a cell calendar aged at 90% SoC versus time, (c) Normalised resistance of continuously cycled cells versus time and, (d) Normalised resistance of calendar aged cell versus time

continuous cycling, EIS data were only collected at the BoL and EoL and are presented in Fig. 5.2. On the other hand, the EIS data for the calendar aged cell, Fig. 5.3, shows the impedance spectra at the BoL, MoL and EoL.

The EIS data shows significant differences in the changes of the characteristic resistances between the cycled versus the calendar aged cells. The cycled cells experience an increase in R_{Ohmic} and R_{SEI} but most noticeably a very large increase in R_{CT}. The calendar aged cells, however, exhibit their most significant change in R_{Ohmic} with some slight changes of R_{CT}.

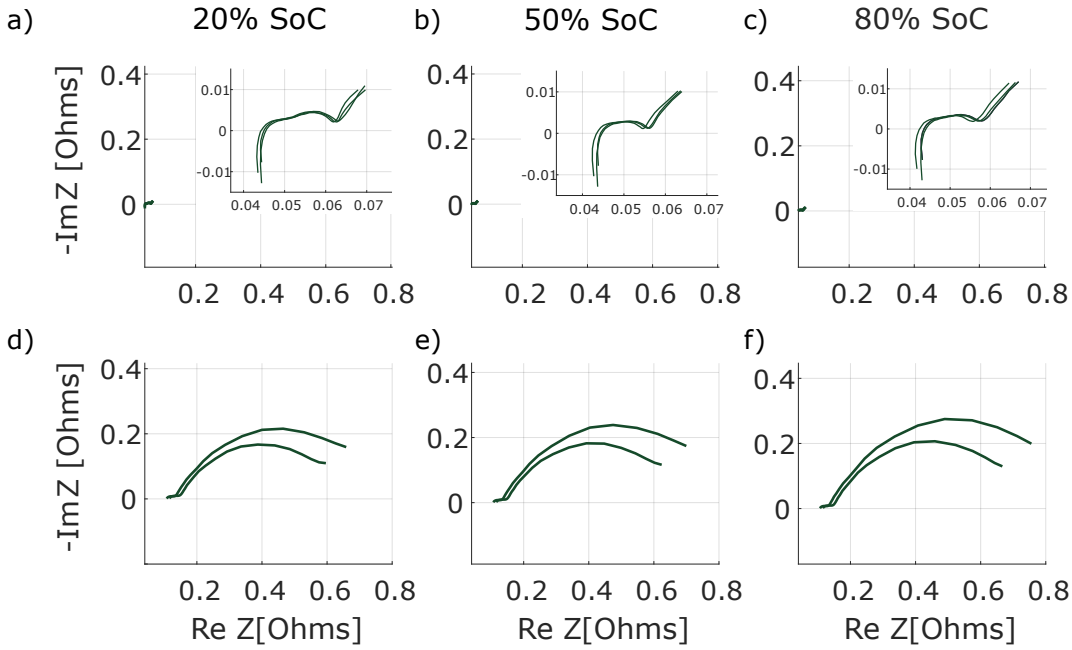

Fig. 5.2 Impedance spectra for cells exposed to continuous CC cycling at BoL at (a) 20%, SoC (b) 50%, (c) 80%, and EoL at (d) 20%, (e) 50% ,(f) 80% SoC

Differential voltage analysis was conducted on groups 5 and 6 using the same techniques as previously outlined. It is clear from the DVA signatures in Fig. 5.4 of cells exposed to cyclic and calendar ageing, that different degradation modes dominate each type of ageing. During calendar ageing, the cell maintains its peak height at P1, P2 and P3 with a shift to lower capacity indicating that the dominant degradation mode is LLI which is likely be due to SEI formation since the cell is being held at a high SoC [27, 74, 19]. The signature for the cycled cell on the other hand shows that it experiences a rapid loss of active material at the negative electrode along with loss of lithium inventory. Due to the different degradation mechanisms taking place under calendar and cyclic ageing, assuming that these various electrochemical and mechanical influences can be consider separately and then summed together may not be valid.

The continuous constant cycling data and calendar ageing capacity fade data given in Fig. 5.1(a)-(b) were used to understand the difference between assuming ageing modes can be superposed and path dependent degradation. Fig. 5.5 shows the average capacity fade

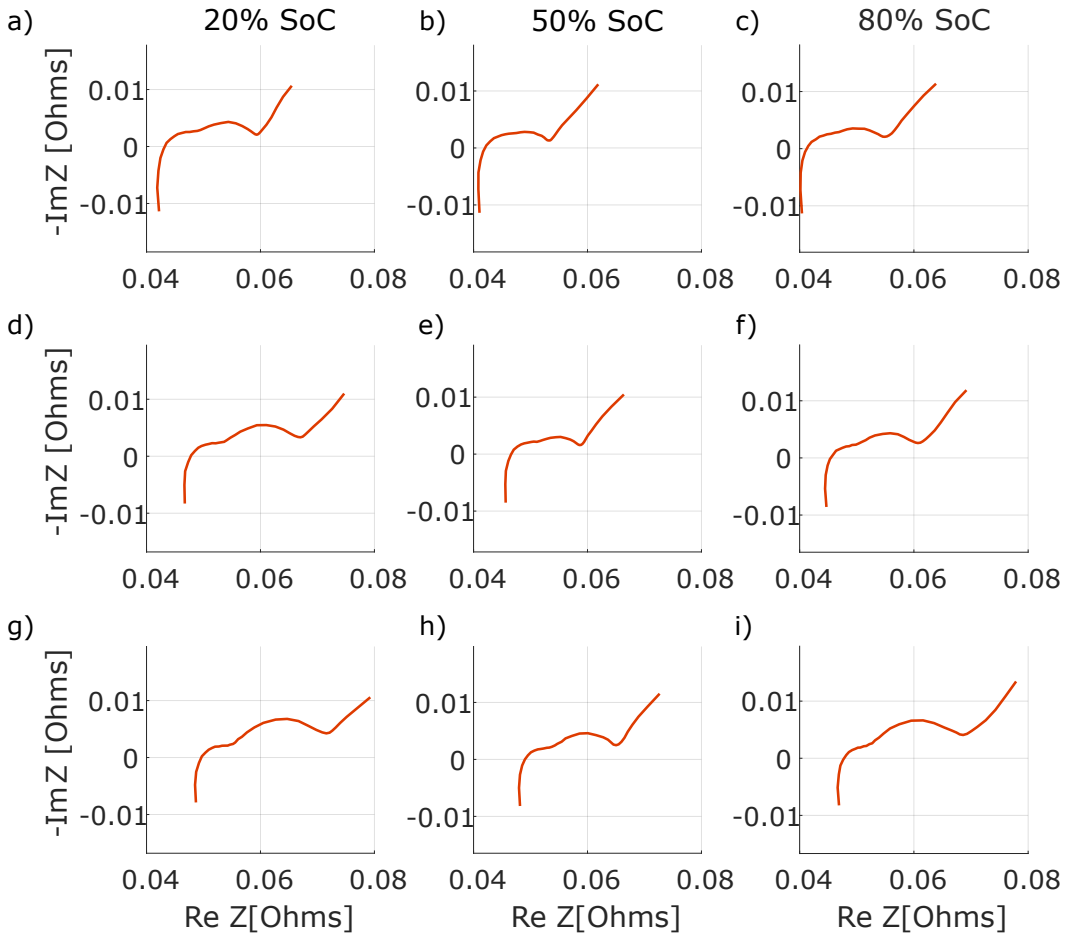

Fig. 5.3 Impedance spectra for the calendar aged cell at BoL at (a) 20%, (b) 50%, (c) 80% SoC; MoL at (d) 20%, (e) 50%, (f) 80% SoC; EoL at (g) 20%, (h) 50% , (i) 80% SoC

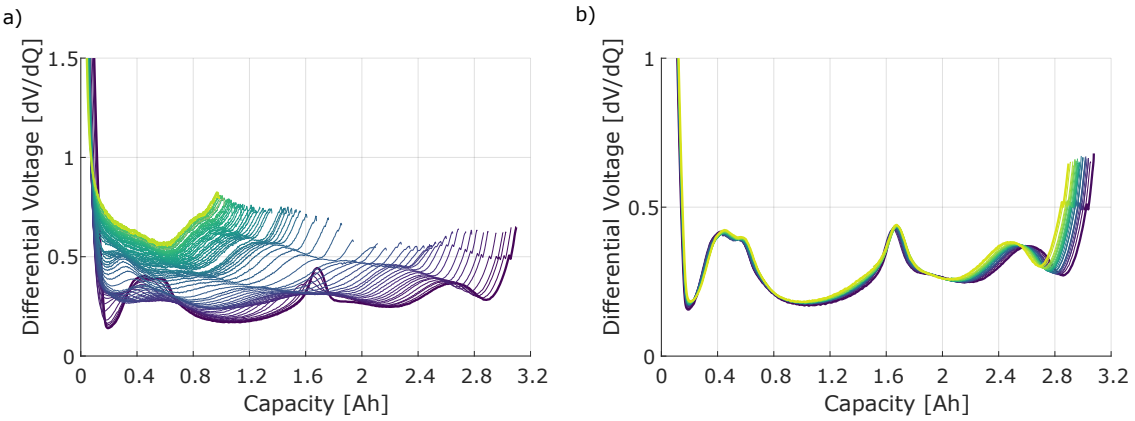

Fig. 5.4 Progression of DVA signatures for (a) a continuously cycled cell and (b) a calendar aged cell

for groups 1 and group 3, the calendar aged cell (group 6) and the continuously cycled cells (group 5). The data collected from experiments (groups 1, 3, 5 and 6) are represented by solid lines. Cells in groups 1 and 3 have experienced 760 days of calendar ageing and 120 days / 623 FEC of cycling by the end of test. The cells in Group 5 lost an average of 0.62 Ah after 120 days and 1.08 Ah after 623 FEC . After 760 days of calendar ageing, the cell in group 6 lost 0.15 Ah. The degradation experienced by cells in group 5 after 120 days/ 623 FEC was summed with the capacity fade experienced by the cell in group 6 after 760 days. This represents the lifetime prediction made with an empirical model that assumes the degradation experienced during calendar and cyclic ageing is cumulative. The cumulative model is shown in dashed lines on Fig. 5.5. The lifetime prediction was conducted for all three cyclic ageing cells in group 5 to gain some insight into the difference in lifetime due to the cell-to-cell variation. The results show that the cumulative calendar and cyclic ageing, in terms of both time and FEC, overestimates the overall rate of capacity fade. The difference between the modelled ageing (assuming that calendar and cyclic effects can be separated and then combined), versus the measured ageing from groups 1 and 3 is very significant when considered as a function of time. However, the comparison as a function of FEC is more important as lifetime predictions should be made based on the charge throughput rather than the time spent cycling. Making lifetime predictions with respect to charge throughput is valuable as it accounts for the difference in cycling conditions (i.e., c-rate). As seen in Fig . 3.2 for example, the cells cycled at a lower c-rate experience less degradation with respect to time but that is only due to the fact that they experience less cycles within the same time. Even taking the best-case cumulative model (i.e., closest to groups 1 and 3), which sums the capacity loss experienced by cells in group 1 and 3 after 623 cycles, and its calendar ageing, it is evident that the rate of degradation is exaggerated. Assuming that the end of life condition for the cell is a loss of 20% of the capacity, the best-case cumulative model with respect to time would reach that criteria in 720 days or 655 days with respect to FEC,

while average of group 3 reaches EoL at 774 days and the average of group 1 could last to 900 days. This also highlights that small changes in the rate of degradation can lead to large changes in the actual lifetime because of the relatively shallow gradient of capacity fade in these situations. Comparing the capacity loss at 867 days (i.e., the end of testing for group 3), group 3 lost 21.8% of its capacity and group 1 lost 19.5% while according to the predictions, the best-case prediction with respect to time lost 24.2% and the best-case prediction with respect to FEC lost 26.1%. This is a significant difference between the predicted capacity fade and the capacity fade experienced due to exposure to combined profiles. The difference increases when compared to the other two predictions made with respect to time and FEC. The worst-case prediction with respect to FEC results in a loss of 37.2% of the cell capacity which is significantly greater than the capacity loss experienced by groups 1 and 3. The underestimation of lifetime, especially with respect to group 1 indicates that the cumulative model does not account for path dependence and the ordering of calendar and cycling ageing, could underestimate the lifetime of the cell as seen by these results.

5.2 Superposition of CCCV Cycling and Calendar Ageing Conditions

For groups 7 and 8, that were exposed to a combined profile of CCCV cycling and calendar ageing at 90% SoC, capacity fade data during calendar ageing was collected as described in the previous section. In this case due to time and channel count limitations, the cycling dataset published by Preger et al. was used to understand the continuous CCCV capacity fade [105] . The study conducted by Preger et al. uses the same NCA cell as this thesis, and exposed the cells to C/2 CCCV cycling with a cut-off condition of 0.05 A in a thermal chamber set to 25°C. The cycling conditions and thermal conditions used make this cycling

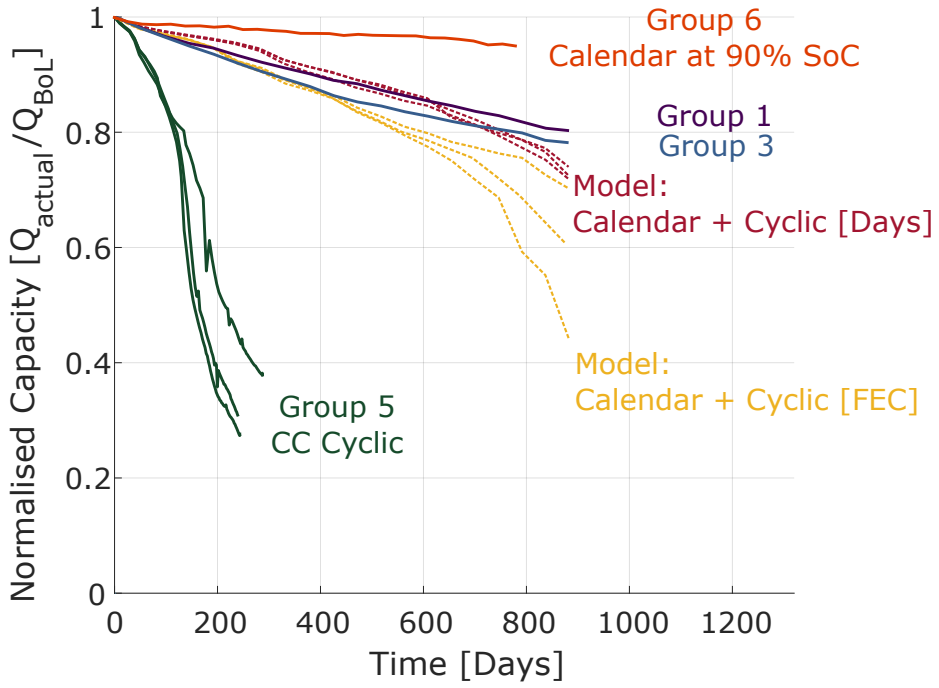

Fig. 5.5 Comparing the normalised capacity fade of cells exposed to calendar ageing, continuous cycling, combined profiles and cumulative capacity fade of calendar + cyclic ageing

data comparable with the cycling conditions used in the combined profiles in experimental campaign 2.

The capacity fade experienced by the cells exposed to continuous CCCV cycling was determined for the same duration of cycling experienced by cells in group 7 and 8, in terms of time and FEC. Groups 7 and 8 cycled for 65 days/ 280 FEC. This was combined with the capacity loss experienced after the 315 days of calendar ageing at 90% SoC for groups 7 and 8. The CCCV cycling for 280 FEC resulted in the loss of 0.55 Ah or 0.61 Ah with respect time. The calendar aged cells lost 0.02 Ah in 315 days. The empirical ageing model result, with respect to FEC, is represented by the blue dashed line in Fig. 5.6 and the result with respect to time is shown in red dashed line. These plots show that assuming the ageing caused by calendar versus cycling modes are independent and cumulative leads to an overestimation of capacity fade, even under CCCV cycling conditions, similar to the results seen for the comparison in the initial experimental campaign with CC cycling Fig. 5.5. The difference

between Fig. 5.5 and Fig. 5.6 however is that the capacity fade prediction with respect to time was the closest to the collected data however incorporating CCCV cycling leads to the capacity fade with respect to FEC providing the closest capacity loss estimation. This highlights the difference in lifetime prediction as a result of the cycling condition. Comparing the capacity lost for each group to that predicted by the superposed models at 380 days, group 7 lost an average of 14.31%, group 8 lost an average of 16.12% , the prediction with respect to FEC lost 18.5% and the model with respect to time lost 21.9%. Group 7, that experienced a shorter duration of continuous cycling and more frequent calendar ageing, exhibits the most divergence from the superposed capacity fade model. This could be because the models do not account for the beneficial impact that the frequent relaxation periods that allow for improved lithium homogeneity has on capacity fade.

A similar comparison was conducted for groups 9 and 10 presented in Fig. 5.7 that incorporates both CCCV cycling and calendar ageing at 4.2 V. The capacity data from calendar ageing at 4.2 V was inferred from the data presented by Keil et al. [89]. Keil et al. conducted calendar ageing at 4.2 V on an NCA 18650 cell at 25 °C, which is comparable to the calendar conditions in the combined load profiles of groups 9 and 10. Groups 9 and 10 experienced 10 months and 10 days of calendar ageing conditions, however the calendar ageing data presented by Keil et al. was terminated after 10 months. The superposition of calendar and cyclic ageing will hence be a slight underestimation. The calendar ageing data from Keil et al. does not show a progression of capacity fade with respect to time, hence only the end point of the cumulative models can be presented and not the trajectory of the cumulative degradation. The capacity fade data during CCCV from Preger et al. was again used to model continuous cyclic ageing. Once again, the superposition of the two modes overestimated the capacity fade compared to the measured combined load profiles. The average capacity loss for group 9 at 380 days was 14.5%, group 10 lost an average of 17.4 % while the prediction with respect to FEC lost 21.5 % and the prediction with respect to

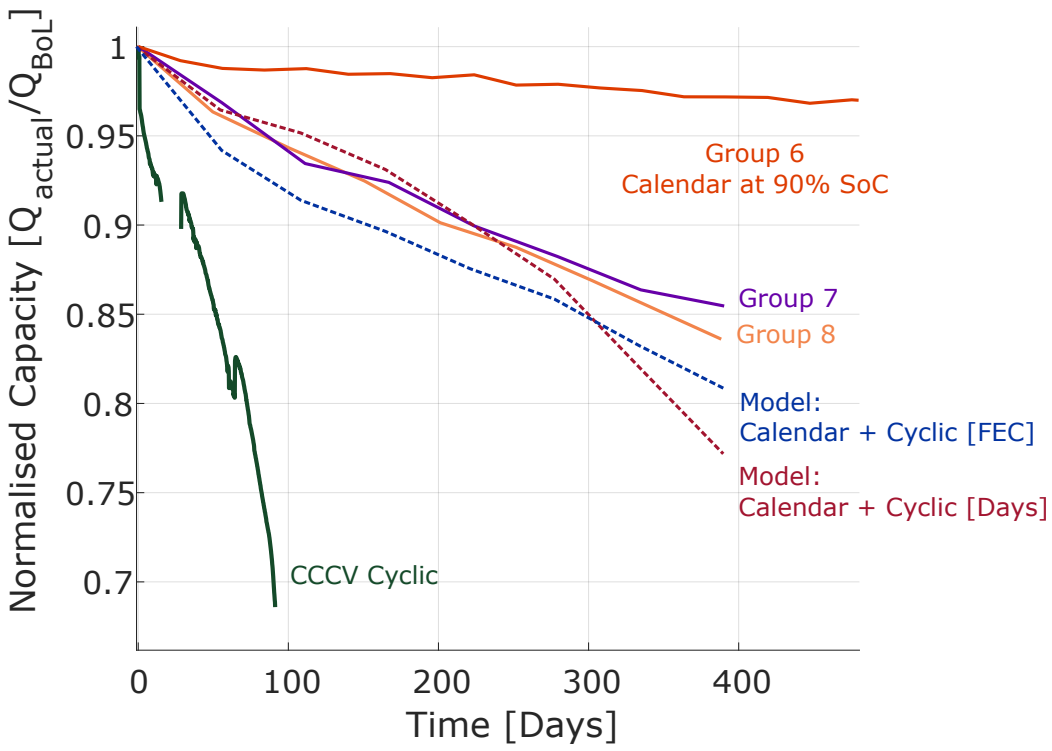

Fig. 5.6 Comparison of the normalised capacity fade of cells in groups 7 and 8 (solid lines) versus an empirical model that superposes CCCV cycling and 90% SoC calendar ageing (dashed lines).

time lost 23.5%. Similar to the two previous comparisons, the models underestimate the lifetime of the cells and similar to Fig. 5.6 , the prediction with respect to FEC is the closest estimation to the collected data. A similar trend is seen in Fig. 5.5 and Fig. 5.6 where the combined profile with shorter continuous cycling experienced the most divergence from the superposed capacity fade models.

5.3 Summary

The preceding comparison between empirical models that separate and then superpose calendar and cyclic ageing vs. measurements from the various groups exposed to combined load profiles clearly shows that the influences of calendar and cyclic ageing are not cumulative.

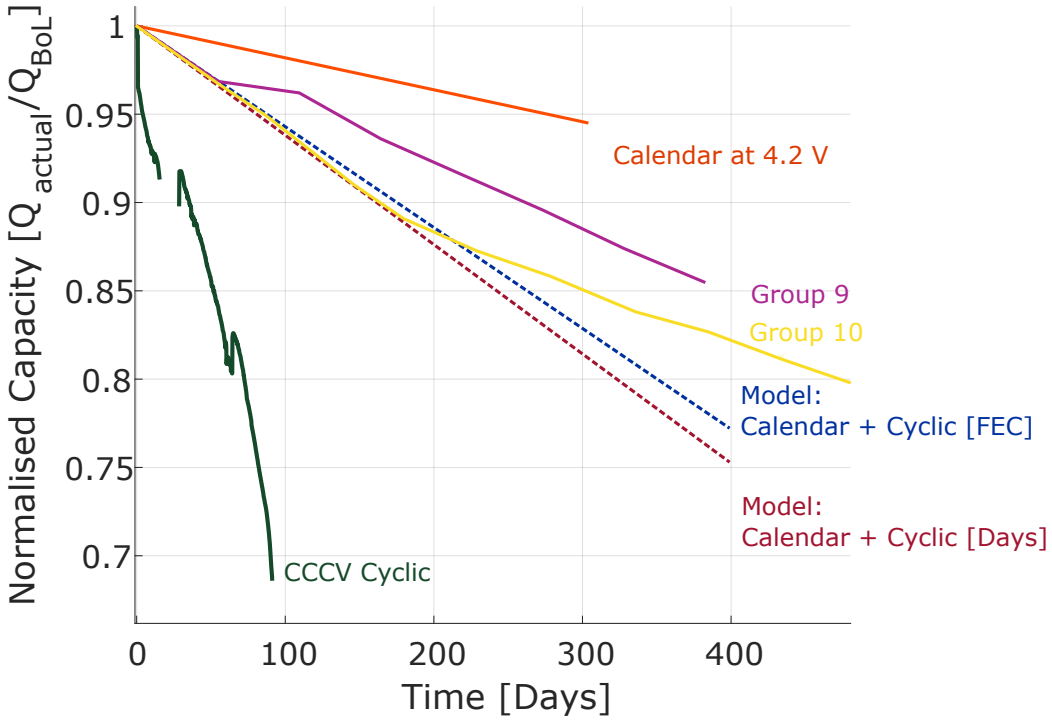

Fig. 5.7 Comparison of the normalised capacity fade of cells in groups 9 and 10 (solid lines) versus an empirical model that superposes CCCV cycling and calendar ageing at 4.2 V (dashes lines).

Assuming that the degradation mechanisms due to calendar and cyclic ageing do not interact results in a significant underestimation of the cell lifetime.

Calculating the difference between the measured ageing due to combined load profiles and the cumulative ageing due to empirical models that separate calendar and cyclic modes shows that the measured data closest to the model prediction is that of group 8 (difference of 2.39%), which experienced 2 days of CCCV cyclic ageing at C/2 followed by 10 days of calendar ageing. This could be due to the more homogenous cycling conditions and the 90% SoC calendar ageing. However, group 10, which also experienced CCCV cycling, exhibits a difference compared to the ageing model of 4.11% , showing that increasing the calendar ageing from 90% to 100% SoC has a significant impact on the accuracy of the superposition assumption. It is crucial to note that as the cell ageing progresses, the difference between the estimated degradation and the measured degradation becomes more prominent. Since groups 7, 8 and 9 have not reached their EoL condition in these comparisons, it is difficult to comment on whether using CC cycling or CCCV cycling would provide more accurate lifetime predictions when using a superposition of calendar and cyclic ageing however from the data presented, CCCV is expected to result in a better prediction with respect to FEC.

Across all three sets of comparisons, groups 1, 7 and 9 experienced the greatest divergence from the modelled degradation trends. All three groups experienced more frequent but shorter relaxation periods that break up the cyclic ageing, compared to their counterpart groups 3, 8 and 10, respectively. This indicates that the relaxation impact due to the calendar ageing periods is important and is not being accounted for in simple empirical models that assume superposition.

The difference between the cumulative models and the degradation data collected suggests that the interaction between the various degradation mechanisms can influence the rate of degradation. For example, as discussed in chapters 3 and 4, a key degradation mechanism encouraging path dependent degradation is the mechanical stress as a result of continuous

cycling, and the significant impact that a relaxation period breaking up the cycling can have on cell lifetime. The relaxation periods during cycling could allow for a reduction in the severity of side reactions encouraged by continuous cycling which would not be accounted for if the cyclic and calendar ageing were simply summed together. The relaxation periods breaking up the continuous cycling allows for improved homogeneity of the lithium distribution and reduces the mechanical stress that leads to particle cracking or the loss of electrical contact. These side reactions, and more importantly, the interaction between the side reactions as a result of the order and periodicity of calendar/cyclic ageing is not accounted for in the cumulative empirical model. To gain insight into the side reactions occurring within the cell, a physics-based model such as a single particle model (SPM) could be used to understand the degradation mechanisms. Since an SPM describes the lithium transport and diffusion, it may provide a more accurate lifetime estimation in the context of path dependent degradation compared to the cumulative model as the individual degradation mechanisms would be accounted for in the model. However, even in a physics-based model, it is unclear whether the interaction between the mechanisms, that results in path dependent degradation, would be captured in the lifetime estimation.

As seen in the data presented in this chapter, cycling with CC results in the most significant difference between the cumulative model and the collected data, especially with respect to FEC. Realistically however, most applications would incorporate a CV step while recharging to ensure the cell is at the required SoC. An EV would experience CC discharge and small CC charges due to regenerative braking however the full charge would include a CV step to ensure the cell has reached 100% SoC. Although the comparison between the data collected with CCCV cycling and the cumulative model in FEC shows a less significant difference than with CC cycling, the underestimation of the lifetime is still significant. The results from this study indicate that the cumulative models are not sensitive to different real applications and drive cycles that cells could be used under. For example, an EV being used for personal

use between work and home would experience short cycling durations with longer periods of time spent under relaxation conditions however an electric taxi/ light weight commercial vehicles will spend a longer duration under cyclic conditions with less frequent relaxation periods breaking up the cycling to allow for relaxation. Even under CCCV cycling conditions that provides the best cumulative model estimation, the lifetime prediction for the EV used for personal driving will be significantly underestimated while the cumulative model will provide a slightly more accurate lifetime estimation for a commercial vehicle, under the conditions tested in this study. The calendar ageing condition increasing from 90% SoC to 100% SoC also resulted in a difference in the rate of degradation, so not only does care need to be taken with regards to the cycling condition but the calendar condition must also be carefully considered in the model. Assuming an EV is recharged and left under calendar ageing conditions for a few hours until the EV is used, the SoC at which the cell is held at can influence the rate of degradation. Some battery management systems limit the cell to being charged to a maximum of 90% SoC while others may allow the cell to be charged to 100% SoC, this difference in calendar ageing condition is also not accounted for in the superimposition model.

Chapter 6

Conclusions

6.1 Conclusions and Contributions

The work presented in this thesis explored the influence of path dependent on the rate of degradation and the accuracy of the cumulative assumption used in empirical models. The conclusion and contributions of the research presented is discussed below in relation to the original objectives of this work as outlined in section 1.4:

6.1.1 Objective 1: Design experiments used to collect data in order to test the hypothesis that path dependence exists.

The combined load profiles and reference performance tests designed in this study presents an approach to isolating the influence of path dependent degradation. The two experimental campaigns outlined in chapters 3 and 4 have been designed to limit all external stress factors to ensure that any divergence seen between degradation trends can be attributed to path dependence as much as possible. Maintaining the same ratio of calendar to cyclic ageing and exposing the cells to the same amount of calendar/cyclic ageing but in different orders allows for the influence of degradation history to be studied. Incorporating different

methods of cycling, two C-rates for cycling and two SoCs of calendar ageing provides a better understanding of the impact of these stress factors on path dependent degradation. Conducting these long-term experiments for approximately 3 years has led to the production of a significant amount of capacity fade, resistance and EIS data which has been made open access for the research community.

6.1.2 Objective 2: Investigate the extent of path dependent degradation under constant current cycling at different C-rates

The hypothesis of the degradation being path dependent was first addressed by exposing cells to combined load profiles that have the same amount of calendar/ cyclic ageing in different orders. All other external stress factors were controlled to ensure the influence of path dependent degradation alone was isolated. Calendar ageing was conducted at 90% SoC and the cells were cycled between the voltage limits using a C/2 and C/4 constant current profile.

It was found that **the order and periodicity of exposure to calendar and cyclic ageing does in some cases impact the overall rate of capacity fade and resistance increase**. The cells exposed to two days of continuous cycling followed by 10 days of calendar ageing (group 3) experienced a greater rate of degradation as compared to cells exposed to 1 day of cyclic ageing followed by 5 days of calendar ageing (group 1). This supports the hypothesis that the history of a cells ageing and the interaction between degradation mechanisms encouraged by calendar/cyclic ageing can impact the rate of degradation. This divergence was more significant for the data plotted against FEC compared to time indicating that the **divergence could be encouraged by the cyclic conditions**. By incorporating different C-rate conditions for cycling (C/2 and C/4), it was identified that **path dependence could be rate dependent** and more prevalent at higher C-rates. The divergence between the groups was more significant in the resistance data than the capacity data which suggests that while

there is **some difference in the overall lifetime due to path dependent degradation, there is a more significant difference in the performance of the cells.**

Constant current cycling especially at high C-rates was found to be most significant in driving path dependence. With the cells in group 3 being exposed to longer continuous cycling compared to group 1, they experience prolonged mechanical stress and volume changes that could encourage the formation of microcracks leading to loss of electrical contact, which could exhibit as loss of active material at the anode. The microcracks could lead to fresh surfaces of active electrode material being exposed to the electrolyte, leading to increased SEI formation. The continuous cycling without relaxation periods could also lead to a lack of lithium homogeneity which could encourage degradation due to increased mechanical stress. Since group 1 only cycled continuously for 1 day, cells in that group may have been able to recover some capacity loss by allowing lithium from the anode overhang region to diffuse through the anode and by the improved homogeneity of lithium distribution during the more frequent relaxation periods. The calendar ageing period after 2 days of continuous cycling for group 3 may not allow the same extent of capacity recovery as it is not as frequent. Alternatively, due to the lower C-rate experienced by groups 2 and 4, the mechanical stress and concentration gradients within the cells in these groups were more limited, allowing a more uniform distribution of lithium in the electrodes, resulting in limited divergence in ageing behaviour.

6.1.3 Objective 3: Examine the difference in the extent of path dependent degradation when cycling under constant current constant voltage conditions

Analysing the degradation data collected from cells exposed to combined load profiles that incorporates constant current constant voltage cycling indicates that **CCCV cycling reduces the difference in the rate of degradation**. Introducing a constant voltage charging

step within the cycling protocol encourages the lithium distribution to homogenise and therefore was expected to impact the degradation trajectories of the cells differently to the CC cycling of the first campaign. This suggests that CCCV cycling reduces the influence of path dependence, possibly due to the periods of low stress during the constant voltage step of the cycling encouraging a more uniform lithium distribution and reducing the mechanical stress caused by continuous de/intercalation. This supports the notion that one of the factors encouraging path dependence is the degree of inhomogeneous lithium distribution. The cells exposed to the combined profiles that incorporate CCCV cycling degrade more rapidly than the cells than incorporate CC cycling. Unlike the CC cycled data however, the divergence between the capacity trends is more prominent than the power fade data. It was noted that the divergence was more evident in the data plotted against time as compared to the data plotted against FEC which may suggest that **the calendar ageing may be encouraging the path dependence more than the cyclic condition** under these test conditions.

6.1.4 Objective 4: Understand the impact of calendar ageing at different states of charge on path dependent degradation

The CC cycling interspersed with more frequent breaks of 90% SoC calendar ageing improved the lifetime of the cells as compared to the cells exposed to longer calendar ageing after longer durations of continuous cycling. A similar but less significant impact was seen when calendar ageing at 90% SoC after cycling under CCCV conditions.

Increasing the calendar ageing to 100% SoC with the CCCV profile seemed to encourage the impact of path dependent degradation. A similar trend was seen where the calendar ageing breaking up the continuous cycling improved the lifetime of the cell. It is concluded that, where cycling is aggressive, **degradation may be slowed by exposing cells to regular calendar ageing periods between the continuous cycling** to allow reduction in mechanical stresses and homogenisation of local concentrations, as discussed further below.

6.1.5 Objective 5: Gain insight into the degradation modes that encourage path dependent degradation

Incremental capacity and differential voltage analyses indicated that for the combined load profiles in both experimental campaigns, it was the **difference in the rate of loss of active material at the anode** that was the most significant degradation mode driving differences in capacity and resistance. The likely cause of this is that cells exposed to CC cycling for a longer continuous duration could be subjected to **increased mechanical stress at the anode**, perhaps caused by expansion and contraction of the electrodes, leading to loss of electrical contact, particle cracking, and loss of active material. This is supported by EIS data showing that the charge transfer resistance increases at different rates, possibly due to loss of active surface area leading to increased current densities in the electrodes. The post-mortem study confirms that LAM at the anode could be resulting in the difference in the rate of degradation.

Changing the cycling condition to CCCV reduces this effect by allowing the lithium concentration distribution in the electrodes to be more uniform, which limits the mechanical stress. It was also found that increasing the calendar ageing condition by 10% SoC impacts the rate of loss of lithium inventory as well as the loss of active material loss at the anode.

6.1.6 Objective 6: Understand the accuracy of lifetime predictions made under the cumulative degradation assumption in empirical models.

A study was conducted to quantify the difference in capacity fade between a cell exposed to a combined load profile (i.e., calendar and cyclic ageing) versus the capacity fade estimated by summing the calendar and cyclic aging with a simple algebraic mode. Simple empirical models tend to treat calendar and cyclic ageing as separable influences on cell ageing. Here it was found that this assumption is generally incorrect and that an accurate lifetime

prediction model needs to consider the impact of path dependence. The study shows that the cumulative calendar and cyclic capacity fade under the conditions the data was collected could overestimate the rate of degradation resulting in an earlier estimation of the end of life. In general, **assuming calendar and cycling ageing are separable may lead to an underestimation of cell lifetime**.

For both experimental campaigns, the cells exposed to shorter continuous cycling experienced the most divergence from the simple cumulative model. This indicates that capacity recovery caused by frequent calendar ageing periods breaking up continuous cycling is not being accounted for in simple cumulative empirical models that separate calendar and cyclic aging. This could mean that using an empirical cumulative model for applications such as EV life prediction for light duty passenger cars, that would often normally experience short periods of cycling interspersed with frequent calendar ageing (i.e., parked on the driveway) may not be accurate and may result in a shorter estimation of the useful lifetime of a battery. Even for heavier use fleets (e.g., taxis), the vehicles would still have significant "down time" e.g., overnight. Conversely, in the heaviest usage industrial applications (e.g., marine, HGVs) intensive cycling could have a disproportionately negative impact on battery lifetime and should be carefully accommodated (e.g., by oversizing systems). To encourage the implementation of batteries and its use in applications such as EVs, the predictions on cell lifetime need to be accurate to ensure that cells are being used to their full capacity.

6.2 Limitations and Future Work

The first limitation of this study is the cell selection used for all the experiments. The only chemistry and form factor explored here was NCA 18650 cylindrical cells, however different chemistries display different degradation behaviours [105, 106, 89]. Path dependence under more aggressive operating conditions that lead to mechanical stress on the electrodes (e.g., higher C-rates, continuous CC cycling) is likely to be a common occurrence across most if

not all lithium-ion chemistries, but the extent to which it matters may depend on the specific battery type, electrode geometry, particle sizes and so on. With the increasing popularity of lithium iron phosphate (LFP) cells in electric vehicles, it would be interesting to study path dependence in LFP. Other chemistries such as lithium nickel manganese cobalt oxide, nickel cobalt oxide and nickel manganese oxide could be investigated as well.

The path dependence seen in this study resulted from anode degradation, with a possible explanation being mechanical stress differences leading to microcracks due to the continuous de/intercalation. Graphite electrodes containing silicon have become increasingly popular due to silicon's improved capacity, however this incurs greater volume expansion during lithiation compared to pure graphite, and this encourages the formation of microcracks [107] . As the silicon transitions from Si to $Li_{15}Si_4$, the anode experiences a 280% volumetric change which can lead to significant mechanical strain [108]. Exposing a cell with a Si-graphite anode to similar combined load profiles as used in this thesis will help determine the extent of the impact that microcracks and structural stress could have on path dependence.

It would also be interesting to understand how path dependence changes with electrode thickness e.g., for an energy cell versus a power cell, and with form factor. It is likely that pouch cells will behave somewhat differently to cylindrical cells due to their varying external mechanical constraints. In this study, cylindrical cells were tested, however pouch or prismatic cells will present different stress factors that could impact the impact of path dependence. As cells are dis/charged, the volume of the cell changes dramatically. In cylindrical cells, the can constrains this volume expansion, but in pouch or prismatic cells, external mechanical constraint must be applied. It has been found that this has a huge impact on degradation, with in some cases greater stack pressure built up between the cell and the constraint leading to more rapid capacity fade [28, 109]. Since mechanical stress within the electrodes due to cycling likely plays a significant role in degradation trends as a

function of usage profiles, it would be interesting to explore the impact of path dependence on pouch/prismatic cells.

Due to battery tester channel limitations, this study only considered 3 cells at each test condition, and this does not provide great statistical confidence. Studies have been conducted that show the extent of cell-to-cell variability for cells from the same manufacturing batch and it is difficult to identify the cell- to-cell variability at the BoL [62]. Hence selecting 3 cells per condition may not provide an accurate representation of overall degradation trends. Exposing a larger set of cells of the same chemistry and format to the same combined load profiles will improve our understanding of intrinsic versus extrinsic variance in battery ageing. Since the extent of divergence between different test groups changes as the cells age, it would also be interesting to continue the tests for a longer duration than studied here until all the cells have lost a minimum of 20% of the initial capacity.

Modifying the combined load profiles used here to incorporate a greater range of different calendar and cyclic ageing conditions and durations would allow further exploration of path dependent ageing. This could include modifying the existing combined load profile with the same cycling and calendar ageing conditions but changing the ratio away from 1:5 of time spent in cycling and calendar ageing conditions. Due to the cell specifications in this study, the maximum C-rate used for cyclic ageing was C/2 and the cells were cycled conservatively. Since it was noted that the influence of path dependence increases with higher C-rates, exposing cells to profiles with higher C-rates would be beneficial to obtain an understanding of the impact of C-rate on path dependence.

Test bench data collection often oversimplifies the conditions that a cell would face compared to a real application, and models that are built using lab datasets are biased towards the data collection conditions. The combined load profiles in both experimental campaigns here incorporated controlled cycling conditions (CC or CCCV) which was selected rather than realistic drive cycles in order to limit cycle-dependent stress factors and to isolate the

influence of path dependent degradation alone. Using CC and CCCV cycling however is not representative of realistic cell usage conditions in most applications. Drawing detailed conclusions about path dependence under realistic usage conditions using the combined load profiles designed in this study is not possible. For an EV application, testing realistic drive cycles including characteristics such as regenerative braking could provide a more realistic view of the impact of path dependant degradation. To further this study, more data needs to be collected on cells exposed to various combined load profiles and stress factors. Exposing cells to a range of temperatures to emulate the differences in pack cooling or environmental temperatures will also add to the understanding of the influence of path dependence on life. Cycling cells including low temperatures would encourage degradation mechanisms such as lithium plating and this could be a significant effect. Conducting a study with higher C-rates, various temperatures and incorporating realistic cycling characteristics that are close to realistic use cases may identify the scenarios for which the superposition model is suitable or unsuitable for estimation for cell lifetime. This would require a very large number of test channels and thermal chambers. This data can be used to compare the degradation as a result of combined load profiles with empirical model lifetime predictions that assume degradation due to calendar and cyclic ageing is cumulative. This will provide clarity on the calendar and cyclic ageing conditions under which the assumption would result in an accurate prediction of cell lifetime.

The results from this study indicate that path dependence is not accounted for in empirical models that assume the influence of calendar and cyclic ageing are cumulative. The data collected in this study could be used to investigate the accuracy of lifetime predictions obtained from electrochemical models. Understanding electrochemical models can accurately account for path dependent degradation will allow for a more informed selection of model depending on the application of the battery. Improving the accuracy of lifetime predictions

will improve warranties for cells and will ensure that the cell is utilised to its full capacity before moving on to second life applications or recycling.

Finally, experimental campaign 2 was more limited than the first campaign due to the impact of COVID-19, which resulted in restricted access to laboratories and offices. This led to the need for remote control of long-term experiments and delays in conducting end of life tests. There were also delays caused by the need for permission to access collaborator facilities and support. Due to these limitations, some planned work on post-mortem analysis was not possible. A post-mortem study was originally planned in order to visually inspect the electrodes in campaign 2 and determine whether the influences seen in the DVA signatures support the electrode degradation seen for the aged cells. The delays also led to the inability to conduct other types of post-mortem tests for both experimental campaigns such as morphological and structural analysis using scanning electron microscopy. Combining scanning electron microscopy with energy dispersive X-ray spectroscopy would have allowed the composition materials of the electrode to be identified, which could have been used to confirm the optical visual inspection of the anode and would have assisted in determining changes in the cathodes with greater accuracy [110, 91]. In order to confirm the impact of path dependent degradation due to changes in the electrodes, a study had been planned to open a representative cell from each group in the second campaign and construct half cells (as per the first campaign). This would allow the DVA signatures of the half cells to be obtained which could have been compared to the fresh half-cell DVA signatures. This could have provided some insight into the degradation experienced by each electrode to determine whether the influences seen in the full cell DVA signatures could be validated.

References

[1] Christoph R Birkl, Matthew R Roberts, Euan Mcturk, Peter G Bruce, and David A Howey. Degradation Diagnostics for Lithium Ion Cells. *Journal of Power Sources*, 341:1–35, 2016.

[2] Fan Yang, Yuanyuan Xie, Yelin Deng, and Chris Yuan. Predictive modeling of battery degradation and greenhouse gas emissions from U.S. state-level electric vehicle operation. *Nature Communications*, 9(1):1–10, 2018.

[3] Madeleine Ecker, Jochen B. Gerschler, Jan Vogel, Stefan Käbitz, Friedrich Hust, Philipp Dechent, and Dirk Uwe Sauer. Development of a lifetime prediction model for lithium-ion batteries based on extended accelerated aging test data. *Journal of Power Sources*, 215:248–257, 2012.

[4] John Wang, Justin Purewal, Ping Liu, Jocelyn Hicks-Garner, Souren Soukazian, Elena Sherman, Adam Sorenson, Luan Vu, Harshad Tataria, and Mark W. Verbrugge. Degradation of lithium ion batteries employing graphite negatives and nickel-cobalt-manganese oxide + spinel manganese oxide positives: Part 1, aging mechanisms and life estimation. *Journal of Power Sources*, 272:1154–1161, 2014.

[5] E. Sarasketa-Zabala, E. Martinez-Laserna, M. Berecibar, I. Gandiaga, L. M. Rodriguez-Martinez, and I. Villarreal. Realistic lifetime prediction approach for Li-ion batteries. *Applied Energy*, 162:839–852, 2016.

[6] M. Schimpe, M. E. von Kuepach, M. Naumann, H. C. Hesse, K. Smith, and A. Jossen. Comprehensive Modeling of Temperature-Dependent Degradation Mechanisms in Lithium Iron Phosphate Batteries. *ECS Transactions*, 80(13):147–170, 2017.

[7] Matthieu Dubarry, George Baure, and Arnaud Devie. Durability and Reliability of EV Batteries under Electric Utility Grid Operations: Path Dependence of Battery Degradation. *Journal of The Electrochemical Society*, 165(5):A773–A783, 2018.

[8] David Linden and Thomas Reddy. *Handbook of Batteries*. McGraw Hill Professional, 3 edition, 2001.

[9] Sheng Shui Zhang. A review on the separators of liquid electrolyte Li-ion batteries. *Journal of Power Sources*, 164(1):351–364, 2007.

[10] Rotem Marom, S. Francis Amalraj, Nicole Leifer, David Jacob, and Doron Aurbach. A review of advanced and practical lithium battery materials. *Journal of Materials Chemistry*, 21(27):9938–9954, 2011.

[11] Arumugam Manthiram. An Outlook on Lithium Ion Battery Technology. *ACS Central Science*, 3(10):1063–1069, 2017.

[12] George E. Blomgren. The Development and Future of Lithium Ion Batteries. *Journal of The Electrochemical Society*, 164(1):A5019–A5025, 2017.

[13] Fitria Savira and Yudi Suharsono. Automotive Li-Ion Batteries: Current Status and Future Perspectives. *Journal of Chemical Information and Modeling*, 01(01):1689–1699, 2013.

[14] R. Spotnitz. Simulation of capacity fade in lithium-ion batteries. *Journal of Power Sources*, 113(1):72–80, 2003.

[15] J. Vetter, P. Novák, M.R. Wagner, C. Veit, K.-C. Möller, J.O. Besenhard, M. Winter, M. Wohlfahrt-Mehrens, C. Vogler, and A. Hammouche. Ageing mechanisms in lithium-ion batteries. *Journal of Power Sources*, 147(1-2):269–281, sep 2005.

[16] Gang Ning and Branko N. Popov. Cycle Life Modeling of Lithium-Ion Batteries. *Journal of The Electrochemical Society*, 151(10):A1584, 2004.

[17] Peng Lu, Chen Li, Eric W. Schneider, and Stephen J. Harris. Chemistry, impedance, and morphology evolution in solid electrolyte interphase films during formation in lithium ion batteries. *Journal of Physical Chemistry C*, 118(2):896–903, 2014.

[18] Seong Jin An, Jianlin Li, Claus Daniel, Debasish Mohanty, Shrikant Nagpure, and David L. Wood. The state of understanding of the lithium-ion-battery graphite solid electrolyte interphase (SEI) and its relationship to formation cycling. *Carbon*, 105:52–76, 2016.

[19] Jorn M. Reniers, Grietus Mulder, and David A. Howey. Review and Performance Comparison of Mechanical-Chemical Degradation Models for Lithium-Ion Batteries. *Journal of The Electrochemical Society*, 166(14):A3189–A3200, 2019.

[20] Victor A. Agubra and Jeffrey W. Fergus. The formation and stability of the solid electrolyte interface on the graphite anode. *Journal of Power Sources*, 268:153–162, 2014.

[21] M. B. Pinson and M. Z. Bazant. Theory of SEI Formation in Rechargeable Batteries: Capacity Fade, Accelerated Aging and Lifetime Prediction. *Journal of the Electrochemical Society*, 160(2):A243–A250, dec 2012.

[22] Qianqian Liu, Chunyu Du, Bin Shen, Pengjian Zuo, Xinqun Cheng, Yulin Ma, Geping Yin, and Yunzhi Gao. Understanding undesirable anode lithium plating issues in lithium-ion batteries. *RSC Advances*, 6(91):88683–88700, 2016.

[23] Ian Campbell. Design optimisation and diagnostics for lithium-ion battery fast charging. 2019.

[24] N. Legrand, B. Knosp, P. Desprez, F. Lapicque, and S. Raël. Physical characterization of the charging process of a Li-ion battery and prediction of Li plating by electrochemical modelling. *Journal of Power Sources*, 245:208–216, 2014.

[25] Ratnakumar V. Bugga and Marshall C. Smart. Lithium Plating Behavior in Lithium-Ion Cells. *ECS Transactions*, 25(36):241–252, 2019.

[26] J. Vetter, P. Novák, M.R. R. Wagner, C. Veit, K.-C. C. Möller, J.O. O. Besenhard, M. Winter, M. Wohlfahrt-Mehrens, C. Vogler, and a. Hammouche. Ageing mechanisms in lithium-ion batteries. *Journal of Power Sources*, 147(1-2):269–281, sep 2005.

[27] Peter Keil, Simon F. Schuster, Jörn Wilhelm, Julian Travi, Andreas Hauser, Ralph C. Karl, and Andreas Jossen. Calendar Aging of Lithium-Ion Batteries. *Journal of The Electrochemical Society*, 163(9):A1872–A1880, 2016.

[28] John Cannarella and Craig B. Arnold. Stress evolution and capacity fade in constrained lithium-ion pouch cells. *Journal of Power Sources*, 245:745–751, 2014.

[29] Doron Aurbach. Review of selected electrode-solution interactions which determine the performance of Li and Li ion batteries. *Journal of Power Sources*, 89(2):206–218, 2000.

[30] M. Wohlfahrt-Mehrens, C. Vogler, and J. Garche. Aging mechanisms of lithium cathode materials. In *Journal of Power Sources*, volume 127, pages 58–64, 2004.

[31] Chun Zhan, Tianpin Wu, Jun Lu, and Khalil Amine. Dissolution, migration, and deposition of transition metal ions in Li-ion batteries exemplified by Mn-based cathodes-A critical review. *Energy and Environmental Science*, 11(2):243–257, 2018.

[32] Kang Joon Park, Jang Yeon Hwang, Hoon Hee Ryu, Filippo Maglia, Sung Jin Kim, Peter Lamp, Chong S. Yoon, and Yang Kook Sun. Degradation Mechanism of Ni-Enriched NCA Cathode for Lithium Batteries: Are Microcracks Really Critical? *ACS Energy Letters*, 4(6):1394–1400, 2019.

[33] Yancheng Zhang and Chao-Yang Wang. Cycle-Life Characterization of Automotive Lithium-Ion Batteries with LiNiO[sub 2] Cathode. *Journal of The Electrochemical Society*, 156(7):A527, 2009.

[34] Christoph Birkl. Diagnosis and prognosis of degradation in lithium-ion batteries. *University of Oxford*, 2017.

[35] Amartya Mukhopadhyay and Brian W. Sheldon. Deformation and stress in electrode materials for Li-ion batteries. *Progress in Materials Science*, 63(February):58–116, 2014.

[36] John Cannarella and Craig B. Arnold. The Effects of Defects on Localized Plating in Lithium-Ion Batteries. *Journal of The Electrochemical Society*, 162(7):A1365–A1373, 2015.

[37] Xuebing Han, Minggao Ouyang, Languang Lu, Jianqiu Li, Yuejiu Zheng, and Zhe Li. A comparative study of commercial lithium ion battery cycle life in electrical vehicle: Aging mechanism identification. *Journal of Power Sources*, 251:38–54, 2014.

[38] Pankaj Arora. Capacity Fade Mechanisms and Side Reactions in Lithium-Ion Batteries. *Journal of The Electrochemical Society*, 145(10):3647, 1998.

[39] M. Rosa Palacín. Understanding ageing in Li-ion batteries: A chemical issue. *Chemical Society Reviews*, 47(13):4924–4933, 2018.

[40] Stefan Käbitz, Jochen Bernhard Gerschler, Madeleine Ecker, Yusuf Yurdagel, Brita Emmermacher, Dave André, Tim Mitsch, and Dirk Uwe Sauer. Cycle and calendar life study of a graphite|LiNi1/3Mn 1/3Co1/3O2 Li-ion high energy system. Part A: Full cell characterization. *Journal of Power Sources*, 239:572–583, 2013.

[41] I. Bloom, B.W Cole, J.J Sohn, S.A Jones, E.G Polzin, V.S Battaglia, G.L Henriksen, C. Motloch, R. Richardson, T. Unkelhaeuser, D. Ingersoll, and H.L Case. An accelerated calendar and cycle life study of Li-ion cells. *Journal of Power Sources*, 101(2):238–247, oct 2001.

[42] M. Ecker, J.B. Gerschler, J. Vogel, S. Käbitz, F. Hust, P. Dechent, and D.U. Sauer. Analyzing calendar aging data towards a lifetime prediction model for lithium-ion batteries. *26th Electric Vehicle Symposium*, pages 47–58, 2012.

[43] Stefan Käbitz, Jochen Bernhard Gerschler, Madeleine Ecker, Yusuf Yurdagel, Brita Emmermacher, Dave André, Tim Mitsch, and Dirk Uwe Sauer. Cycle and calendar life study of a graphite|LiNi1/3Mn 1/3Co1/3O2 Li-ion high energy system. Part A: Full cell characterization. *Journal of Power Sources*, 239:572–583, 2013.

[44] Johannes Schmalstieg, Stefan Käbitz, Madeleine Ecker, and Dirk Uwe Sauer. From Accelerated Aging Tests to a Lifetime Prediction Model : Analyzing Lithium-Ion Batteries. *27th World Electric Vehicle Symposium and Exhibition, EVS 2014; Barcelona; Spain*, pages 1–12, 2014.

[45] John Wang, Ping Liu, Jocelyn Hicks-Garner, Elena Sherman, Souren Soukiazian, Mark Verbrugge, Harshad Tataria, James Musser, and Peter Finamore. Cycle-life model for graphite-LiFePO4 cells. *Journal of Power Sources*, 196(8):3942–3948, apr 2011.

[46] Peter Keil and Andreas Jossen. Aging of Lithium-Ion Batteries in Electric Vehicles : Impact of Regenerative Braking. *EVS28 International Electric Vehicle Symposium and Exhibition*, (May):1–11, 2015.

[47] Robert Burrell, Alana Zulke, Peter Keil, and Harry Hoster. Communication—Identifying and Managing Reversible Capacity Losses that Falsify Cycle Ageing Tests of Lithium-Ion Cells. *Journal of The Electrochemical Society*, 167(13):130544, 2020.

[48] J. C. Burns, a. Kassam, N. N. Sinha, L. E. Downie, L. Solnickova, B. M. Way, and J. R. Dahn. Predicting and Extending the Lifetime of Li-Ion Batteries. *Journal of the Electrochemical Society*, 160(9):A1451–A1456, 2013.

[49] Stefan Käbitz, Jochen Bernhard Gerschler, Madeleine Ecker, Yusuf Yurdagel, Brita Emmermacher, Dave André, Tim Mitsch, and Dirk Uwe Sauer. Cycle and calendar life study of a graphite|LiNi1/3Mn 1/3Co1/3O2 Li-ion high energy system. Part A: Full cell characterization. *Journal of Power Sources*, 239:572–583, 2013.

[50] Mohammad Kassem, Julien Bernard, Renaud Revel, Serge Pelissier, and C Delacourt. Calendar aging of a graphite / LiFePO4 cell To cite this version :. 2013.

[51] I. Bloom, B. W. Cole, J. J. Sohn, S. A. Jones, E. G. Polzin, V. S. Battaglia, G. L. Henriksen, C. Motloch, R. Richardson, T. Unkelhaeuser, D. Ingersoll, and H. L. Case. An accelerated calendar and cycle life study of Li-ion cells. *Journal of Power Sources*, 101(2):238–247, 2001.

[52] Matthieu Dubarry, M. Berecibar, A. Devie, D. Anseán, N. Omar, and I. Villarreal. State of health battery estimator enabling degradation diagnosis: Model and algorithm description. *Journal of Power Sources*, 360:59–69, 2017.

[53] Kandler Smith, Ying Shi, and Shriram Santhanagopalan. Degradation mechanisms and lifetime prediction for lithium-ion batteries; A control perspective. In *2015 American Control Conference (ACC)*, pages 728–730. IEEE, jul 2015.

[54] Peter Keil and Andreas Jossen. Aging of lithium-ion batteries in electric vehicles:. *Dissertation*, 7(1):41–51, 2017.

[55] E. V. Thomas, I. Bloom, J. P. Christophersen, and V. S. Battaglia. Statistical methodology for predicting the life of lithium-ion cells via accelerated degradation testing. *Journal of Power Sources*, 184(1):312–317, 2008.

[56] Zeyu Ma, Jiuchun Jiang, Wei Shi, Weige Zhang, and Chunting Chris Mi. Investigation of path dependence in commercial lithium-ion cells for pure electric bus applications: Aging mechanism identification. *Journal of Power Sources*, 274:29–40, 2015.

[57] Matthieu Dubarry, Arnaud Devie, and Katherine McKenzie. Durability and reliability of electric vehicle batteries under electric utility grid operations: Bidirectional charging impact analysis. *Journal of Power Sources*, 358:39–49, 2017.

[58] Kevin L. Gering, Sergiy V. Sazhin, David K. Jamison, Christopher J. Michelbacher, Bor Yann Liaw, Matthieu Dubarry, and Mikael Cugnet. Investigation of path dependence in commercial lithium-ion cells chosen for plug-in hybrid vehicle duty cycle protocols. *Journal of Power Sources*, 196(7):3395–3403, 2011.

[59] Jens Groot, Maciej Swierczynski, Ana Irina Stan, and Søren Knudsen Kær. On the complex ageing characteristics of high-power LiFePO4/graphite battery cells cycled with high charge and discharge currents. *Journal of Power Sources*, 286:475–487, 2015.

[60] Clemens Guenther, Benjamin Schott, Wilfried Hennings, Paul Waldowski, and Michael A. Danzer. Model-based investigation of electric vehicle battery aging by means of vehicle-to-grid scenario simulations. *Journal of Power Sources*, 239:604–610, 2013.

[61] Zackrisson Mats. Life cycle assessment of long life lithium electrode for electric vehicle batteries-cells for Leaf, Tesla and Volvo bus. page 56, 2017.

[62] Thorsten Baumhöfer, Manuel Brühl, Susanne Rothgang, and Dirk Uwe Sauer. Production caused variation in capacity aging trend and correlation to initial cell performance. *Journal of Power Sources*, 247:332–338, feb 2014.

[63] Alexander Uwe Schmid, Moritz Kurka, and Kai Peter Birke. Reproducibility of Li-ion cell reassembling processes and their influence on coin cell aging. *Journal of Energy Storage*, 24(April):100732, 2019.

[64] Evgenij Barsoukov and J. Ross Macdonald. *Impedance Spectroscopy-Theory , Experiment , and*, volume 125. second edition, 2005.

[65] James Taylor, Anup Barai, T. R. Ashwin, Yue Guo, Mark Amor-Segan, and James Marco. An insight into the errors and uncertainty of the lithium-ion battery characterisation experiments. *Journal of Energy Storage*, 24(May):100761, 2019.

[66] Anup Barai, Kotub Uddin, Matthieu Dubarry, Limhi Somerville, Andrew McGordon, Paul Jennings, and Ira Bloom. A comparison of methodologies for the non-invasive characterisation of commercial Li-ion cells. *Progress in Energy and Combustion Science*, 72:1–31, 2019.

[67] Jorge Varela Barreras, Trishna Raj, David A. Howey, and Erik Schaltz. Results of screening over 200 pristine lithium-ion cells. *2017 IEEE Vehicle Power and Propulsion Conference, VPPC 2017 - Proceedings*, 2018-Janua(Cccv):1–6, 2018.

[68] Wesley Chang, Clement Bommier, Thomas Fair, Justin Yeung, Shripad Patil, and Daniel Steingart. Understanding Adverse Effects of Temperature Shifts on Li-Ion Batteries: An Operando Acoustic Study. *Journal of The Electrochemical Society*, 167(9):090503, 2020.

[69] Y. Ji, Y. Zhang, and C.-Y. Wang. Li-Ion Cell Operation at Low Temperatures. *Journal of the Electrochemical Society*, 160(4):A636–A649, feb 2013.

[70] Anna Tomaszewska, Zhengyu Chu, Xuning Feng, Simon O'Kane, Xinhua Liu, Jingyi Chen, Chenzhen Ji, Elizabeth Endler, Ruihe Li, Lishuo Liu, Yalun Li, Siqi Zheng, Sebastian Vetterlein, Ming Gao, Jiuyu Du, Michael Parkes, Minggao Ouyang, Monica Marinescu, Gregory Offer, and Billy Wu. Lithium-ion battery fast charging: A review. *eTransportation*, 1:100011, 2019.

[71] Ankit Verma, Kandler Smith, Shriram Santhanagopalan, Daniel Abraham, Koffi Pierre Yao, and Partha P. Mukherjee. Galvanostatic Intermittent Titration and Performance Based Analysis of LiNi 0.5 Co 0.2 Mn 0.3 O 2 Cathode . *Journal of The Electrochemical Society*, 164(13):A3380–A3392, 2017.

[72] Christoph R. Birkl, Matthew R. Roberts, Euan McTurk, Peter G. Bruce, and David A. Howey. Degradation diagnostics for lithium ion cells. *Journal of Power Sources*, 341:373–386, 2017.

[73] Xuebing Han, Minggao Ouyang, Languang Lu, Jianqiu Li, Yuejiu Zheng, and Zhe Li. A comparative study of commercial lithium ion battery cycle life in electrical vehicle: Aging mechanism identification. *Journal of Power Sources*, 251:38–54, 2014.

[74] Matthieu Dubarry, Cyril Truchot, and Bor Yann Liaw. Synthesize battery degradation modes via a diagnostic and prognostic model. *Journal of Power Sources*, 219:204–216, dec 2012.

[75] Ira Bloom, Andrew N. Jansen, Daniel P. Abraham, Jamie Knuth, Scott A. Jones, Vincent S. Battaglia, and Gary L. Henriksen. Differential voltage analyses of high-power, lithium-ion cells 1. Technique and application. *Journal of Power Sources*, 139(1-2):295–303, 2005.

[76] Peter Keil and Andreas Jossen. Calendar Aging of NCA Lithium-Ion Batteries Investigated by Differential Voltage Analysis and Coulomb Tracking. *Journal of The Electrochemical Society*, 164(1):A6066–A6074, 2017.

[77] Matthieu Dubarry, Cyril Truchot, and Bor Yann Liaw. Cell degradation in commercial LiFePO4 cells with high-power and high-energy designs. *Journal of Power Sources*, 258:408–419, 2014.

[78] C R Birkl, E McTurk, M R Roberts, P G Bruce, and D A Howey. A Parametric Open Circuit Voltage Model for Lithium Ion Batteries. *Journal of The Electrochemical Society*, 162(12):A2271–A2280, 2015.

[79] Barbara Stiaszny, Jörg C. Ziegler, Elke E. Krauß, Jan P. Schmidt, and Ellen Ivers-Tiffée. Electrochemical characterization and post-mortem analysis of aged LiMn 2O4-Li(Ni0.5Mn0.3Co 0.2)O2/graphite lithium ion batteries. Part I: Cycle aging. *Journal of Power Sources*, 251:439–450, 2014.

[80] USABC. Electric Vehicle Battery Test Procedures Manual Rev. 2. *United States Advanced Battery Consortium*, (January):129, 1996.

[81] INL. Battery Test Manual For Electric Vehicles. (June):65, 2015.

[82] Marius Bauer, Clemens Guenther, Michael Kasper, Mathias Petzl, and Michael A. Danzer. Discrimination of degradation processes in lithium-ion cells based on the sensitivity of aging indicators towards capacity loss. *Journal of Power Sources*, 283:494–504, 2015.

[83] Peter Keil and Andreas Jossen. Calendar Aging of NCA Lithium-Ion Batteries Investigated by Differential Voltage Analysis and Coulomb Tracking. *Journal of The Electrochemical Society*, 164(1):A6066–A6074, 2017.

[84] Nina Meddings, Marco Heinrich, Frédéric Overney, Jong Sook Lee, Vanesa Ruiz, Emilio Napolitano, Steffen Seitz, Gareth Hinds, Rinaldo Raccichini, Miran Gaberšček, and Juyeon Park. Application of electrochemical impedance spectroscopy to commercial Li-ion cells: A review. *Journal of Power Sources*, 480(September), 2020.

[85] Victoria Julia Ovejas and Angel Cuadras. Impedance characterization of an LCO-NMC/graphite cell: Ohmic conduction, sei transport and charge-transfer phenomenon. *Batteries*, 4(3), 2018.

[86] Simon F. Schuster, Tobias Bach, Elena Fleder, Jana Müller, Martin Brand, Gerhard Sextl, and Andreas Jossen. Nonlinear aging characteristics of lithium-ion cells under different operational conditions. *Journal of Energy Storage*, 1:44–53, 2015.

[87] Carlos Pastor-Fernandez, W. Dhammika Widanage, James Marco, Miguel Angel Gama-Valdez, and Gael H. Chouchelamane. Identification and quantification of ageing mechanisms in Lithium-ion batteries using the EIS technique. *2016 IEEE Transportation Electrification Conference and Expo, ITEC 2016*, pages 1–6, 2016.

[88] Jan Philipp Schmidt, Thorsten Chrobak, Moses Ender, Jörg Illig, Dino Klotz, and Ellen Ivers-Tiffée. Studies on LiFePO4 as cathode material using impedance spectroscopy. *Journal of Power Sources*, 196(12):5342–5348, 2011.

[89] Peter Keil, Simon F. Schuster, Jörn Wilhelm, Julian Travi, Andreas Hauser, Ralph C. Karl, and Andreas Jossen. Calendar Aging of Lithium-Ion Batteries. *Journal of The Electrochemical Society*, 163(9):A1872–A1880, 2016.

[90] P. Ramadass, Bala Haran, Ralph White, and Branko N. Popov. Capacity fade of Sony 18650 cells cycled at elevated temperatures: Part II. Capacity fade analysis. *Journal of Power Sources*, 112(2):614–620, 2002.

[91] Christoph R. Birkl, Euan McTurk, Stefanie Zekoll, Felix H. Richter, Matthew R. Roberts, Peter G. Bruce, and David A. Howey. Degradation Diagnostics for Commercial Lithium-Ion Cells Tested at -10C. *Journal of The Electrochemical Society*, 164(12):A2644–A2653, 2017.

[92] A. J. Louli, Jing Li, S. Trussler, Christopher R. Fell, and J. R. Dahn. Volume, Pressure and Thickness Evolution of Li-Ion Pouch Cells with Silicon-Composite Negative Electrodes. *Journal of The Electrochemical Society*, 164(12):A2689–A2696, 2017.

[93] Muhammad Rashid and Amit Gupta. Effect of Relaxation Periods over Cycling Performance of a Li-Ion Battery. *Journal of The Electrochemical Society*, 162(2):A3145–A3153, 2015.

[94] Meinert Lewerenz, Philipp Dechent, and Dirk Uwe Sauer. Investigation of capacity recovery during rest period at different states-of-charge after cycle life test for prismatic Li(Ni 1/3 Mn 1/3 Co 1/3)O 2 -graphite cells. *Journal of Energy Storage*, 21(January):680–690, 2019.

[95] Meinert Lewerenz, Georg Fuchs, Lisa Becker, and Dirk Uwe Sauer. Irreversible calendar aging and quantification of the reversible capacity loss caused by anode overhang. *Journal of Energy Storage*, 18(February):149–159, 2018.

[96] Gang Ning, Bala Haran, and Branko N. Popov. Capacity fade study of lithium-ion batteries cycled at high discharge rates. *Journal of Power Sources*, 117(1-2):160–169, 2003.

[97] Simon F. Schuster, Tobias Bach, Elena Fleder, Jana Müller, Martin Brand, Gerhard Sextl, and Andreas Jossen. Nonlinear aging characteristics of lithium-ion cells under different operational conditions. *Journal of Energy Storage*, 1(1):44–53, 2015.

[98] Daniel P. Abraham, Steven D. Poppen, Andrew N. Jansen, Jun Liu, and Dennis W. Dees. Application of a lithium-tin reference electrode to determine electrode contributions to impedance rise in high-power lithium-ion cells. *Electrochimica Acta*, 49(26):4763–4775, 2004.

[99] T. Waldmann, G. Bisle, B.-I. Hogg, S. Stumpp, M. a. Danzer, M. Kasper, P. Axmann, and M. Wohlfahrt-Mehrens. Influence of Cell Design on Temperatures and Temperature Gradients in Lithium-Ion Cells: An In Operando Study. *Journal of the Electrochemical Society*, 162(6):A921–A927, 2015.

[100] Koffi P.C. Yao, John S. Okasinski, Kaushik Kalaga, Ilya A. Shkrob, and Daniel P. Abraham. Quantifying lithium concentration gradients in the graphite electrode of Li-ion cells using: Operando energy dispersive X-ray diffraction. *Energy and Environmental Science*, 12(2):656–665, 2019.

[101] Shabbir Ahmed, Ira Bloom, Andrew N. Jansen, Tanvir Tanim, Eric J. Dufek, Ahmad Pesaran, Andrew Burnham, Richard B. Carlson, Fernando Dias, Keith Hardy, Matthew Keyser, Cory Kreuzer, Anthony Markel, Andrew Meintz, Christopher Michelbacher, Manish Mohanpurkar, Paul A. Nelson, David C. Robertson, Don Scoffield, Matthew Shirk, Thomas Stephens, Ram Vijayagopal, and Jiucai Zhang. Enabling fast charging – A battery technology gap assessment. *Journal of Power Sources*, 367:250–262, 2017.

[102] Matilda Klett, Rickard Eriksson, Jens Groot, Pontus Svens, Katarzyna Ciosek Högström, Rakel Wreland Lindström, Helena Berg, Torbjörn Gustafson, Göran Lindbergh, and Kristina Edström. Non-uniform aging of cycled commercial LiFePO4//graphite cylindrical cells revealed by post-mortem analysis. *Journal of Power Sources*, 257:126–137, 2014.

[103] Jörn Wilhelm, Stefan Seidlmayer, Peter Keil, Jörg Schuster, Armin Kriele, Ralph Gilles, and Andreas Jossen. Cycling capacity recovery effect: A coulombic efficiency and post-mortem study. *Journal of Power Sources*, 365:327–338, 2017.

[104] A. Shellikeri, V. Watson, D. Adams, E. E. Kalu, J. A. Read, T. R. Jow, J. S. Zheng, and J. P. Zheng. Investigation of Pre-lithiation in Graphite and Hard-Carbon Anodes Using Different Lithium Source Structures. *Journal of The Electrochemical Society*, 164(14):A3914–A3924, 2017.

[105] Yuliya Preger, Heather M. Barkholtz, Armando Fresquez, Daniel L. Campbell, Benjamin W. Juba, Jessica Romàn-Kustas, Summer R. Ferreira, and Babu Chalamala. Degradation of Commercial Lithium-Ion Cells as a Function of Chemistry and Cycling Conditions. *Journal of The Electrochemical Society*, 167(12):120532, 2020.

[106] Noshin Omar, Bavo Verbrugge, Grietus Mulder, Peter Van Den Bossche, Joeri Van Mierlo, Mohamed Daowd, Miguel Dhaens, and Stijn Pauwels. Evaluation of performance characteristics of various lithium-ion batteries for use in BEV application. *2010 IEEE Vehicle Power and Propulsion Conference, VPPC 2010*, 2010.

[107] Yu Miao, Patrick Hynan, Annette Von Jouanne, and Alexandre Yokochi. Current li-ion battery technologies in electric vehicles and opportunities for advancements. *Energies*, 12(6):1–20, 2019.

[108] M. N. Obrovac and Leif Christensen. Structural changes in silicon anodes during lithium insertion/extraction. *Electrochemical and Solid-State Letters*, 7(5), 2004.

[109] Martin Wünsch, Jörg Kaufman, and Dirk Uwe Sauer. Investigation of the influence of different bracing of automotive pouch cells on cyclic liefetime and impedance spectra. *Journal of Energy Storage*, 21(October 2018):149–155, 2019.

[110] Matilda Klett, Rickard Eriksson, Jens Groot, Pontus Svens, Katarzyna Ciosek Högström, Rakel Wreland Lindström, Helena Berg, Torbjörn Gustafson, Göran Lindbergh, and Kristina Edström. Non-uniform aging of cycled commercial LiFePO4//graphite cylindrical cells revealed by post-mortem analysis. *Journal of Power Sources*, 257:126–137, 2014.

Appendix A

Data Collection and Load Profile Test Procedures

This section provides the test procedures used to collect the data presented in this thesis.

A.1 Data Collection Test Procedures

The reference performance test procedure described below is conducted periodically during the combined load profiles that are shown in sections A.2.

Table A.1 RPT Test Procedure

Step	Method		End Condition
1	Rest		t=3h
2	CCCV Charge	I=1.5A	I $\leq$ 0.05A
		V=4.2V	
3	Rest		t=1h
4	CC Discharge	I=1.5A	V$\leq$2.5V
			Set variable: VAR1 = Capacity
5	Rest		t=1h
6	CCCV Charge	I=1.5A	I $\leq$ 0.05A
		V=4.2V	
			Set variable: VAR2 = Capacity
7	Rest		t=2h
Pseudo OCV			
8	CC Discharge	I=0.125A	V$\leq$2.5V
9	Rest		t= 30m
10	CCCV Charge	I=0.125A	I $\leq$ 0.05A
		V=4.2V	
11	Rest		t=1h

Table A.2 RPT Test Procedure Continued

Step	Method		End Condition
Pulse Power Characterisation Test			
12	CC Discharge	I=1.5A	Function:Capacity $\geq$ VAR1*0.2
13	Rest		t=1h
14	CC Discharge	I=1.5A	t=36s
15	Rest		t=30m
16	CC Charge	I=1.5A	t=36s
17	Rest		t=30m
18	CC Discharge	I=10.0A	t=36s
19	Rest		t=1h
20	CC Discharge	I=1.5A	Function:Capacity $\geq$ (VAR1*0.3)-0.1
21	Rest		t=1h
22	CC Discharge	I=1.5A	t=36s
23	Rest		t=30m
24	CC Charge	I=1.5A	t=36s
25	Rest		t=30m
26	CC Discharge	I=10.0A	t=36s
27	Rest		t=1h
28	CC Discharge	I=1.5A	Function:Capacity $\geq$ (VAR1*0.3)-0.1
29	Rest		t=1h
30	CC Discharge	I=1.5A	t=36s
31	Rest		t=30m
32	CC Charge	I=1.5A	t=36s
33	Rest		t=30m
34	CC Discharge	I=10.0A	t=36s
35	Rest		t=1h
36	End		

Table A.3 Electrochemical Impedance Spectroscopy Test Procedure

Step	Method		End Condition
1	Rest		t=3h
2	CCCV Charge	I=1.5A	I $\leq$ 0.05A
		V=4.2V	
3	Rest		t=1h
4	CC Discharge	I=1.5A	V$\leq$2.5V
			Set variable: VAR1 = Capacity
5	Rest		t=1h
6	CCCV Charge	I=1.5A	I $\leq$ 0.05A
		V=4.2V	
7	Rest		t=1h
8	CC Discharge	I=1.5A	Function:Capacity $\geq$ VAR1*0.2
9	Rest		t=1h
10	GEIS	I=0.1A	frequency:10mHz-5kHz
11	CC Discharge	I=1.5A	Function:Capacity $\geq$ VAR1*0.3
12	Rest		t=1h
13	GEIS	I=0.1A	frequency:10mHz-5kHz
14	CC Discharge	I=1.5A	Function:Capacity $\geq$ VAR1*0.2
15	Rest		t=1h
16	GEIS	I=0.1A	frequency:10mHz-5kHz
17	End		

Table A.4 Galvanostatic Intermittent Titration Technique Test Procedure

Step	Method		End Condition
1	CCCV Charge	I=1.5A	I $\leq$ 0.05A
		V=4.2V	
			Set variable: VAR2 = Capacity
2	Do 1		
3	CC Discharge	I=1.5A	Function:Capacity $\geq$ VAR1*0.1
4	Rest		t=2h
5	Loop1		10
6	CC Discharge	I=1.5A	V$\leq$2.5V
7	Rest		4h
8	Do 2		
9	CC Charge	I=1.5A	Function:Capacity $\geq$ VAR2*0.1
10	Rest		t=2h
11	Loop2		10
12	CCCV Charge	I=1.5A	I $\leq$ 0.05A
		V=4.2V	
13	End		

A.2 Combined Load Profile Test Procedures

A.2.1 Experiemental Campaign 1 Profiles

Table A.5 Group 1 Test Procedure

Step	Method		End Condition
1	Rest		t = 5s
2	CCCV Charge	I=1.5A	I $\leq$ 0.05A
		V=4.2V	
3	Do1		
4	Do2		
5	Do3		
6	CC Discharge	I=1.5A	V$\leq$2.5V
			Set variable: VAR3 = Capacity
7	CC Charge	I=1.5A	V$\geq$4.2V
8	Loop3		6
9	CCCV Charge	I=1.5A	I$\leq$0.05A
		V=4.2V	
10	Rest		t= 30m
11	CC Discharge	I=1.5A	Function:Capacity $\geq$ VAR3*0.1
12	Rest		t=120h
13	Loop2		8
14	Rest		t=5s
15	RPT Subroutine		
16	Rest		t=5s
17	Loop1		100
18	End		

Table A.6 Group 2 Test Procedure

Step	Method		End Condition
1	Rest		t = 5s
2	CCCV Charge	I=1.5A V=4.2V	I $\leq$ 0.05A
3	Do1		
4	Do2		
5	Do3		
6	CC Discharge	I=0.75A	V$\leq$2.5V Set variable: VAR3 = Capacity
7	CC Charge	I=0.75A	V$\geq$4.2V
8	Loop3		3
9	CCCV Charge	I=1.5A V=4.2V	I$\leq$0.05A
10	Rest		t= 30m
11	CC Discharge	I=0.75A	Function:Capacity $\geq$ VAR3*0.1
12	Rest		t=120h
13	Loop2		16
14	Rest		t=5s
15	RPT Subroutine		
16	Rest		t=5s
17	Loop1		100
18	End		

Table A.7 Group 3 Test Procedure

Step	Method		End Condition
1	Rest		t = 5s
2	CCCV Charge	I=1.5A	I $\leq$ 0.05A
		V=4.2V	
3	Do1		
4	Do2		
5	Do3		
6	CC Discharge	I=1.5A	V$\leq$2.5V
			Set variable: VAR3 = Capacity
7	CC Charge	I=1.5A	V$\geq$4.2V
8	Loop3		12
9	CCCV Charge	I=1.5A	I$\leq$0.05A
		V=4.2V	
10	Rest		t= 30m
11	CC Discharge	I=1.5A	Function:Capacity $\geq$ VAR3*0.1
12	Rest		t=240h
13	Loop2		4
14	Rest		t=5s
15	RPT Subroutine		
16	Rest		t=5s
17	Loop1		100
18	End		

Table A.8 Group 4 Test Procedure

Step	Method		End Condition
1	Rest		t = 5s
2	CCCV Charge	I=1.5A	I $\leq$ 0.05A
		V=4.2V	
3	Do1		
4	Do2		
5	Do3		
6	CC Discharge	I=0.75A	V$\leq$2.5V
			Set variable: VAR3 = Capacity
7	CC Charge	I=0.75A	V$\geq$4.2V
8	Loop3		6
9	CCCV Charge	I=1.5A	I$\leq$0.05A
		V=4.2V	
10	Rest		t= 30m
11	CC Discharge	I=0.75A	Function:Capacity $\geq$ VAR3*0.1
12	Rest		t=240h
13	Loop2		8
14	Rest		t=5s
15	RPT Subroutine		
16	Rest		t=5s
17	Loop1		100
18	End		

Table A.9 Group 5 Test Procedure

Step	Method		End Condition
1	Rest		t = 5s
2	CCCV Charge	I=1.5A	I $\leq$ 0.05A
		V=4.2V	
3	Do1		
4	Do2		
5	CC Discharge	I= 1.5 A	V$\leq$2.5 V
6	CC Charge	I=1.5 A	V$\geq$4.2V
7	Loop 2		48
8	CC Charge	I=1.5 A	V$\geq$4.2V
9	Rest		t=5 s
10	RPT Subroutine		
11	Rest		t=5 s
10	Loop 1		100
12	End		

Table A.10 Group 6 Test Procedure

Step	Method		End Condition
1	Rest		t = 5s
2	Do1		
3	CC Discharge	I= 1.5 A	V$\leq$2.5 V
			Set variable: VAR1 = Capacity
4	CCCV Charge	I=1.5A	I $\leq$ 0.05A
		V=4.2V	
5	CC Discharge	I=1.5A	Function:Capacity $\geq$ VAR1*0.1
6	Rest		t=672 h
7	RPT Subroutine		
8	Rest		t=5 s
9	Loop 1		100
10	End		

A.2.2 Experiemental Campaign 2 Profiles

Table A.11 Group 7 Test Procedure

Step	Method		End Condition
1	Rest		t = 5s
2	CCCV Charge	I=1.5A	I $\leq$ 0.05A
		V=4.2V	
3	Do1		
4	Do2		
5	Do3		
6	CC Discharge	I=1.5A	V$\leq$2.5V
			Set variable: VAR3 = Capacity
7	CCCV Charge	I=1.5A	I $\leq$ 0.05A
		V=4.2V	
8	Loop3		5
9	CCCV Charge	I=1.5A	I$\leq$0.05A
		V=4.2V	
10	Rest		t= 30m
11	CC Discharge	I=1.5A	Function:Capacity $\geq$ VAR3*0.1
12	Rest		t=120h
13	Loop2		9
14	Rest		t=5s

Table A.12 Group 7 Test Procedure Continued

Step	Method		End Condition
15	Do4		
16	CC Discharge	I=1.5A	V$\leq$2.5V
17	CCCV Charge	I=1.5A	I $\leq$ 0.05A
		V=4.2V	
18	Loop4		3
19	Rest		t=5s
15	RPT Subroutine		
16	Rest		t=5s
17	Loop1		100
18	End		

Table A.13 Group 8 Test Procedure

Step	Method		End Condition
1	Rest		t = 5s
2	CCCV Charge	I=1.5A	I $\leq$ 0.05A
		V=4.2V	
3	Do1		
4	Do2		
5	Do3		
6	CC Discharge	I=1.5A	V$\leq$2.5V
			Set variable: VAR3 = Capacity
7	CCCV Charge	I=1.5A	I $\leq$ 0.05A
		V=4.2V	
8	Loop3		10
9	CCCV Charge	I=1.5A	I$\leq$0.05A
		V=4.2V	
10	Rest		t= 30m
11	CC Discharge	I=1.5A	Function:Capacity $\geq$ VAR3*0.1
12	Rest		t=240h
13	Loop2		4
14	Rest		t=5s
15	Do4		
16	CC Discharge	I=1.5A	V$\leq$2.5V
17	CCCV Charge	I=1.5A	I $\leq$ 0.05A
		V=4.2V	
18	Loop4		8
19	Rest		t=5s
15	RPT Subroutine		
16	Rest		t=5s
17	Loop1		100
18	End		

Table A.14 Group 9 Test Procedure

Step	Method		End Condition
1	Rest		t = 5s
2	CCCV Charge	I=1.5A	I $\leq$ 0.05A
		V=4.2V	
3	Do1		
4	Do2		
5	Do3		
6	CC Discharge	I=1.5A	V$\leq$2.5V
7	CCCV Charge	I=1.5A	I $\leq$ 0.05A
		V=4.2V	
8	Loop3		5
9	CCCV Charge	I=1.5A	I$\leq$0.05A
		V=4.2V	
10	Rest		t= 120m
11	Loop2		9
12	Rest		t=5s
13	Do4		
14	CC Discharge	I=1.5A	V$\leq$2.5V
15	CCCV Charge	I=1.5A	I $\leq$ 0.05A
		V=4.2V	
16	Loop4		3
17	Rest		t=5s
18	RPT Subroutine		
19	Rest		t=5s
20	Loop1		100
21	End		

Table A.15 Group 10 Test Procedure

Step	Method		End Condition
1	Rest		t = 5s
2	CCCV Charge	I=1.5A	I $\leq$ 0.05A
		V=4.2V	
3	Do1		
4	Do2		
5	Do3		
6	CC Discharge	I=1.5A	V$\leq$2.5V
7	CCCV Charge	I=1.5A	I $\leq$ 0.05A
		V=4.2V	
8	Loop3		10
9	CCCV Charge	I=1.5A	I$\leq$0.05A
		V=4.2V	
10	Rest		t= 240m
11	Loop2		4
12	Rest		t=5s
13	Do4		
14	CC Discharge	I=1.5A	V$\leq$2.5V
15	CCCV Charge	I=1.5A	I $\leq$ 0.05A
		V=4.2V	
16	Loop4		8
17	Rest		t=5s
18	RPT Subroutine		
19	Rest		t=5s
20	Loop1		100
21	End		

Appendix B

Additional Degradation Data

This section presents the raw data collected for experimental campaigns 1 and 2.

B.1 Raw Capacity Data

B.2 Raw Resistance Data

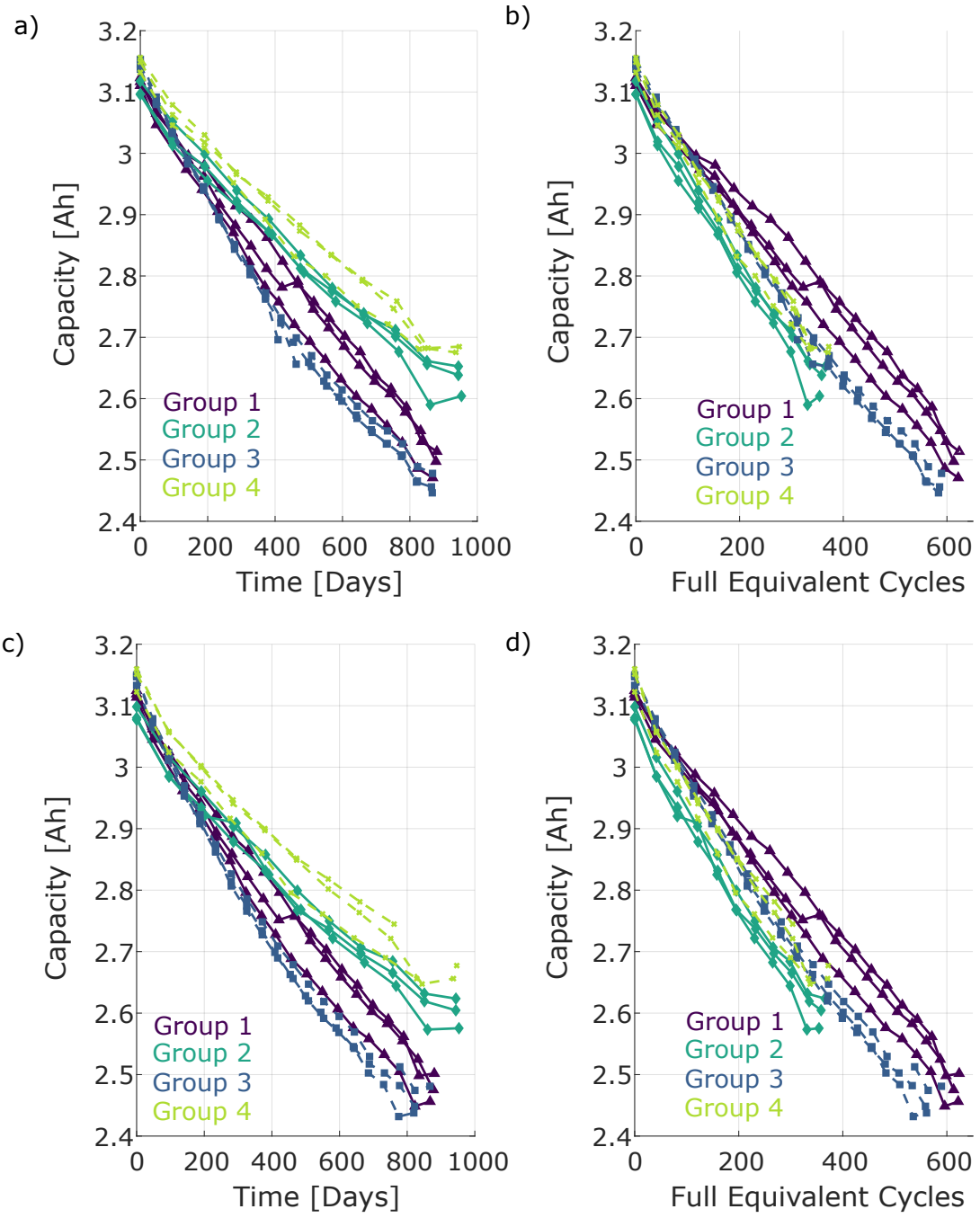

Fig. B.1 Raw capacity data for groups 1,2,3 and 4 during (a),(b) discharge and (c),(d) charge.

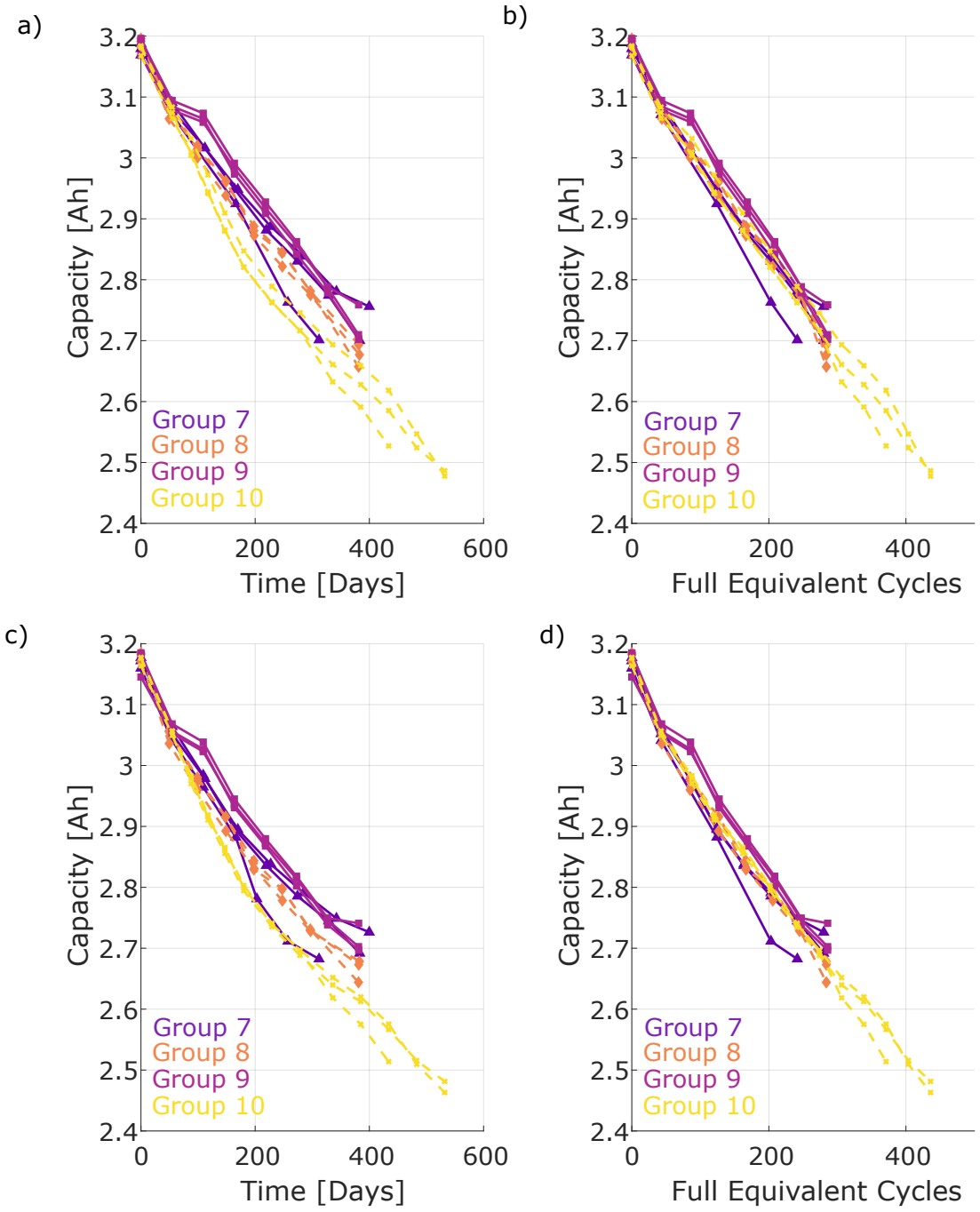

Fig. B.2 Raw capacity data for groups 7, 8, 9 and 10 during (a),(b) discharge and (c),(d) charge.

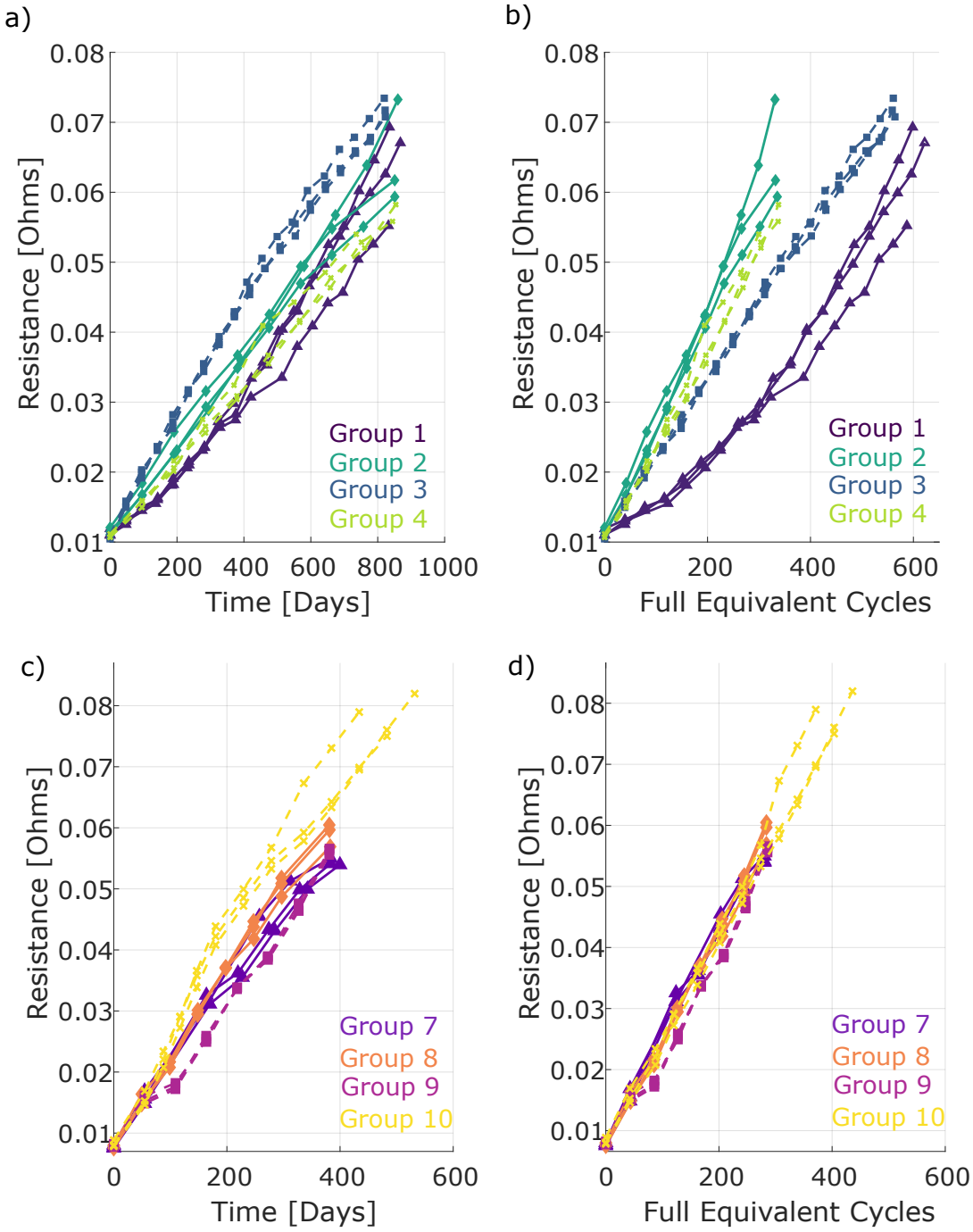

Fig. B.3 Raw resistance data at 50% SoC with a 1.5 A discharge pulse for (a),(b) experimental camapaigns 1 and (c),(d) experimental campaign 2

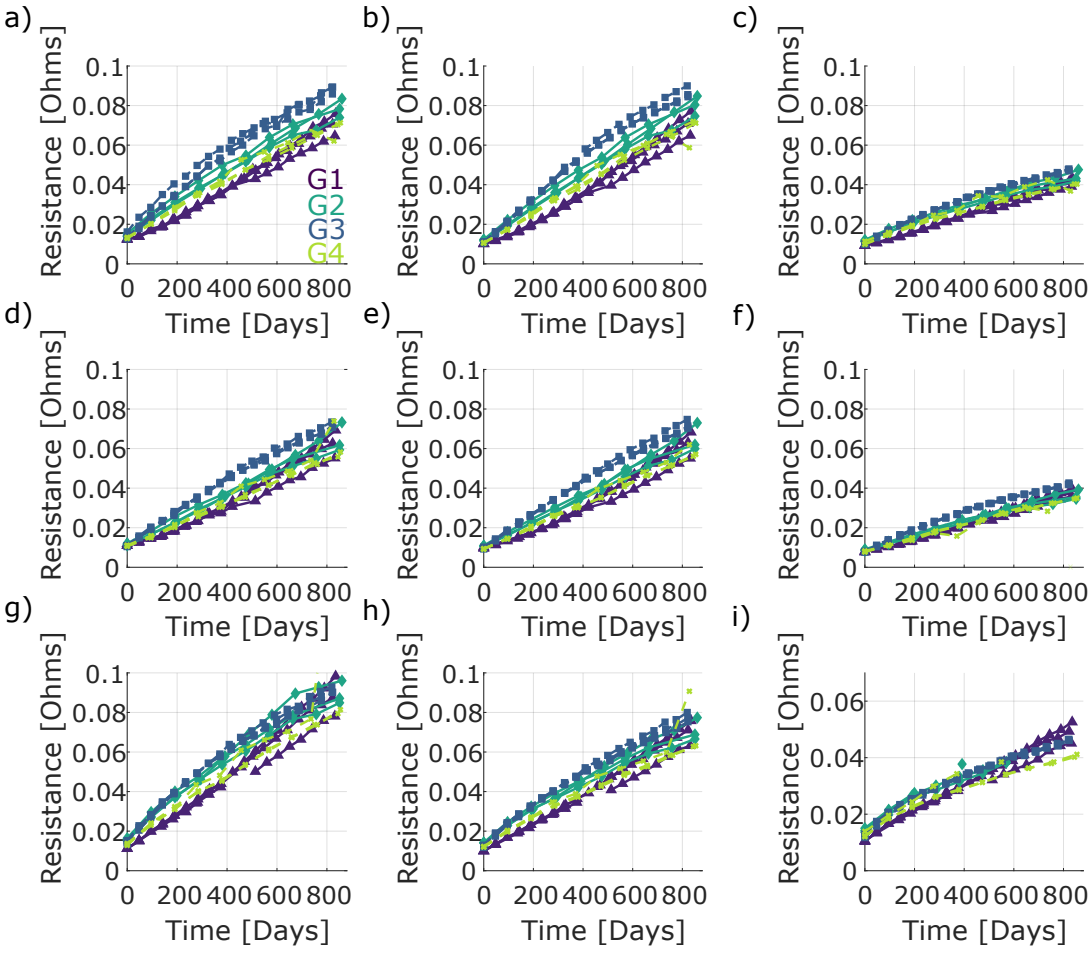

Fig. B.4 Raw DC resistance for experimental camapaign 1 (a),(b),(c) taken at 80% SoC with 1.5A discharge, 1.5A charge and 10A discharge pulse respectively; (d),(e),(f) taken at 50% SoC with 1.5A discharge, 1.5A charge and 10A discharge pulse respectively; (g),(h),(i) taken at 20% SoC with 1.5A discharge, 1.5A charge and 10A discharge pulse respectively

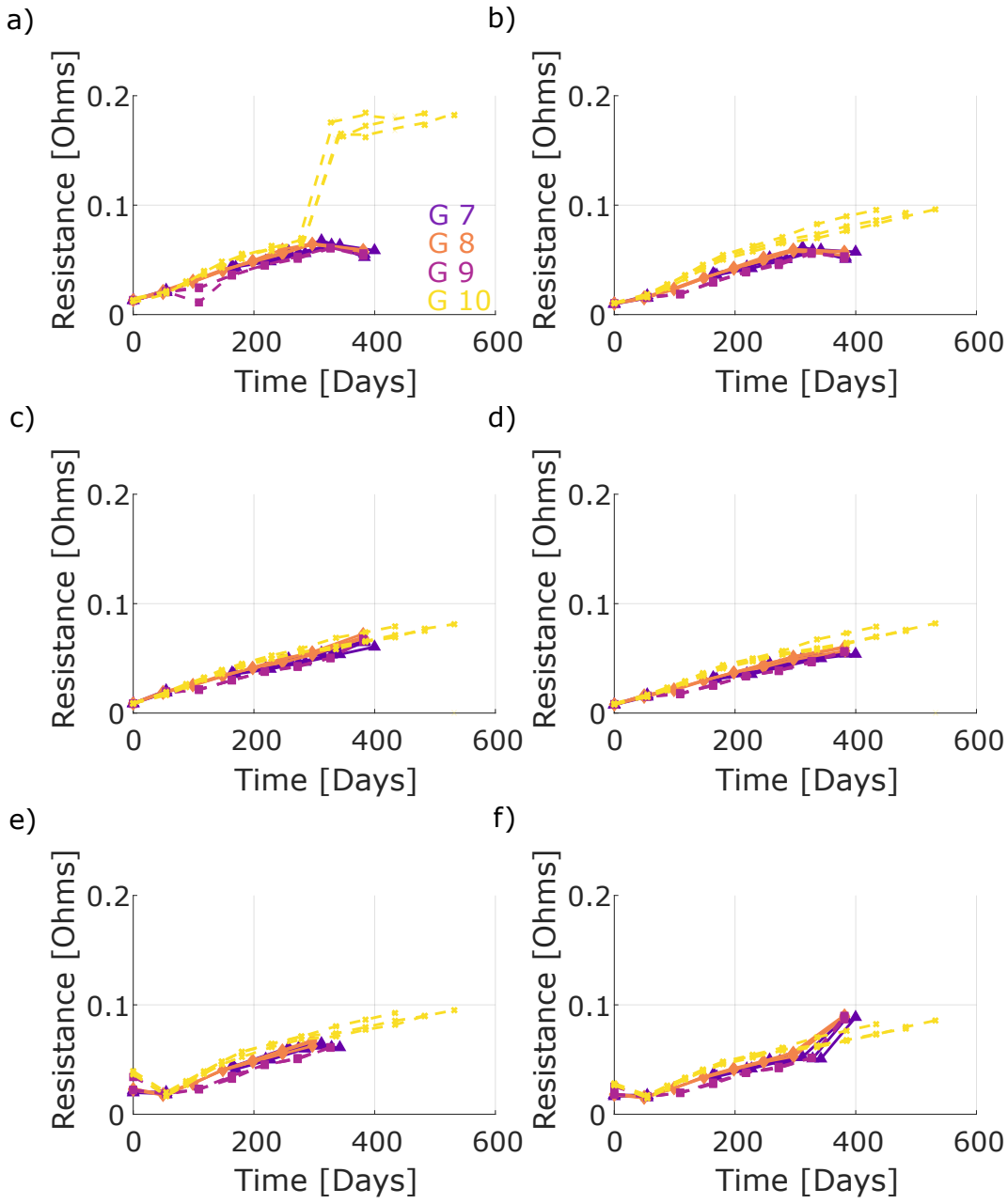

Fig. B.5 Raw DC resistance for experimental campagin 2 (a),(b),(c) taken at 80% SoC with 1.5A discharge, 1.5A charge and 10A discharge pulse respectively; (d),(e),(f) taken at 50% SoC with 1.5A discharge, 1.5A charge and 10A discharge pulse respectively; (g),(h),(i) taken at 20% SoC with 1.5A discharge, 1.5A charge and 10A discharge pulse respectively